THE STRUCTURAL AND FUNCTIONAL ROLES OF MITOCHONDRIAL FISSION ADAPTORS IN YEAST AND HUMANS

by

Sajjan Koirala

A dissertation submitted to the faculty of
The University of Utah
in partial fulfillment of the requirements for the degree of

Doctor of Philosophy

Department of Biochemistry

The University of Utah

December 2012

Copyright © Sajjan Koirala 2012

All Rights Reserved

The University of Utah Graduate School

STATEMENT OF DISSERTATION APPROVAL

The dissertation of **Sajjan Koirala**

has been approved by the following supervisory committee members:

Janet M. Shaw	, Chair	**10/22/2012** Date Approved
Don Ayer	, Member	**10/22/2012** Date Approved
Michael S. Kay	, Member	**10/22/2012** Date Approved
Wesley I. Sundquist	, Member	**10/23/2012** Date Approved
Dennis R. Winge	, Member	**10/22/2012** Date Approved

and by **Wesley I. Sundquist and Christopher P. Hill** , Chair of the Department of **Biochemistry**

and by Charles A. Wight, Dean of The Graduate School.

ABSTRACT

The mitochondrion is an essential organelle in eukaryotic cells. The major functions of mitochondria are ATP production, calcium homeostasis, heme and lipid biosynthesis and apoptosis. Mitochondria form a dynamic tubular spaghetti-like network that fuses, divides and moves within the cell. The molecular events that regulate mitochondrial dynamics are important for various cellular and developmental processes and are linked to cellular dysfunction and disease. This dissertation focuses on the molecular machineries that carry out mitochondrial fission in yeast and human.

Mitochondrial fission requires both dynamin-related GTPases (called Dnm1/Drp1 in yeast/human) and membrane adaptors. In yeast, a tail-anchored protein called Fis1 and an adaptor protein called Mdv1 recruit Dnm1 to the membrane. Mdv1 interacts with Dnm1 and stimulates Dnm1 self-assembly. Although Fis1 is conserved in humans, an Mdv1 ortholog is absent. Instead, humans have at least three other membrane anchored proteins (Mff, MiD49, MiD51/MIEF1) whose roles in fission are poorly defined.

Studies presented in this thesis address two key issues related to mitochondrial fission. First, experiments in Chapter 2 address how the structure of the yeast mitochondrial adaptor (Mdv1) affects Dnm1 function. A structural study of the Mdv1 central domain shows that this region forms an unusually long antiparallel coiled coil which positions the β-propeller domains of Mdv1 to interact with Dnm1 as it transitions from the cytoplasm to mitochondria. *In vivo* studies with altered coiled coil domains

demonstrates the importance of this domain in Mdv1-Fis1 binding, Dnm1 mitochondrial recruitment and Dnm1-mediated mitochondrial fission. Second, experiments in Chapter 3 determine whether multiple human adaptors are capable of working independently to elicit Drp1-mediated membrane fission. *In vivo* studies using the yeast and human adaptors in a minimal yeast system show that Fis1 is dispensable for mitochondrial membrane scission. These studies also demonstrate that Mdv1, Mff, or MiDs can work in parallel with their corresponding DRPs to catalyze membrane fission. Importantly, co-assembly of MiD49 protein with Drp1 dramatically decreases the diameter of assembled Drp1 structures. Together, these studies advance our understanding of how adaptors and fission dynamins work together to achieve membrane constriction and fission, and raise important questions for future studies.

TABLE OF CONTENTS

LIST OF FIGURES

Figure

LIST OF TABLES

Table

CHAPTER 1

INTRODUCTION

The General Organization and Function of Mitochondria

The mitochondrion is a doubled-membraned organelle that is present in virtually all eukaryotic cells. According to the endosymbiont theory, the present day mitochondrion originated from the engulfment of an α-proteobacterium by a primordial eukaryotic cell (Gray et al., 1999; Henze and Martin, 2003; Margulis, 1981; Wallace, 2005).

The mitochondrion contains outer and inner mitochondrial membranes as depicted in Figure 1.1. These two membranes are vastly different in their composition and function but both play critical roles in the compartmentalization of the organelle. The aqueous space between the outer and inner membrane is called the intermembrane space. The inner mitochondrial membrane forms highly convoluted membrane invaginations called cristae. The cristae structures house protein complexes involved in ATP production through oxidative phosphorylation reactions. The inner mitochondrial membrane encloses an aqueous compartment called the matrix. In addition to the circular mitochondrial DNA genome (which encodes RNAs and proteins necessary for respiratory function), the matrix also contains enzymes of the citric acid cycle and (in some organisms) the beta-oxidation pathway.

Apart from performing various metabolic and ATP generating functions, mitochondria play critical roles in cellular calcium storage and signaling (Szabadkai et al., 2004). Calcium ion concentrations inside mitochondria can regulate the activity of some dehydrogenase enzymes (Denton, 2009; McCormack and Denton, 1980). In addition, the calcium ion concentration inside the mitochondrion has been shown to be critical for apoptosis (Pinton et al., 2008). Apoptotic cell death also requires loss of mito-

Figure 1.1. Compartments of the Mitochondrion.
The mitochondrion contain two membranes, the outer and inner membranes. The inner membrane folds inward forming convoluted invaginations called cristae, marked by the red rectangle. The space between the two membranes is called the intermembrane space. The inner most aqueous part of the mitochondrion is called the matrix.

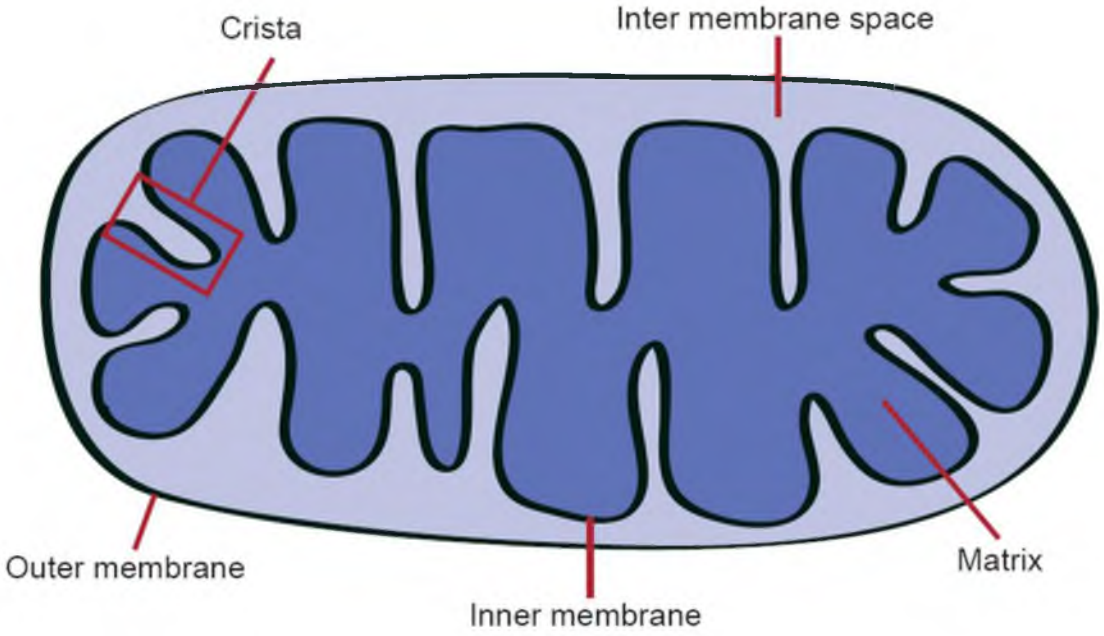
Crista
Inter membrane space
Outer membrane
Inner membrane
Matrix

chondrial membrane potential and the release of cytochrome c from the mitochondrial inner membrane (Lasorsa et al., 2003; Pinton et al., 2001; Szabadkai and Rizzuto, 2004; Szalai et al., 1999). Together, mitochondrial integrity and composition are very important for cell growth, signaling and survival.

Mitochondrial Dynamics and Human Diseases

Mitochondria appear as bean or oval-shaped organelles in transmission electron microscopy (TEM) images (Figure 1.2). Although TEM images are extremely useful in showing the structural details within an organelle, the TEM images do not accurately portray the actual shape and size of an organelle since TEM images are static and obtained from ultra-thin sections of a chemically fixed specimen. Thanks to the discovery of fluorescent proteins, live cell imaging studies over the last 10-15 years have shown that mitochondria are highly dynamic organelles that constantly change their shape, size, number and distribution (Chan, 2006a, b; Nunnari et al., 1997; Okamoto and Shaw, 2005). There are at least four distinct pathways that regulate the dynamic behavior of mitochondria. These pathways include mitochondrial fission, fusion, tubulation and transport (Bereiter-Hahn and Voth, 1994; Boldogh et al., 2001; Nunnari et al., 1997). Genetic studies in *Saccharomyces cerevisiae* (budding yeast) have been instrumental in the identification of molecular machineries that control these mitochondrial dynamics (Bleazard et al., 1999; Hermann et al., 1998; Mozdy et al., 2000; Okamoto and Shaw, 2005; Sesaki and Jensen, 1999; Tieu et al., 2002). Moreover, recent studies carried out in various multicellular organisms show that mitochondrial dynamics and molecular

Figure 1.2. Transmission Electron Microscopy (TEM) Image of Mitochondria.
Lung cell mitochondrion showing convoluted cristae invaginations. Scale bar 100 nm. Courtesy of Louisa Howard, Dartmouth College, Hanover, NH, U.S.A.

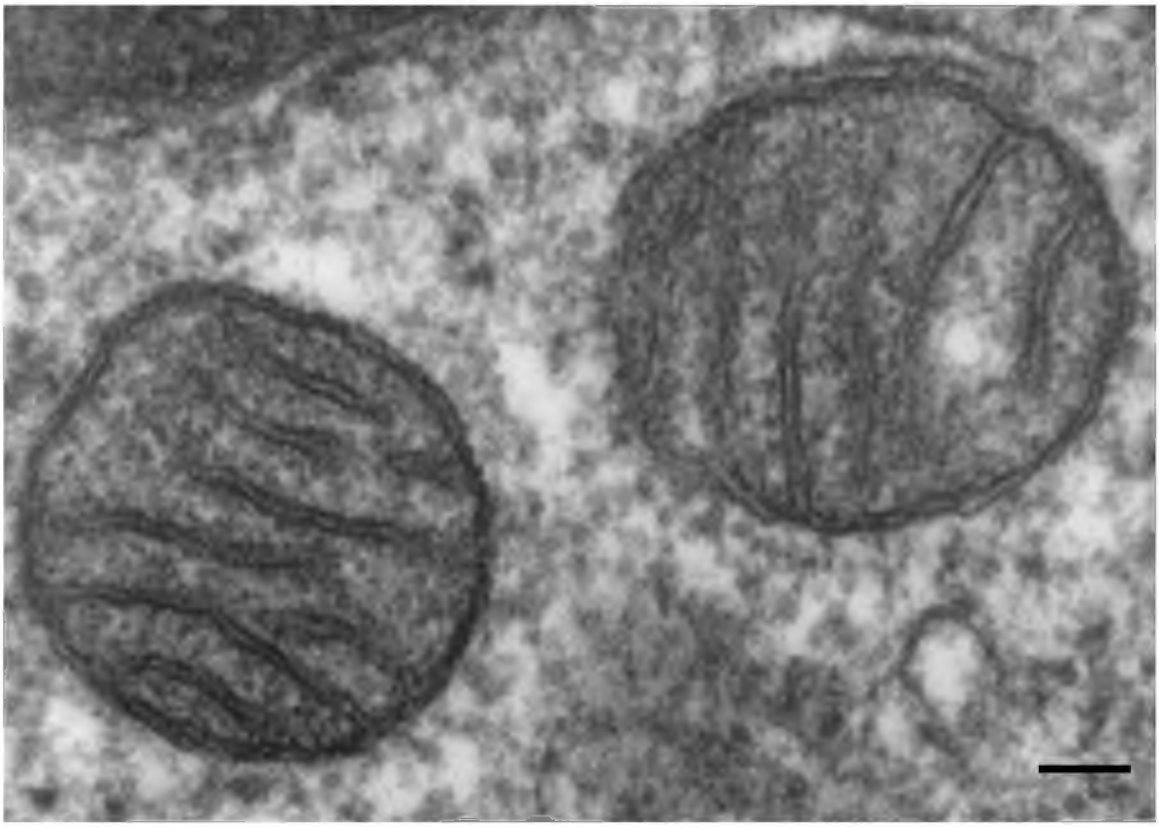

machines are conserved in all eukaryotes studied thus far and are very important for the health of the organism (Chan, 2006b).

It is now clear that mitochondria form highly dynamic branched tubular networks that distribute outward from the nuclear periphery into the cytoplasm (Okamoto and Shaw, 2005). Microscopy studies using fluorescently labeled mitochondria show that these organelles actively divide, fuse, change their shape and move around the cytoplasm. In cells that are very long such as neurons, mitochondria travel long distances between the cell body and synaptic terminals using cytoskeletal tracks and motor proteins (Bereiter-Hahn and Voth, 1994; Boldogh et al., 2001; Chen and Chan, 2005; Nunnari et al., 1997; Okamoto and Shaw, 2005). Genetic and mass spectrometric screens have identified proteins that are responsible for dynamically modulating these organelles. All genes required for mitochondrial dynamics are encoded by the nuclear genome (Angelini et al., 2009). Gene knockout studies indicate that the mitochondrial dynamics are crucial for the development and life of an organism (Liesa et al., 2009).

Regulated fission and fusion allows mitochondria to exchange their contents, including mtDNA, RNAs and proteins (Twig et al., 2008). This exchange helps maintain a healthy organelle in the mother cell that can also be duplicated and transported into daughter cells during division (Nakada et al., 2001; Twig et al., 2008). Dysfunction of proteins required for mitochondrial dynamics can contribute to aging and cause human diseases (Chan, 2006a; Chang et al., 2010), including neurodegenerative diseases such as Huntington's disease, Alzheimer's disease, Parkinson's disease (Mattson et al., 2008; Reddy et al., 2009; Wang et al., 2009), cardiovascular disease (Ong and Hausenloy, 2010) and skeletal muscle atrophy (Romanello et al., 2010). Due to the link between

mitochondrial dynamics dysfunction and disease, understanding how these processes keep cells, tissues and organisms healthy is getting much more attention of late.

Mitochondrial Fission in Yeast and Man

Mitochondria cannot be created *de novo*. Daughter cells have to inherit at least a copy of a mitochondrion from the mother cells in order to survive (Boldogh et al., 2005). How does a cell overcome this problem and generate sufficient mitochondrial mass and copy number in the mother cell, so a portion of which can be inherited by the daughters during division? Some ground breaking discoveries in late nineties identified proteins that modulate mitochondrial copy number (Okamoto and Shaw, 2005). These are the proteins involved in mitochondrial fission and fusion. Genetic and fluorescence microscopy studies in *Saccharomyces cerevisiae* established the concept of dynamic balance between these two opposing events (Bleazard et al., 1999; Sesaki and Jensen, 1999). Both of these processes are controlled by independent sets of proteins. When proteins essential for either of these two membrane remodeling events are knocked out in yeast cells, continuous membrane fission or fusion leads to the formation of mitochondrial fragmentation or nets, respectively (Okamoto and Shaw, 2005). Excessive mitochondrial fragmentation leads to mitochondrial DNA loss and respiratory defects in yeast. Likewise, excessive mitochondrial fusion makes it hard for yeast cells to pass mitochondria to daughter cells during sporulation (Gorsich and Shaw, 2004). These findings highlight the importance of the balance between these two membrane-remodeling events. More recent studies in multicellular organisms of the plant and animal kingdoms established that mitochondrial fission and fusion and the protein machineries that control these processes are at least partially conserved in different eukaryotic

kingdoms. The studies in this thesis focus on understanding of the molecular players and the mechanisms of mitochondrial fission.

Saccharomyces cerevisiae has been the prototype organism for studying the process of mitochondrial fission. In yeast, mitochondrial fission requires three proteins; Dnm1, Fis1 and Mdv1. Dnm1 is a dynamin related GTPase that acts as the mechanochemical enzyme that severs the mitochondrial compartment (Otsuga et al., 1998). Fis1 is anchored to the outer mitochondrial membrane via its C-terminus and faces the cytoplasm (Mozdy et al., 2000). Mdv1 is an adaptor that localizes to the mitochondrial outer membrane via its interaction with Fis1 (Tieu and Nunnari, 2000) A complex formed between Fis1 and Mdv1 on the membrane recruits Dnm1 by direct binding between Mdv1 and Dnm1. Fluorescence microscopy studies show that Mdv1 and Dnm1 further assemble into large complexes. Time-lapse imaging studies show that mitochondrial fission occurs in a stochastic manner at sites where both Mdv1 and Dnm1 are assembled (Cerveny and Jensen, 2003; Cerveny et al., 2001; Fekkes et al., 2000; Karren et al., 2005; Tieu and Nunnari, 2000; Tieu et al., 2002). The cellular signaling circuitry that controls the localization and assembly of Mdv1 and Dnm1 on mitochondria is not understood.

In addition to yeast, mitochondrial fission has been well studied in worms, flies, plants and mammals. As part of my thesis work, I studied the fission process using yeast and human proteins. Table 1.1 summarizes the mitochondrial fission proteins in yeast and humans. Two components of the mitochondrial fission machinery, the dynamin-related GTPase Dnm1/Drp1 and the membrane anchor Fis1/hFis1, are conserved in these two or-

Table 1.1 Conserved and Nonconserved Mitochondrial Fission Components in Yeast and Humans

	Yeast	Role in fission	Human	Role in fission
Dynamin-related GTPase	Dnm1	Essential	Drp1	Essential
Membrane anchor	yFis1	Essential	hFis1	Not determined
Adaptor	Mdv1	Essential		
Adaptor	Caf4	Nonessential		
Membrane anchor			Mff	Essential
Membrane anchor			hMiD49	Not determined
Membrane anchor			hMiD51	Not determined

Green: conserved among eukaryotes, Purple: conserved among fungi, Blue: conserved among metazoans, Orange: conserved among vertebrates.

ganisms (Table 1.1 purple shading). In yeast, Mdv1 and its nonessential paralog Caf4 (Griffin et al., 2005) interact with Fis1 on the outer mitochondrial membrane and, in turn, bind and recruit Dnm1 to the membrane. To date, Mdv1/Caf4 orthologs have not been identified outside of the fungal kingdom. Recent studies in mammals have identified three additional membrane localized mitochondrial fission proteins called Mff, MiD49 and MiD51 (MIEF1) (Gandre-Babbe and van der Bliek, 2008; Otera et al., 2010; Palmer et al., 2011; Zhao et al., 2011). Mff is a mitochondrial receptor for Drp1 that is conserved in metazoans but not in yeast. MiD49 and MiD51 are paralogs that are found only in vertebrates (Zhao et al., 2012). There are no sequence or domain similarities between Fis1, Mff, MiD49/MiD51 or Mdv1/Caf4 (Figure 1.3). Table 1.2 summarizes the amino acid sequence identity of fission proteins from yeast and human.

Dynamin-Related Mitochondrial Fission GTPases

The amino acid identities between mitochondrial fission GTPases and classical dynamin are shown in Table 1.2. The mitochondrial fission GTPases are not only conserved and have similar domain structures but are also related to other GTPases, which act in membrane remodeling (Figure 1.3). The most studied and the best understood membrane remodeling GTPase member is classical dynamin, which severs the necks of clathrin-coated pits to release clathrin-coated vesicles during endocytosis. Both classical dynamins and mitochondrial dynamin related proteins (DRPs) contain GTPase, middle and GTPase effector domains (GED) (Figure 1.3). The classical dynamins have a membrane interaction domain called the pleckstrin homology (PH) domain, while the mitochondrial DRPs have an insert B domain in place of the PH

Table 1.2. Amino Acid Sequence Identity among Mitochondrial Fission Proteins.

	Protein A	Protein B	Amino acids sequence identity (%)
1	hDynamin1	hDrp1	33
2	hDynamin1	yDnm1	32
3	hDrp1	yDnm1	43
4	hFis1	yFis1	22
5	Mdv1	Caf4	30
6	hMff	Mdv1	7
7	hMff	hFis1	11
8	hMff	hMiD49	10
9	hMff	hMiD51	9
10	hMiD49	Mdv1	11
11	hMiD49	hFis1	6
12	hMiD49	hMiD51	45
13	hMiD51	Mdv1	8
14	hMiD51	hFis1	8

h: human, y: yeast, very dark shade: very significant identity, dark shade: significant identity, light shade: noteworthy identity, no shade: insignificant identity

Global alignment of each pairs of sequences was performed using the CLUSTALO program, UNIPROT.

Figure 1.3. Domain Structures of Mitochondrial Fission Proteins.
A. Domain structures of classical dynamin and mitochondrial fission dynamin-related proteins (DRPs), including GTPase, Middle, Pleckstrin Homology (PH), GTPase Effector Domain (GED), Proline Rich Domain (PRD) and Insert B. **B.** Domain structures of yeast fission adaptors (yFis1, Mdv1 and Caf4), including tetratricopeptide (TPR), transmembrane domain (TM), N-terminal extension (NTE), coiled coil (CC) and WD40 repeats predicted to form a β-propeller. **C.** Domain structures of human fission adaptors (hFis1, Mff, MiD49, MiD51 (MIEF1), including TPR, TM and CC. Question marks indicate regions with no predicted domains in these proteins.

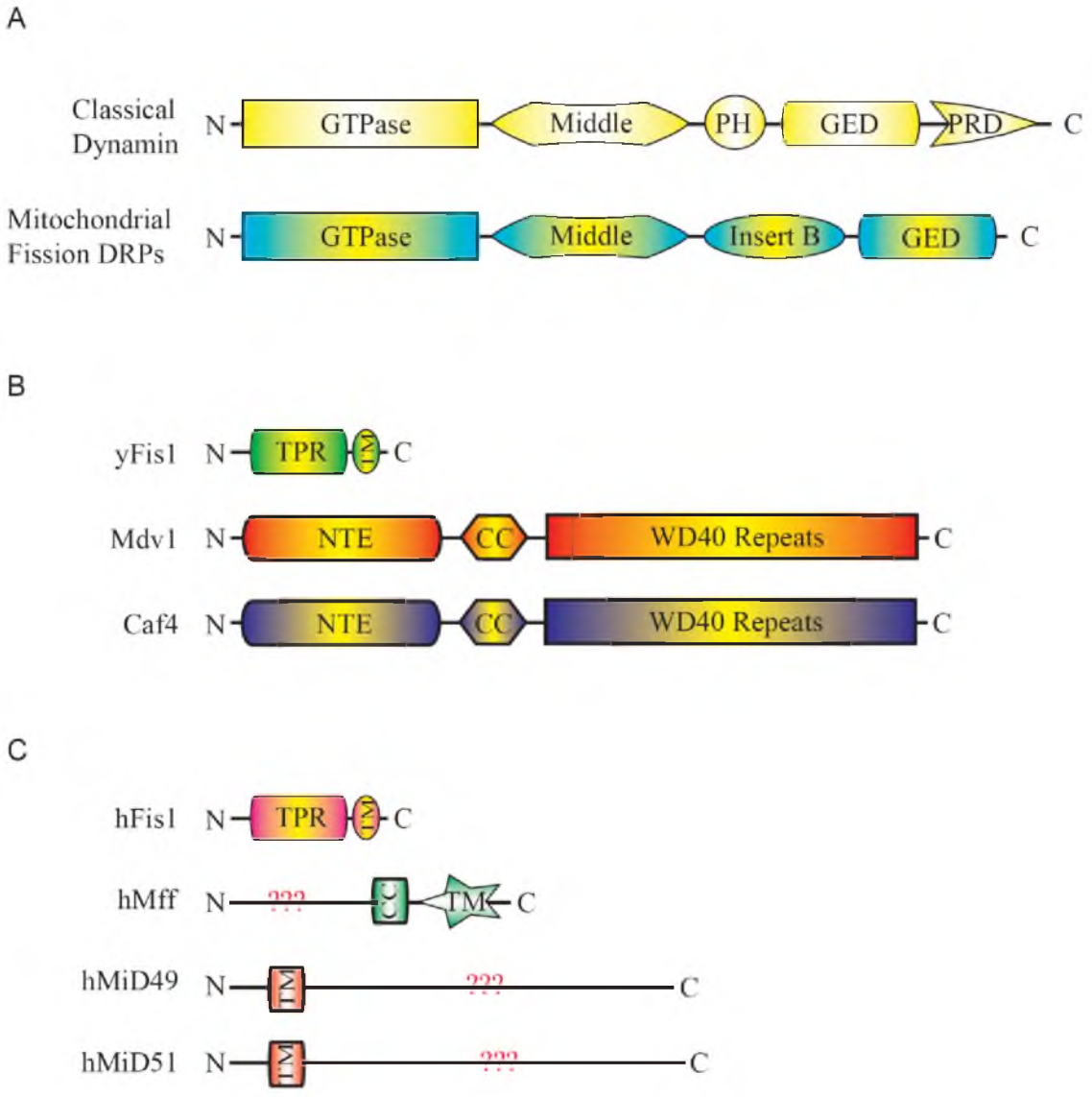
A
Classical Dynamin
N
GTPase
Middle
PH
GED
PRD
C
Mitochondrial Fission DRPs
N
GTPase
Middle
Insert B
GED
C
B
yFis1
N
TPR
TM
C
Mdv1
N
NTE
CC
WD40 Repeats
C
Caf4
N
NTE
CC
WD40 Repeats
C
C
hFis1
N
TPR
TM
C
hMff
N
???
TM
C
hMiD49
N
TM
???
C
hMiD51
N
TM
???
C

domain that is required for the interaction with the mitochondrial adaptors (Bui et. al., 2012). Dynamins also have a proline rich domain (PRD) at their C-termini that interacts with SH3 domain containing proteins such as amphiphysin, endophilin and cortactin (Cestra et al., 1999). Mitochondrial DRPs do not have the PRD domain.

Dynamin family members possess the following five properties. First, they have GTPase domains that can bind and hydrolyze GTP. Their affinity for nucleotide and intrinsic hydrolysis rate is great enough that they do not strictly require GTPase activating proteins (GAPs) or GTPase exchange factors (GEFs) for activity. Second, they can self-assemble and form spirals of various diameters. Self-interaction within the spiral stimulates the GTPase activity of the protein. Third, *in vitro* self-assembly of these proteins is dependent upon the buffer ionic strength, i.e., at low ionic strengths, dynamins self-assemble and at high ionic strengths, they disassemble. Fourth, GTP binding favors dynamin assembly but GTP hydrolysis favors their disassembly. Fifth, they act as mechanochemical enzymes to remodel specific biological membranes in a GTP hydrolysis dependent manner (Praefcke and McMahon, 2004). This remodeling can take the form of fission or fusion.

In vivo, mitochondrial fission DRPs require adaptor proteins for their membrane localization. In yeast, Fis1-Mdv1 or Fis1-Caf4 complexes on the mitochondrial membrane recruit the Dnm1 GTPase to the mitochondrial surface where it assembles and catalyzes fission. *In vitro* studies indicate that Mdv1 not only binds Dnm1 directly but also stimulates the assembly, and indirectly the GTPase activity of Dnm1 (Lackner et al., 2009). Although membrane-anchored Fis1 was originally reported to bind and recruit Drp1 for fission in mammals (Yoon et al., 2003) a direct interaction between these two

proteins is no longer thought to occur. Instead, new mitochondrial adaptors have been identified and are implicated in human Drp1 function (Table 1.1) (Gandre-Babbe and van der Bliek, 2008; Otera et al., 2010; Palmer et al., 2011; Zhao et al., 2011). Chapter three of this dissertation characterizes human Drp1 and other mitochondrial fission adaptors to establish their roles in Drp1 membrane recruitment and fission.

Molecular Architecture of the Yeast Mitochondrial Fission Adaptor for Dnm1 Mitochondrial Recruitment and Fission

In yeast, mitochondrial fission requires a concerted effort of three proteins (Figure 1.3). The membrane bound Fis1 recruits soluble Mdv1 from the cytoplasm via an interaction between the TPR domain of Fis1 and the NTE of Mdv1 (Karren et al., 2005). The C-terminal WD40 repeats of Mdv1 are predicted to form a β-propeller domain that interacts with Dnm1 (Tieu et al., 2002). Recent studies from our lab indicate that a novel motif within the insert B domain of Dnm1 is essential for Mdv1 β-propeller interactions (Bui et al., 2012).

There have been several attempts made to understand the molecular details of Fis1-Mdv1-Dnm1 complex formation. The crystal structure of the Fis1 cytoplasmic domain has been solved (Suzuki et al., 2005). Very recently, the Dnm1 cryo-EM structure was also published (Mears et al., 2011). Attempts to solve the co-crystal structures of full-length fission proteins have not been very successful. Some inroads have been made, including the solution of a co-crystal structure of a short helix (~13 aa) of the NTE of Mdv1 and the TPR domain of Fis1 (Zhang and Chan, 2007). However, at the time I began my thesis studies, the field lacked a clear model for the molecular architecture of the Fis1-Mdv1 complex on the membrane. Such a model was necessary to

understand the role of Fis1-Mdv1 in binding and positioning cytoplasmic Dnm1 for further assembly on the membrane.

To understand the role of Mdv1 in Dnm1 membrane recruitment and mitochondrial fission, I collaborated with researchers in the Biochemistry Department to solve the structure of the predicted Mdv1 coiled coil (CC) domain and characterized its function in fission complex assembly and fission (described in Chapter 2 of this thesis). Previous co-IP and yeast two hybrid studies had indicated that the Mdv1 CC might regulate Mdv1 self-interaction (Griffin et al., 2005). More importantly, a suppressor mutation in the middle of the predicted Mdv1 CC was shown to mitigate the negative effect of TPR point mutations on Fis1-Mdv1 interactions (Karren et al., 2005). I purified the Mdv1 coiled coil domain, determined its oligomeric state and solved the crystal structure in collaboration with other labs in the Department (details of our collaborators in this study can be found in the Chapter 2). We found that the Mdv1 CC formed a dimeric antiparallel CC at least 92 Å long. Using a mutational analysis, I was able to show that the Mdv1 CC sequence, length and formation were important for optimal Dnm1 membrane recruitment and function. These studies also indicated that spatial positioning of β-propeller domains by the Mdv1 CC was important for Dnm1 mediated mitochondrial fission (see fission complex assembly model, Figure 1.4).

Multiple Adaptors Regulate Mitochondrial Fission DRP Assembly and Function

Although the mitochondrial fission DRPs are evolutionarily conserved in eukaryotes, with the exception of Fis1, the corresponding adaptors that recruit the DRPs to the mitochondria surface are not (Table 1.1). In Chapter 3 of this thesis, I directly test

Figure 1.4. Model of Yeast Mitochondrial Fission Complex Assembly.
Step I: Monomeric Fis1 constitutively localizes to the mitochondrial outer membrane via its C-terminal transmembrane domain. **Step II:** Soluble Mdv1 dimers from the cytoplasm are recruited to the mitochondrial membrane. **Step III:** Soluble Dnm1 dimers assemble on the Fis1-Mdv1 complexes on the membrane by binding to the beta-propeller domain of Mdv1. This is thought to result in the co-assembly of Mdv1 with Dnm1 to produce fission competent fission complexes. **Step IV:** Disassembly of fission complexes thought to be triggered by GTP hydrolysis by Dnm1.

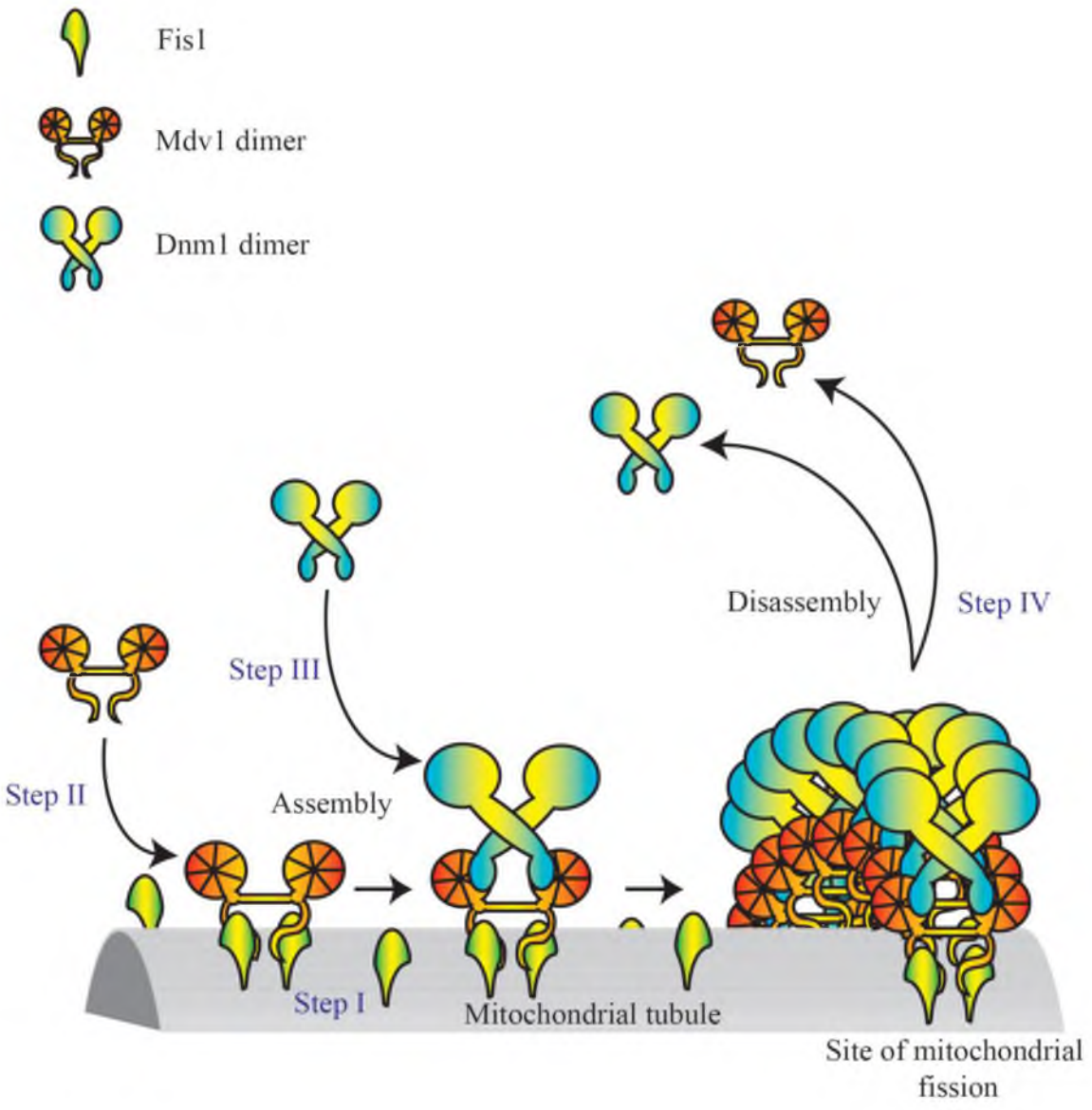
Fis1
Mdv1 dimer
Dnm1 dimer
Step II
Step III
Assembly
Disassembly
Step IV
Step I
Mitochondrial tubule
Site of mitochondrial fission

the function of Fis1 in fission complex assembly and mitochondrial fission after Dnm1 membrane recruitment. The key to this analysis was the generation of a yeast strain missing all known mitochondrial fission genes (*fis1Δmdv1Δcaf4Δdnm1Δ*). Using this strain, I was able to directly tether full-length and truncated Mdv1 constructs to the mitochondrial membrane and ask whether they could function with cytoplasmic Dnm1 in fission when Fis1 was absent. I also tested whether the functions of both Mdv1 and Fis1 could be bypassed by tethering Dnm1 to the mitochondrial membrane. The results of my studies conclusively demonstrated that yeast Fis1 played no role in mitochondrial fission other than bringing Mdv1 to the mitochondrial membrane. The studies also suggested that Mdv1 was essential after Dnm1-recruitment to complete fission.

I extended these studies to dissect the function of individual human adaptors in mitochondrial fission. As summarized in Table 1.1, humans have four adaptors that are implicated in Drp1 membrane recruitment and function (Otera et al., 2010; Palmer et al., 2011; Yoon et al., 2003). Whether these proteins worked independently or together was not known. None of these four proteins have any sequence or domain similarities with the yeast Mdv1 adaptor (Table 1.2). Except for the MiD49/MiD51 paralogs, these proteins also are not similar to one another (Table 1.2). Although Mff had been shown to act in Drp1 recruitment (Otera et al., 2010), whether it was sufficient for Drp1 mediated fission was not known. Moreover, conflicting roles had been proposed for the MiD49 and MiD51 (also called MIEF1) adaptors. One study suggested both proteins were required for mitochondrial fission (Palmer et al., 2011), while another proposed they functioned either to promote mitochondrial fusion or to inhibit mitochondrial fission (Zhao et al., 2011). By expressing different combinations of Drp1 and human adaptors in the yeast

tester strain, I was able to show that: 1) hFis1 plus hDrp1 are not sufficient for mitochondrial fission. 2) hFis1 is not sufficient to target GFP-hDrp1 to mitochondria. 3) hMff plus hDrp1, or hMiD49 plus hDrp1, or hMiD51 plus hDrp1 are each sufficient to target GFP-hDrp1 to the mitochondrial membrane and complete membrane fission. These studies for the first time show that only two proteins, a membrane adaptor and the mitochondrial fission GTPase, are capable of remodeling mitochondrial membranes *in vivo*.

Structural studies with the purified components of human mitochondrial fission (hDrp1 and hMiD49) are also presented in Chapter 3. I characterized the GTP hydrolysis properties of human Drp1. Collaborative negative-staining transmission electron microscopy (TEM) studies were used to define the assembly properties of hDrp1 in the presence and absence of the MiD49 adaptor. These biochemical studies provide the first demonstration that a mitochondrial adaptor can alter the polymer structure of a mitochondrial dynamin.

Refererences

Angelini, C., Bello, L., Spinazzi, M., and Ferrati, C. (2009). Mitochondrial disorders of the nuclear genome. Acta myologica : myopathies and cardiomyopathies : official journal of the Mediterranean Society of Myology / edited by the Gaetano Conte Academy for the Study of Striated Muscle Siseases *28*, 16-23.

Bereiter-Hahn, J., and Voth, M. (1994). Dynamics of mitochondria in living cells: shape changes, dislocations, fusion, and fission of mitochondria. Microscopy Research and Technique *27*, 198-219.

Bleazard, W., McCaffery, J.M., King, E.J., Bale, S., Mozdy, A., Tieu, Q., Nunnari, J., and Shaw, J.M. (1999). The dynamin-related GTPase Dnm1 regulates mitochondrial fission in yeast. Nature Cell Biology *1*, 298-304.

Boldogh, I.R., Fehrenbacher, K.L., Yang, H.C., and Pon, L.A. (2005). Mitochondrial movement and inheritance in budding yeast. Gene *354*, 28-36.

Boldogh, I.R., Yang, H.C., and Pon, L.A. (2001). Mitochondrial inheritance in budding yeast. Traffic *2*, 368-374.

Bui, H.T., Karren, M.A., Bhar, D., and Shaw, J.M. (2012). A novel motif in the yeast mitochondrial dynamin Dnm1 is essential for adaptor binding and membrane recruitment. J Cell Biol *199*, 613-622.

Cerveny, K.L., and Jensen, R.E. (2003). The WD-repeats of Net2p interact with Dnm1p and Fis1p to regulate division of mitochondria. Mol Biol Cell *14*, 4126-4139.

Cerveny, K.L., McCaffery, J.M., and Jensen, R.E. (2001). Division of mitochondria requires a novel DMN1-interacting protein, Net2p. Mol Biol Cell *12*, 309-321.

Cestra, G., Castagnoli, L., Dente, L., Minenkova, O., Petrelli, A., Migone, N., Hoffmuller, U., Schneider-Mergener, J., and Cesareni, G. (1999). The SH3 domains of endophilin and amphiphysin bind to the proline-rich region of synaptojanin 1 at distinct sites that display an unconventional binding specificity. J Biol Chem *274*, 32001-32007.

Chan, D.C. (2006a). Mitochondria: dynamic organelles in disease, aging, and development. Cell *125*, 1241-1252.

Chan, D.C. (2006b). Mitochondrial fusion and fission in mammals. Annu Rev Cell Dev Biol *22*, 79-99.

Chang, C.R., Manlandro, C.M., Arnoult, D., Stadler, J., Posey, A.E., Hill, R.B., and Blackstone, C. (2010). A lethal de novo mutation in the middle domain of the dynamin-related GTPase Drp1 impairs higher order assembly and mitochondrial division. J Biol Chem *285*, 32494-32503.

Chen, H., and Chan, D.C. (2005). Emerging functions of mammalian mitochondrial fusion and fission. Human Molecular Genetics *14 Spec No. 2*, R283-289.

Denton, R.M. (2009). Regulation of mitochondrial dehydrogenases by calcium ions. Biochimica et Biophysica Acta *1787*, 1309-1316.

Fekkes, P., Shepard, K.A., and Yaffe, M.P. (2000). Gag3p, an outer membrane protein required for fission of mitochondrial tubules. J Cell Biol *151*, 333-340.

Gandre-Babbe, S., and van der Bliek, A.M. (2008). The novel tail-anchored membrane protein Mff controls mitochondrial and peroxisomal fission in mammalian cells. Mol Biol Cell *19*, 2402-2412.

Gorsich, S.W., and Shaw, J.M. (2004). Importance of mitochondrial dynamics during meiosis and sporulation. Mol Biol Cell *15*, 4369-4381.

Gray, M.W., Burger, G., and Lang, B.F. (1999). Mitochondrial evolution. Science *283*, 1476-1481.

Griffin, E.E., Graumann, J., and Chan, D.C. (2005). The WD40 protein Caf4p is a component of the mitochondrial fission machinery and recruits Dnm1p to mitochondria. J Cell Biol *170*, 237-248.

Henze, K., and Martin, W. (2003). Evolutionary biology: essence of mitochondria. Nature *426*, 127-128.

Hermann, G.J., Thatcher, J.W., Mills, J.P., Hales, K.G., Fuller, M.T., Nunnari, J., and Shaw, J.M. (1998). Mitochondrial fusion in yeast requires the transmembrane GTPase Fzo1p. J Cell Biol *143*, 359-373.

Karren, M.A., Coonrod, E.M., Anderson, T.K., and Shaw, J.M. (2005). The role of Fis1p-Mdv1p interactions in mitochondrial fission complex assembly. J Cell Biol *171*, 291-301.

Lackner, L.L., Horner, J.S., and Nunnari, J. (2009). Mechanistic analysis of a dynamin effector. Science *325*, 874-877.

Lasorsa, F.M., Pinton, P., Palmieri, L., Fiermonte, G., Rizzuto, R., and Palmieri, F. (2003). Recombinant expression of the Ca(2+)-sensitive aspartate/glutamate carrier increases mitochondrial ATP production in agonist-stimulated Chinese hamster ovary cells. J Biol Chem *278*, 38686-38692.

Liesa, M., Palacin, M., and Zorzano, A. (2009). Mitochondrial dynamics in mammalian health and disease. Physiological Reviews *89*, 799-845.

Margulis, L. (1981). Symbiosis in cell evolution : life and its environment on the early Earth (San Francisco: W. H. Freeman).

Mattson, M.P., Gleichmann, M., and Cheng, A. (2008). Mitochondria in neuroplasticity and neurological disorders. Neuron *60*, 748-766.

McCormack, J.G., and Denton, R.M. (1980). Role of calcium ions in the regulation of intramitochondrial metabolism. Properties of the Ca2+-sensitive dehydrogenases within intact uncoupled mitochondria from the white and brown adipose tissue of the rat. Biochem J *190*, 95-105.

Mears, J.A., Lackner, L.L., Fang, S., Ingerman, E., Nunnari, J., and Hinshaw, J.E. (2011). Conformational changes in Dnm1 support a contractile mechanism for mitochondrial fission. Nat Struct Mol Biol *18*, 20-26.

Mozdy, A.D., McCaffery, J.M., and Shaw, J.M. (2000). Dnm1p GTPase-mediated mitochondrial fission is a multi-step process requiring the novel integral membrane component Fis1p. J Cell Biol *151*, 367-380.

Nakada, K., Inoue, K., Ono, T., Isobe, K., Ogura, A., Goto, Y.I., Nonaka, I., and Hayashi, J.I. (2001). Inter-mitochondrial complementation: Mitochondria-specific system preventing mice from expression of disease phenotypes by mutant mtDNA. Nature Medicine *7*, 934-940.

Nunnari, J., Marshall, W.F., Straight, A., Murray, A., Sedat, J.W., and Walter, P. (1997). Mitochondrial transmission during mating in Saccharomyces cerevisiae is determined by mitochondrial fusion and fission and the intramitochondrial segregation of mitochondrial DNA. Mol Biol Cell *8*, 1233-1242.

Okamoto, K., and Shaw, J.M. (2005). Mitochondrial morphology and dynamics in yeast and multicellular eukaryotes. Annu Rev Genet *39*, 503-536.

Ong, S.B., and Hausenloy, D.J. (2010). Mitochondrial morphology and cardiovascular disease. Cardiovascular Research *88*, 16-29.

Otera, H., Wang, C., Cleland, M.M., Setoguchi, K., Yokota, S., Youle, R.J., and Mihara, K. (2010). Mff is an essential factor for mitochondrial recruitment of Drp1 during mitochondrial fission in mammalian cells. J Cell Biol *191*, 1141-1158.

Otsuga, D., Keegan, B.R., Brisch, E., Thatcher, J.W., Hermann, G.J., Bleazard, W., and Shaw, J.M. (1998). The dynamin-related GTPase, Dnm1p, controls mitochondrial morphology in yeast. J Cell Biol *143*, 333-349.

Palmer, C.S., Osellame, L.D., Laine, D., Koutsopoulos, O.S., Frazier, A.E., and Ryan, M.T. (2011). MiD49 and MiD51, new components of the mitochondrial fission machinery. EMBO Reports *12*, 565-573.

Pinton, P., Ferrari, D., Rapizzi, E., Di Virgilio, F., Pozzan, T., and Rizzuto, R. (2001). The Ca2+ concentration of the endoplasmic reticulum is a key determinant of ceramide-induced apoptosis: significance for the molecular mechanism of Bcl-2 action. EMBO J *20*, 2690-2701.

Pinton, P., Giorgi, C., Siviero, R., Zecchini, E., and Rizzuto, R. (2008). Calcium and apoptosis: ER-mitochondria Ca2+ transfer in the control of apoptosis. Oncogene *27*, 6407-6418.

Praefcke, G.J., and McMahon, H.T. (2004). The dynamin superfamily: universal membrane tubulation and fission molecules? Nature Reviews Molecular Cell Biology *5*, 133-147.

Reddy, P.H., Mao, P., and Manczak, M. (2009). Mitochondrial structural and functional dynamics in Huntington's disease. Brain Research Reviews *61*, 33-48.

Romanello, V., Guadagnin, E., Gomes, L., Roder, I., Sandri, C., Petersen, Y., Milan, G., Masiero, E., Del Piccolo, P., Foretz, M., *et al.* (2010). Mitochondrial fission and remodelling contributes to muscle atrophy. EMBO J *29*, 1774-1785.

Sesaki, H., and Jensen, R.E. (1999). Division versus fusion: Dnm1p and Fzo1p antagonistically regulate mitochondrial shape. J Cell Biol *147*, 699-706.

Suzuki, M., Neutzner, A., Tjandra, N., and Youle, R.J. (2005). Novel structure of the N terminus in yeast Fis1 correlates with a specialized function in mitochondrial fission. J Biol Chem *280*, 21444-21452.

Szabadkai, G., and Rizzuto, R. (2004). Participation of endoplasmic reticulum and mitochondrial calcium handling in apoptosis: more than just neighborhood? FEBS Letters *567*, 111-115.

Szabadkai, G., Simoni, A.M., Chami, M., Wieckowski, M.R., Youle, R.J., and Rizzuto, R. (2004). Drp-1-dependent division of the mitochondrial network blocks intraorganellar Ca2+ waves and protects against Ca2+-mediated apoptosis. Mol Cell *16*, 59-68.

Szalai, G., Krishnamurthy, R., and Hajnoczky, G. (1999). Apoptosis driven by IP(3)-linked mitochondrial calcium signals. EMBO J *18*, 6349-6361.

Tieu, Q., and Nunnari, J. (2000). Mdv1p Is a WD Repeat Protein that Interacts with the Dynamin-related GTPase, Dnm1p, to Trigger Mitochondrial Division. J Cell Biol *151*, 353-366.

Tieu, Q., Okreglak, V., Naylor, K., and Nunnari, J. (2002). The WD repeat protein, Mdv1p, functions as a molecular adaptor by interacting with Dnm1p and Fis1p during mitochondrial fission. J Cell Biol *158*, 445-452.

Twig, G., Hyde, B., and Shirihai, O.S. (2008). Mitochondrial fusion, fission and autophagy as a quality control axis: the bioenergetic view. Biochimica et Biophysica Acta *1777*, 1092-1097.

Wallace, D.C. (2005). A mitochondrial paradigm of metabolic and degenerative diseases, aging, and cancer: a dawn for evolutionary medicine. Annu Rev Genet *39*, 359-407.

Wang, X., Su, B., Zheng, L., Perry, G., Smith, M.A., and Zhu, X. (2009). The role of abnormal mitochondrial dynamics in the pathogenesis of Alzheimer's disease. Journal of Neurochemistry *109 Suppl 1*, 153-159.

Yoon, Y., Krueger, E.W., Oswald, B.J., and McNiven, M.A. (2003). The mitochondrial protein hFis1 regulates mitochondrial fission in mammalian cells through an interaction with the dynamin-like protein DLP1. Molecular and Cellular Biology *23*, 5409-5420.

Zhang, Y., and Chan, D.C. (2007). Structural basis for recruitment of mitochondrial fission complexes by Fis1. Proc Natl Acad Sci U S A *104*, 18526-18530.

Zhao, J., Lendahl, U., and Nister, M. (2012). Regulation of mitochondrial dynamics: convergences and divergences between yeast and vertebrates. Cell Mol Life Sci.

Zhao, J., Liu, T., Jin, S., Wang, X., Qu, M., Uhlen, P., Tomilin, N., Shupliakov, O., Lendahl, U., and Nister, M. (2011). Human MIEF1 recruits Drp1 to mitochondrial outer membranes and promotes mitochondrial fusion rather than fission. EMBO J *30*, 2762-2778.

CHAPTER 2

MOLECULAR ARCHITECTURE OF A DYNAMIN ADAPTOR: IMPLICATIONS FOR ASSEMBLY OF MITOCHONDRIAL FISSION COMPLEXES

Authors

Sajjan Koirala, Huyen T. Bui, Heidi L. Schubert, Debra Eckert, Christopher P. Hill, Michael S. Kay, Janet M. Shaw

Reproduced in this dissertation after obtaining copyright permission from the Rockefeller University Press.

©2010 Rockefeller University Press. Originally published in Journal of Cell Biology. Vol.191: No. 6: Pages 1127-1139: doi: 10.1083/jcb.201005046

Published December 13, 2010

JCB: Article

THE JOURNAL OF CELL BIOLOGY

Molecular architecture of a dynamin adaptor: implications for assembly of mitochondrial fission complexes

Sajjan Koirala, Huyen T. Bui, Heidi L. Schubert, Debra M. Eckert, Christopher P. Hill, Michael S. Kay, and Janet M. Shaw

Department of Biochemistry, University of Utah, Salt Lake City, UT 84112

Recruitment and assembly of some dynamin-related guanosine triphosphatases depends on adaptor proteins restricted to distinct cellular membranes. The yeast Mdv1 adaptor localizes to mitochondria by binding to the membrane protein Fis1. Subsequent Mdv1 binding to the mitochondrial dynamin Dnm1 stimulates Dnm1 assembly into spirals, which encircle and divide the mitochondrial compartment. In this study, we report that dimeric Mdv1 is joined at its center by a 92-Å antiparallel coiled coil (CC). Modeling of the Fis1–Mdv1 complex using available crystal structures suggests that the Mdv1 CC lies parallel to the bilayer with N termini at opposite ends bound to Fis1 and C-terminal β-propeller domains (Dnm1-binding sites) extending into the cytoplasm. A CC length of appropriate length and sequence is necessary for optimal Mdv1 interaction with Fis1 and Dnm1 and is important for proper Dnm1 assembly before membrane scission. Our results provide a framework for understanding how adaptors act as scaffolds to orient and stabilize the assembly of dynamins on membranes.

Introduction

In eukaryotes, mitochondrial fission regulates organelle copy number and mitochondrial function in metabolism, development, and programmed cell death (Chen and Chan, 2005; Okamoto and Shaw, 2005). Fission begins when a dynamin-related GTPase is recruited from the cytoplasm to the outer membrane, where it assembles into large polymers that hydrolyze GTP and sever the mitochondrial compartment. Protein–protein interactions between the GTPase and a membrane-anchored receptor are essential for the recruitment step and are also thought to provide a structural scaffold that promotes GTPase assembly.

The membrane receptor for yeast mitochondrial fission is a complex composed of two proteins, membrane-anchored Fis1 (Mozdy et al., 2000) and its binding partner, Mdv1 (Tieu and Nunnari, 2000; Cerveny et al., 2001; Tieu et al., 2002; Cerveny and Jensen, 2003). Mdv1 functions as an adaptor to bridge the interaction between Fis1 and the cytoplasmic Dnm1 GTPase. Binding of Dnm1 to Mdv1 nucleates the polymerization of Dnm1 dimers into spirals that encircle and constrict the membrane (Bleazard et al., 1999; Ingerman et al., 2005; Bhar et al., 2006; Lackner et al., 2009). Mdv1 coassembles with Dnm1 in these spirals to generate functional fission complexes (Shaw and Nunnari, 2002). Although fission complexes could, in principle, assemble uniformly on the mitochondrial surface, assembly usually occurs at discrete sites on tubular mitochondria in living cells.

The architectural features of the Mdv1–Fis1 receptor required for Dnm1 recruitment and assembly remain unclear. Structural analysis of the Fis1 cytoplasmic domain reveals a single tetratricopeptide repeat (TPR; Suzuki et al., 2005). The N terminus of Mdv1 contains a short, helix-loop-helix motif that surrounds and clamps the surface of the Fis1 TPR domain (Zhang and Chan, 2007). The C terminus of Mdv1, which is required for Dnm1 binding, is predicted to form a multibladed β-propeller. The N- and C-terminal domains are linked by a predicted heptad repeat (HR). Because Mdv1 acts both to recruit Dnm1 and nucleate Dnm1 assembly, defining the structure,

Correspondence to Michael S. Kay: kay@biochem.utah.edu; or Janet M. Shaw: shaw@biochem.utah.edu

Abbreviations used in this paper: CC, coiled coil; CD, circular dichroism; DIC, differential interference contrast; ES, equilibrium sedimentation; HR, heptad repeat; IP, immunoprecipitation; MBP, maltose-binding protein; NTE, N-terminal extension; TPR, tetratricopeptide repeat; WCE, whole cell extract; WT, wild type.

© 2010 Koirala et al. This article is distributed under the terms of an Attribution–Noncommercial–Share Alike–No Mirror Sites license for the first six months after the publication date (see http://www.rupress.org/terms). After six months it is available under a Creative Commons License (Attribution–Noncommercial–Share Alike 3.0 Unported license, as described at http://creativecommons.org/licenses/by-nc-sa/3.0/).

Supplemental Material can be found at: http://jcb.rupress.org/content/suppl/2010/12/10/jcb.201005046.DC1.html

The Rockefeller University Press $30.00
J. Cell Biol. Vol. 191 No. 6 1127–1139
www.jcb.org/cgi/doi/10.1083/jcb.201005046

Published December 13, 2010

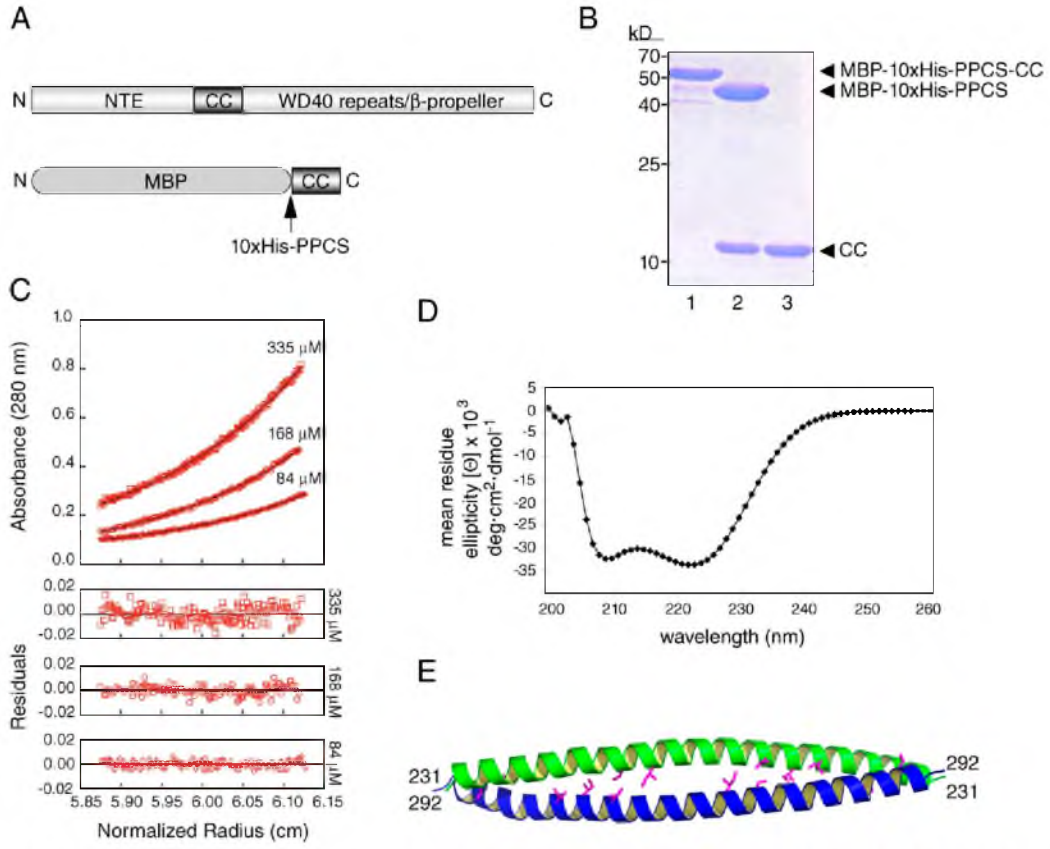

Figure 1. **Mdv1 self-assembles via a dimeric, antiparallel CC.** (A, top) Domain structure of Mdv1, including the NTE, predicted CC, and WD repeats predicted to form a β-propeller. (bottom) The construct used for purification of the Mdv1 CC domain includes the MBP fused to 10xHis, the PreScission protease cleavage site (PPCS), and Mdv1 residues 231–299 (CC; MBP-10xHis-PPCS-CC). (B) SDS-PAGE analysis of purified MBP-10xHis-PPCS-CC fusion protein stained with Coomassie brilliant blue (lane 1), PreScission protease–cleaved MBP-10xHis-PPCS + CC (lane 2), and purified CC (lane 3). (C) Sedimentation equilibrium profile of the Mdv1 CC fragment at the indicated initial loading concentrations (open symbols) with the corresponding fit of 16,263 D ($MW_{obs}/MW_{monomer}$ = 1.95). Residuals for the nonlinear least-squared fits are shown below. (D) CD wavelength scan of $CC^{231–299}$ dimer. (E) Crystal structure of $CC^{231–292}$ dimer at a 2.6-Å resolution. Hydrophobic side chains of residues L233, L237, I251, I254, L268, I272, and I275 are shown in magenta.

oligomeric state, and orientation of this domain is important to understand how Mdv1 initially interacts with the Dnm1 dimer and how this interaction positions the Dnm1 dimer for further polymerization.

In this study, we present the structure of the Mdv1 HR, which forms an unusually long (92 Å) antiparallel coiled coil (CC). We also provide a structural model of dimeric Mdv1 bound to two uncomplexed Fis1 molecules anchored at the mitochondrial membrane. This model shows how the CC positions the two β-propeller domains of Mdv1 to interact with Dnm1 as it transitions from the cytoplasm to mitochondria. In vivo experiments indicate that formation of the Mdv1 antiparallel CC and CC length are important for Fis1 binding, Dnm1 recruitment and assembly, coassembly of Mdv1 into the fission complex, and mitochondrial fission. Surprisingly, restoring Mdv1 oligomerization using a heterologous antiparallel CC rescues Dnm1, but not Fis1, interactions. Thus, the sequence of the Mdv1 CC plays an important but unanticipated role in Mdv1–Fis1 binding. Using a substitution exposed at the surface of the CC, we show that the CC sequence can function to stabilize the Mdv1–Fis1 complex. The combined data reveal new insights into the formation of functional mitochondrial fission complexes.

Results

Structure of the Mdv1 CC

The Mdv1 sequence was analyzed using the MultiCoil CC prediction program (Wolf et al., 1997). The ends (231–299) for the expression construct were chosen based on the total probability score (P > 0.2). Mdv1 $CC^{231–299}$ was expressed as a maltose-binding protein (MBP) fusion protein in *Escherichia coli*, released by proteolytic cleavage, and purified to homogeneity (see Materials and methods; Fig. 1, A and B). Equilibrium sedimentation (ES) centrifugation (Fig. 1 C) and circular dichroism (CD) analyses (Fig. 1 D) indicated that Mdv1 $CC^{231–299}$ is a dimer exhibiting double minima typical of a strong α-helix.

Published December 13, 2010

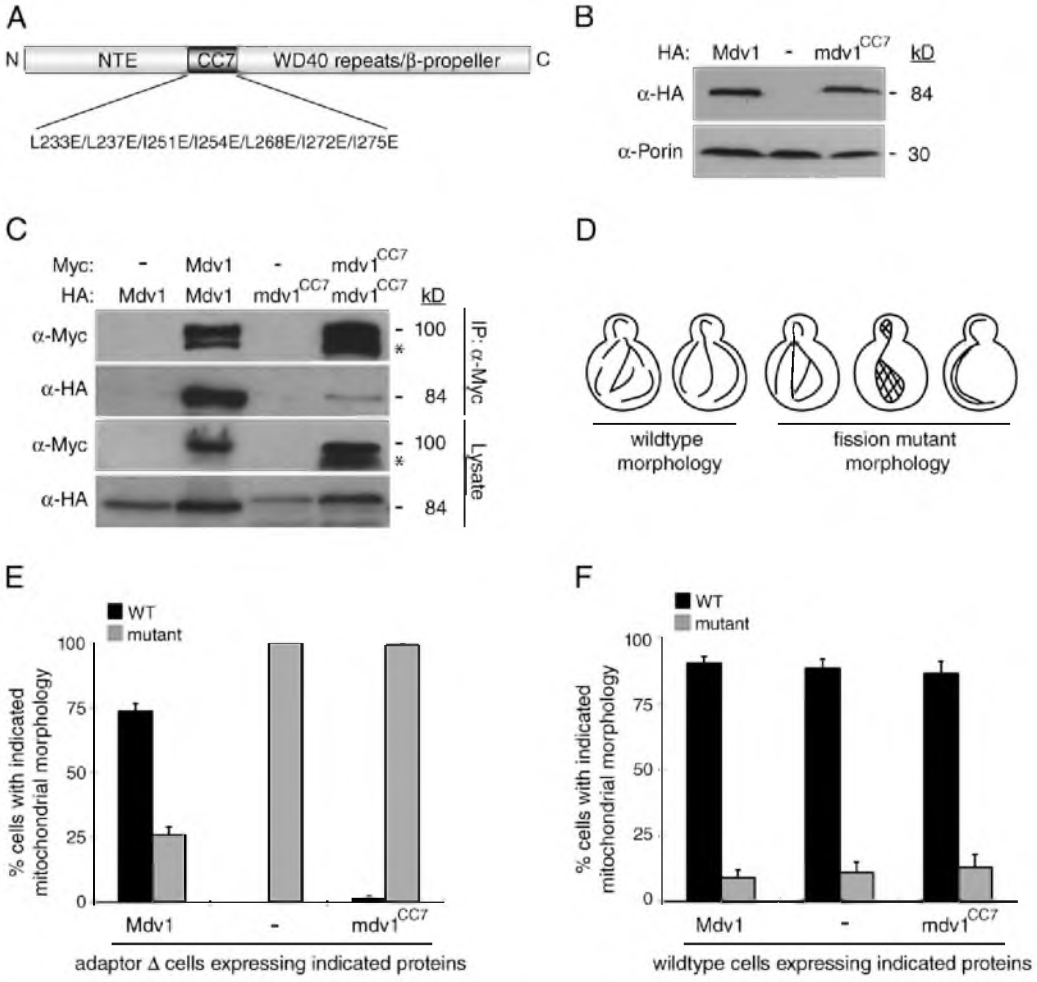

Figure 2. **Disruption of Mdv1 CC formation blocks mitochondrial fission.** (A) Schematic of the mdv1^{CC7} mutant protein. Substitutions introduced at a and d positions in the CC to generate the mdv1^{CC7} mutant protein are listed below the diagram. (B) Steady-state abundance of C-terminal HA-tagged Mdv1 and mdv1^{CC7} mutant proteins expressed in adaptor Δ cells. The mdv1^{CC7} protein sometimes migrates at a higher molecular mass than WT Mdv1 (Figs. 3 A, 4 A, and 6). WCEs separated by SDS-PAGE were immunoblotted with anti-HA and anti-porin antibodies. (C) Lysates from cells expressing the indicated C-terminal Myc- and HA-tagged Mdv1 proteins were used for IP with anti-Myc agarose beads. Lysates (bottom) and immunoprecipitated fractions (top) were analyzed by SDS-PAGE and Western blotting with anti-Myc and anti-HA antibodies. Asterisks mark protein breakdown products. (D) Cartoons depicting mitochondrial morphologies scored in quantification experiments as WT or fission mutant. (E and F) Quantification of mitochondrial morphologies in adaptor Δ (E) or WT (F) cells expressing Mdv1 and mdv1^{CC7} mutant proteins. Black and gray bars and error bars represent the mean and standard deviation of at least three independent experiments ($n = 100$).

The crystal structure of a selenomethionine-substituted Mdv1 CC$^{231–291}$ construct (L248M and L281M; 2.6 Å; Fig. 1 E and Table S2) revealed that residues 231–292 of this polypeptide fold into a single, 92-Å helix that forms an antiparallel homodimer. This structure is unusual, as intermolecular homodimeric CCs are predominantly parallel. To our knowledge, the structure of only one other homodimeric antiparallel CC of this length (>90 Å) has been reported, also in a protein required for mitochondrial membrane dynamics (Mfn1 HR2, 95 Å; Koshiba et al., 2004). The electrostatic surface of the structure is not highly positive (unpublished data), suggesting that Mdv1 CC$^{231–292}$ does not associate directly with negatively charged lipids exposed at the cytoplasmic face of the outer mitochondrial membrane.

The Mdv1 CC is essential for mitochondrial fission

To determine whether the antiparallel CC interaction in Mdv1 was required for mitochondrial fission, we changed isoleucine and leucine residues contributing to formation of the hydrophobic interface in this structure to glutamate in the full-length protein (Figs. 1 E and 2 A, magenta side chains). Consistent with

Published December 13, 2010

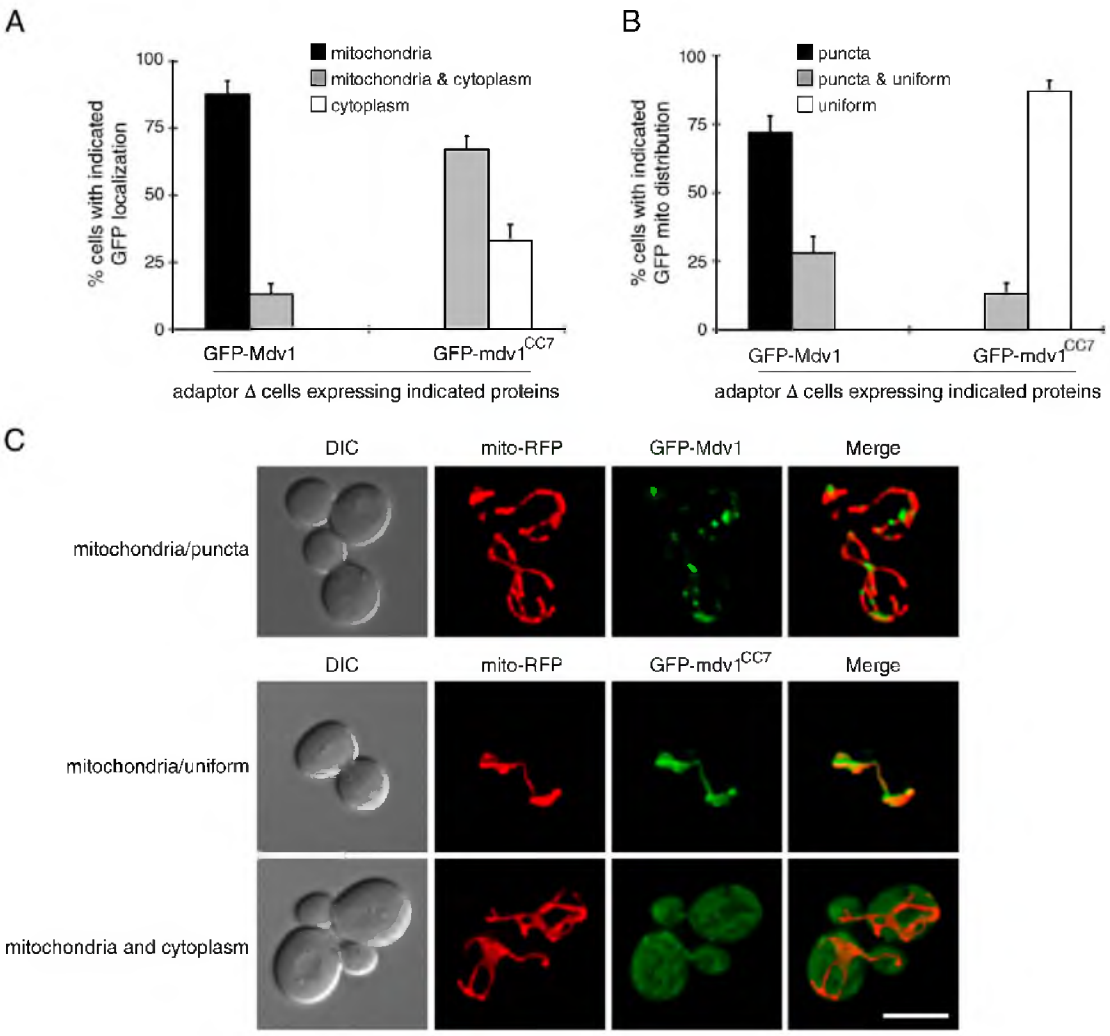

Figure 3. **CC formation promotes mitochondrial recruitment and assembly of the Mdv1 fission adaptor.** (A) Subcellular localization of N-terminal GFP-tagged Mdv1 and mdv1^{CC7} proteins imaged in adaptor Δ cells. (B) Mitochondrial distribution of GFP-tagged Mdv1 and mdv1^{CC7} proteins imaged in adaptor Δ cells. Bars and error bars represent the mean and standard deviation of at least three independent experiments (n = 100). (C) Representative images of GFP-Mdv1 and GFP-mdv1^{CC7} localization and distribution quantified in A and B. DIC, mitochondrial matrix–targeted dsRed (mito-RFP), and merged RFP and GFP images are shown. Bar, 5 µm.

the extended length of this CC, glutamate substitution of all seven isoleucine and leucine residues depicted in Fig. 2 A was necessary to disrupt Mdv1 function (unpublished data). Western blotting of yeast whole cell extracts (WCEs) indicated that the abundance of the mutant adaptor protein, hereafter referred to as mdv1^{CC7}, was similar to that of wild-type (WT) Mdv1 (Figs. 2 B and S4 A). However, these mutations nearly abolished the ability of mdv1^{CC7} to self-interact in coimmunoprecipitation (co-IP) experiments (Fig. 2 C).

We tested the ability of mdv1^{CC7} to support mitochondrial fission in adaptor-null (adaptor Δ) yeast cells lacking Mdv1 and its paralogue Caf4 (Griffin et al., 2005). Although Mdv1 is required for the majority of mitochondrial fission that occurs in vivo, deletion of both Mdv1 and Caf4 is necessary to completely abolish fission. The adaptor Δ strain exhibits severe fission defects, including interconnected, netlike, or collapsed mitochondrial tubules (Fig. 2, D and E). Although expression of Mdv1 restored WT morphology in ~75% of the population, expression of mdv1^{CC7} failed to rescue fission defects (Fig. 2, D and E). Thus, dimerization of Mdv1 via its antiparallel CC plays a critical role in mitochondrial fission. When expressed from the uninduced *MET25* promoter, steady-state abundance of Mdv1 is fourfold higher than that of Mdv1 expressed from its native promoter (Karren et al., 2005; unpublished data). Although expressing

Published December 13, 2010

fourfold higher levels of mdv1^{CC7} protein did not cause dominant fission defects in WT cells (Fig. 2 F), dominant-negative fission phenotypes began to appear when expression was further elevated by a 4-h induction of the *MET25* promoter (Fig. S4 C, ~16-fold overexpression). This dominant-negative effect suggests that mdv1^{CC7} continues to interact with one or more of its other two binding partners, effectively interfering with the WT fission machinery.

CC formation promotes mitochondrial recruitment and assembly of the Mdv1 fission adaptor

We used the mdv1^{CC7} mutant protein to test the importance of Mdv1 CC formation for its membrane recruitment. Experiments in intact cells expressing GFP-mdv1^{CC7} revealed that the localization of the mutant protein was compromised relative to WT. In control experiments, the majority of WT GFP-Mdv1 colocalized with RFP-labeled mitochondrial tubules (Fig. 3, A and C, top), whereas a small fraction of cells also displayed dual localization to mitochondria and the cytoplasm (Fig. 3 A). In contrast, GFP-mdv1^{CC7} did not localize exclusively with mitochondria. Instead, yeast cells expressing GFP-mdv1^{CC7} exhibited dual mitochondrial and cytoplasmic localization or exclusively cytoplasmic localization of the adaptor protein (Fig. 3, A and C, bottom). Western blotting indicated that this cytoplasmic localization was not caused by proteolysis and release of GFP from the N terminus of the fusion protein (unpublished data).

After membrane recruitment, localization of a subpopulation of Mdv1 appears punctate because of its coassembly with the Dnm1 GTPase into fission complexes (Tieu and Nunnari, 2000; Cerveny et al., 2001; Griffin et al., 2005; Karren et al., 2005; Naylor et al., 2006). Although mitochondrial localized GFP-Mdv1 was largely punctate (Fig. 3 B), GFP-mdv1^{CC7} failed to coassemble into punctate fission complexes and uniformly labeled mitochondrial membranes in the majority of cells (Fig. 3, B and C, middle). This uniform mitochondrial labeling resulted from association of Mdv1 with Fis1 and was abolished in cells lacking Fis1 (mdv1^{CC7} had no effect on Fis1 localization; unpublished data). These combined data indicate that CC formation promotes both Mdv1 recruitment to Fis1 on mitochondria and subsequent higher order assembly of Mdv1 into fission complexes.

Mitochondrial recruitment and self-assembly of the Dnm1 GTPase requires Mdv1 CC formation

The Dnm1 GTPase interacts with the C terminus of Mdv1 (Tieu et al., 2002; Cerveny and Jensen, 2003), which is predicted to form a multibladed β-propeller. This interaction promotes the self-assembly of Dnm1 into rings and spirals (Lackner et al., 2009) that are visualized as mitochondrial puncta (fission complexes) when labeled with a fluorescent marker (Otsuga et al., 1998). We tested whether Mdv1 dimerization in vivo was required for Mdv1–Dnm1 interaction and Dnm1 assembly into mitochondrial puncta. Although HA-tagged Mdv1 efficiently coprecipitated Dnm1 from cell lysates, complex formation between mdv1^{CC7}-HA and Dnm1 was significantly reduced (Fig. 4 A). This reduced interaction was also apparent in vivo. Although GFP-Dnm1 efficiently assembled into puncta on mitochondria when cells expressed WT Mdv1 (Fig. 4, B and C, top), the fraction of cytoplasmic GFP-Dnm1 increased in cells expressing mdv1^{CC7} (Fig. 4, B and C, bottom). Residual GFP-Dnm1 puncta on mitochondria in mdv1^{CC7}–expressing cells were often smaller and less-evenly distributed on the organelle tubules (Fig. 4 C, middle). This may be caused in part by the fact that mdv1^{CC7} uniformly labels mitochondrial membranes (RFP-mdv1^{CC7}; Fig. 4 D) but does not efficiently coassemble into puncta with Dnm1 (Fig. 3 C, middle and bottom). When combined with our finding that GFP-mdv1^{CC7} fails to form mitochondrial puncta and cannot support fission (Fig. 2 E; and Fig. 3 C, middle and bottom), these results provide a direct demonstration that dimeric Mdv1 must coassemble with the Dnm1 GTPase to form functional fission complexes.

Mdv1 dimerization via a heterologous antiparallel CC partially restores adaptor function

To determine whether physical CC formation was sufficient for adaptor function, we generated a chimeric protein, which replaced the Mdv1 CC with residues 674–734 of the mammalian mitofusin protein Mfn1 (mdv1^{HR2}; Fig. 5 A). In crystallographic experiments, this Mfn1 domain forms an antiparallel CC similar in length to the Mdv1 CC (95 Å; Koshiba et al., 2004). As observed for WT Mdv1, the mdv1^{HR2} chimera was stably expressed (Figs. 5 B and S4 A), localized with mitochondria in differential fractionation and fluorescence microscopy experiments (Figs. 5 C and S1 A), and was able to self-interact in co-IP experiments (Fig. 5 D). Unlike WT Mdv1, mdv1^{HR2} only partially rescued mitochondrial fission and morphology defects in the adaptor Δ strain (Figs. 5 E and S1 B). This partial rescue could not be attributed to defects in mdv1^{HR2}–Dnm1 interactions because mdv1^{HR2}-HA coimmunoprecipitated Dnm1 and the WT adaptor (Fig. 5 F), formed mitochondrial puncta in vivo when labeled with GFP (Fig. S1 C), and also promoted assembly of GFP-Dnm1 into punctate mitochondrial fission complexes (Fig. S1 D). These results were surprising because they suggested that dimerization of Mdv1 via an antiparallel CC is important but not sufficient for the adaptor's function in mitochondrial fission. Instead, the sequence of the Mdv1 CC may also contribute to adaptor function.

The sequence of the Mdv1 CC is critical for interaction with Fis1

We noticed that the mitochondrial localization of mdv1^{HR2} decreased relative to Mdv1 when Dnm1 was absent (Fig. S1 E). Under these conditions, stable mitochondrial association of mdv1^{HR2} depends entirely upon interactions with Fis1. Thus, the inability of mdv1^{HR2} to fully rescue fission defects in vivo could result from a reduced Fis1 interaction. It has been unclear whether the Mdv1 CC is necessary for interaction with Fis1. A crystal structure showed that α-helices in the N-terminal extension (NTE) of fission adaptor proteins bind directly to the cytoplasmic tetratricopeptide domain of Fis1 (Zhang and Chan, 2007). Mutations predicted to disrupt contact sites in this complex interfered with Mdv1–Fis1 interactions and reduced fission in vivo.

Published December 13, 2010

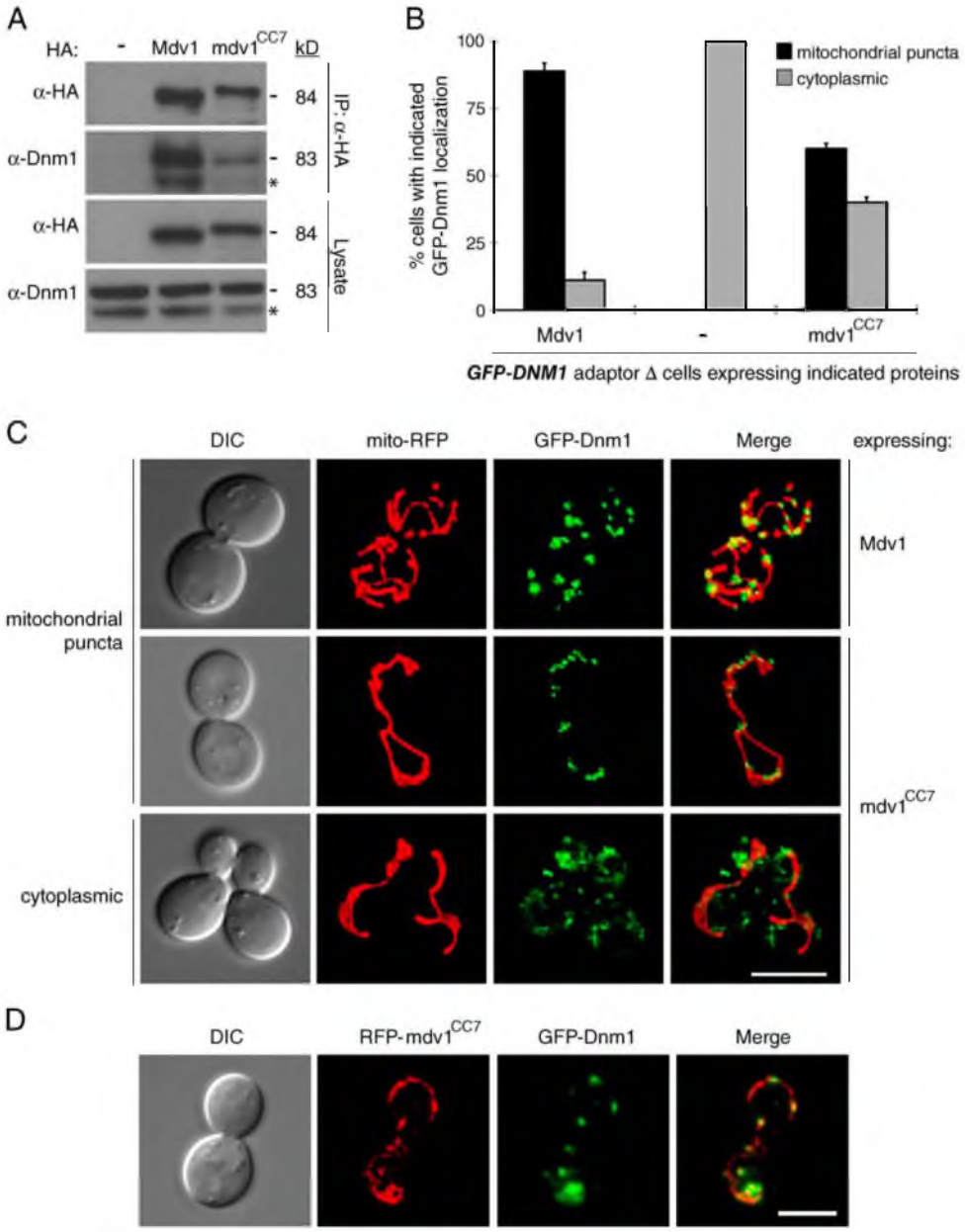

Figure 4. **Efficient Dnm1–Mdv1 interaction and Dnm1 assembly into functional mitochondrial fission complexes requires Mdv1 CC formation.** (A) Lysates from cells expressing the indicated C-terminal HA-tagged Mdv1 proteins were used for IP with anti-HA agarose beads. Lysate (bottom) and immunoprecipitated fractions (top) were analyzed by SDS-PAGE and Western blotting with anti-HA and anti-Dnm1 antibodies. Asterisks mark protein breakdown products. (B) Localization of genomically expressed GFP-Dnm1 in cells expressing Mdv1 or mdv1^{CC7}. Bars and error bars represent the mean and standard deviation of at least three independent experiments ($n = 100$). (C) Representative images of GFP-Dnm1 localization quantified in B. DIC, mitochondrial matrix–targeted RFP (mito-RFP), GFP-Dnm1, and merged RFP and GFP images are shown. (D) Colocalization of RFP-mdv^{CC7} and GFP-Dnm1. DIC and merged RFP with GFP images are shown. Bars, 5 µm.

However, genetic suppressor experiments from our laboratory suggested that the Mdv1 CC also contributes to the Mdv1–Fis1 interaction. We previously screened for suppressors of a Fis1 protein–destabilizing mutation (*fis1-3*; Karren et al., 2005). *fis1-3* contains E78D, I85T, and Y88H substitutions in the concave surface of the Fis1 TPR domain that destabilize the protein at an

Published December 13, 2010

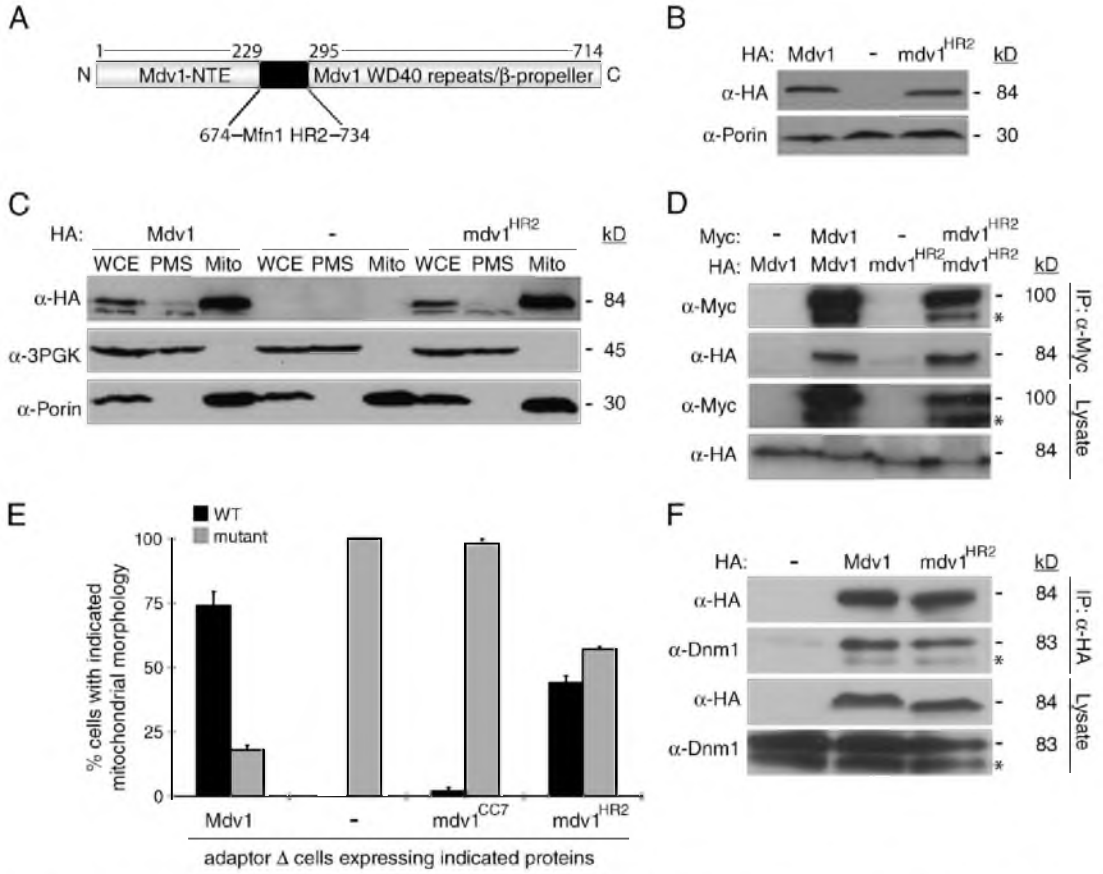

Figure 5. **Dimerization via a heterologous antiparallel CC partially restores Mdv1 adaptor function.** (A) Schematic representation of the mdv1^{HR2} chimera. Residues 230–294 encompassing the Mdv1 antiparallel CC are replaced by residues 674–734 of the Mfn1 HR2 domain. (B) Steady-state abundance of C-terminal HA-tagged Mdv1 and mdv1^{HR2} mutant proteins expressed in fission adaptor Δ cells. WCEs separated by SDS-PAGE were immunoblotted with anti-HA and anti-porin antibodies. (C) Differential sedimentation and Western blot analysis of cytoplasmic 3PGK, mitochondrial porin, and HA-tagged Mdv1 and mdv1^{HR2} proteins in WCE, postmitochondrial supernatant (PMS), and mitochondrial (Mito) fractions. (D) Lysates from cells expressing the indicated C-terminal Myc- and HA-tagged Mdv1 and mdv1^{HR2} proteins were used for IP with anti-Myc agarose beads. Lysate (bottom) and immunoprecipitated fractions (top) were analyzed by SDS-PAGE and Western blotting with anti-HA and anti-Myc antibodies. (E) Quantification of mitochondrial morphologies in adaptor Δ cells expressing Mdv1, mdv1^{CC7} mutant, or mdv1^{HR2} chimeric proteins. Bars and error bars represent the mean and standard deviation of at least three independent experiments (n = 100). (F) Lysates from cells expressing HA-tagged Mdv1 or mdv1^{HR2} were used for IP with anti-HA agarose beads. Lysates (bottom) and immunoprecipitated fractions (top) were analyzed by SDS-PAGE and Western blotting with anti-HA and anti-Dnm1 antibodies. Asterisks mark protein breakdown products.

elevated temperature (37°C). We identified an E250G substitution in the Mdv1 CC domain (at position g in the HR; Fig. S2) that stabilized Mdv1–Fis1 complex formation and restored mitochondrial fission at 37°C in the *fis1-3* strain. These findings strongly suggest that the CC sequence is important for Mdv1–Fis1 interaction. To test this idea, we examined the ability of mdv1^{HR2} to interact with Fis1. As shown in Fig. 6, Myc-tagged Fis1 efficiently coprecipitated HA-tagged Mdv1 from cell lysates, whereas coprecipitation of the CC defective mdv1^{CC7}-HA protein was reduced. Significantly, coprecipitation of mdv1^{HR2}-HA with Myc-Fis1 was also reduced despite the fact that this chimeric adaptor protein can self-interact via the heterologous Mfn1 HR2 domain. Quantification of these Fis1–Mdv1 coIP interactions confirmed that Fis1 complex formation with mdv1^{CC7} and mdv1^{HR2} proteins are reduced, whereas Fis1 interaction with the mdv1^{E250G} suppressor is enhanced relative to WT (Fig. 6 B). The straightforward interpretation of these results is that the sequence of the Mdv1 CC (and not just its dimerization capability) is critical for Mdv1 binding to Fis1 during early steps in fission complex assembly.

The length of the Mdv1 CC is optimized for mitochondrial fission

To test the influence of CC length on Mdv1 function, we generated variants lacking two (mdv1$^{\Delta 2HR}$) or four (mdv1$^{\Delta 4HR}$) HRs of the native Mdv1 CC (Fig. 7 A). Both ΔHR proteins were stably expressed at similar steady-state abundance, continued to self-interact, localized to mitochondria in a Fis1-dependent manner,

Published December 13, 2010

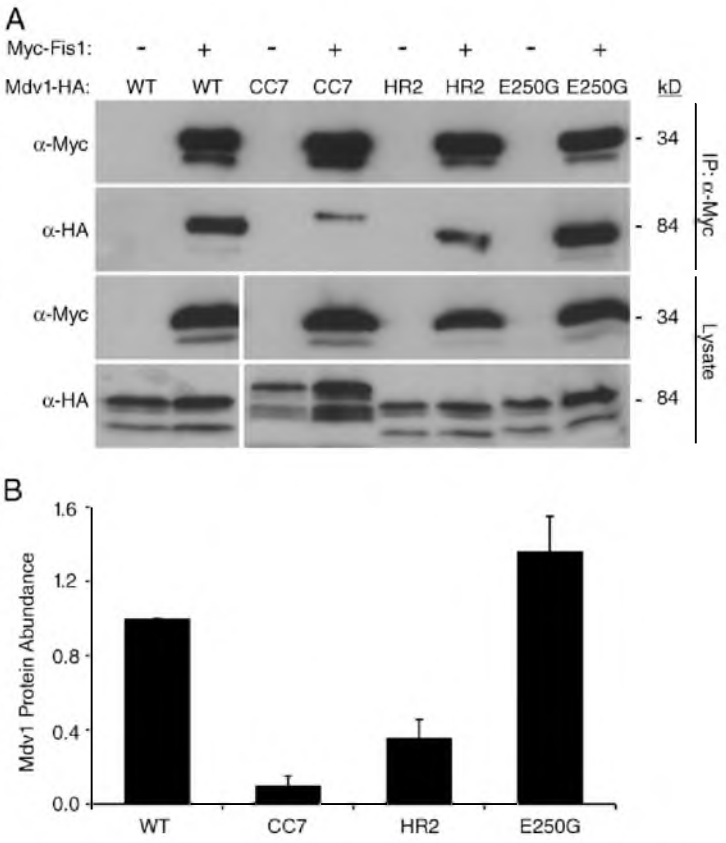

Figure 6. **The Mdv1 CC sequence contributes to efficient Fis1 binding.** (A) Lysates from cells expressing the indicated Mdv1-HA variants and Myc-Fis1 were used for coIP with anti-Myc agarose beads. Lysate (bottom) and IP fractions (top) were analyzed by SDS-PAGE and ECL Western blotting with anti-HA and anti-Myc antibodies. Lower molecular mass bands in all lanes are protein breakdown products. (B) Quantification of coIPs shown in A. Myc- and HA-tagged proteins were detected using a fluorescent secondary antibody followed by scanning on an imaging system. The mean intensity of each Mdv1-HA protein band was normalized to the Myc-Fis1 signal in the same coIP. Bars represent the abundance of Mdv1-HA signal in each coIP relative to the WT. Error bars represent the mean and standard deviation from three independent experiments.

and promoted Dnm1 assembly into mitochondrial fission complexes in vivo (Fig. S3, A, B, and D; Fig. S4, A and B; and not depicted). However, the ΔHR Mdv1 variants did not form mitochondrial puncta as efficiently as WT Mdv1 and exhibited increased uniform labeling of mitochondrial tubules (Fig. S3 C). Moreover, neither ΔHR protein rescued fission defects in the adaptor Δ strain and WT (Fig. 7 B). Thus, the ΔHR Mdv1 variants have a reduced ability to assemble and function in fission. Like the mdv1^{CC7} mutant, the ΔHR variants continued to interact with binding partners in vivo and caused dominant-negative fission defects when overexpressed in a WT strain (Fig. S4 C and not depicted). The dominant-negative defects induced by the ΔHR variants were more severe than those caused by overexpression of mdv1^{CC7} or WT Mdv1, indicating that they have greater ability to interfere with the WT fission machinery in vivo.

We also compared the ability of the ΔHR and E250G Mdv1 variants to restore mitochondrial fission at 25°C and 37°C in cells harboring the *fis1-3* allele. In the *fis1-3 mdv1Δ* strain grown at an elevated temperature, mitochondrial fission is rescued by expression of Mdv1^{E250G} but not WT Mdv1 (Fig. 7 C). The mdv1$^{\Delta 2HR}$ and mdv1$^{\Delta 4HR}$ proteins rescued mitochondrial fission defects at 37°C but less efficiently than Mdv1^{E250G}. In addition, neither mdv1$^{\Delta 2HR}$ nor mdv1$^{\Delta 4HR}$ rescued fission defects and WT or Mdv1^{E250G} at the permissive temperature (25°C).

As with mdv1^{HR2}, we observed that mitochondrial localization of mdv1$^{\Delta 2HR}$ and mdv1$^{\Delta 4HR}$ decreased relative to WT Mdv1 in cells lacking Dnm1 (unpublished data). Because Mdv1 mitochondrial localization in *dnm1Δ* is Fis1 dependent, it is likely that shortening the native Mdv1 CC domain compromises the Fis1–Mdv1 interaction. Based on these combined results, we conclude that the overall length of the native CC is optimized for Mdv1 adaptor function in mitochondrial fission complex assembly and fission.

Discussion

Mdv1 is essential for the membrane recruitment and assembly of the mitochondrial dynamin Dnm1. By combining the new structure of the Mdv1 CC domain with a previously reported Fis1–Mdv1 NTE structure (Zhang and Chan, 2007), we provide a working model for the architecture of the Fis1–Mdv1 complex on the membrane. As depicted in Fig. 8, formation of a 92-Å antiparallel CC between two Mdv1 polypeptides forms an extended dimer. The NTE of each Mdv1 subunit is bound to distinct Fis1 TPR-like domains exposed at the cytoplasmic face of the mitochondrial membrane. Cryo-EM structures suggest that dimeric Dnm1 is the basic subunit for assembly of Dnm1 spirals (Hinshaw, J., personal communication), and two-hybrid

Published December 13, 2010

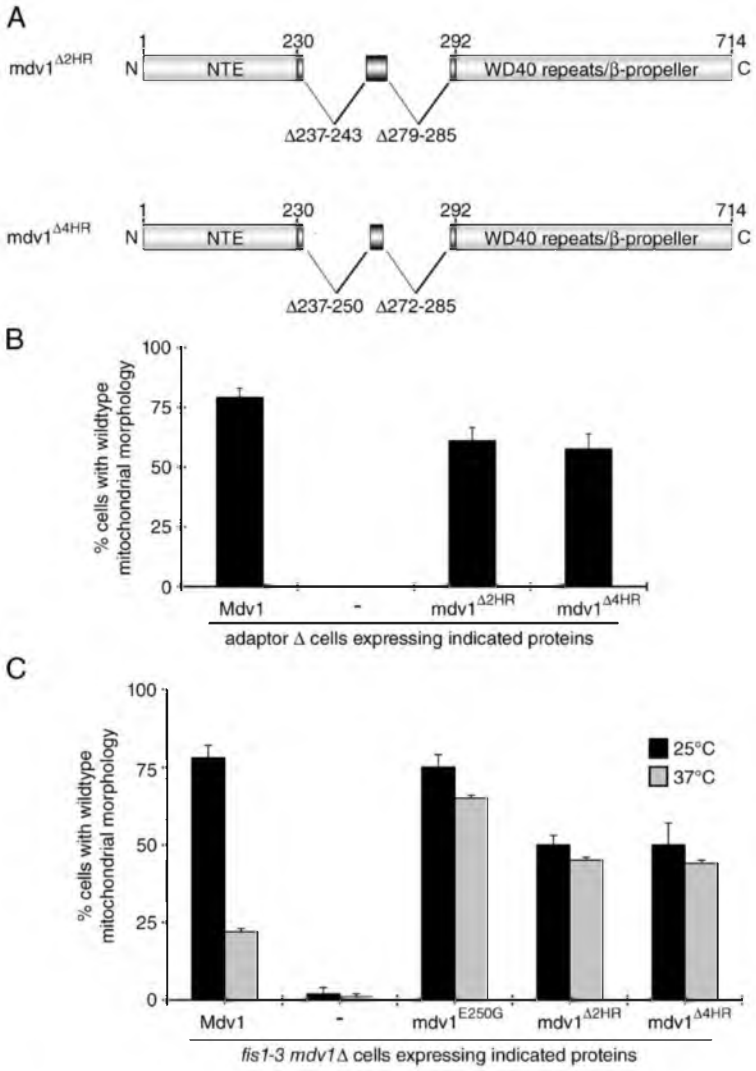

Figure 7. **Effect of CC shortening on Mdv1 function.** (A) Schematic of the mdv1$^{\Delta 2HR}$ and mdv1$^{\Delta 4HR}$ proteins. Residues corresponding to HR deletions are shown below each diagram. (B) Quantification of mitochondrial morphologies in adaptor Δ cells expressing Mdv1, mdv1$^{\Delta 2HR}$, and mdv1$^{\Delta 4HR}$ proteins. (C) Quantification of mitochondrial morphologies at 25 and 37°C in *fis1-3 mdv1Δ* cells expressing WT and mutant Mdv1 proteins. Black and gray bars and error bars represent the mean and standard deviation of at least three independent experiments ($n = 100$).

and co-IP analyses indicate that the predicted Mdv1 β-propeller domain is sufficient for Dnm1 interaction (Tieu et al., 2002; Cerveny and Jensen, 2003). Thus, Mdv1 β-propeller domains at each end of the CC would provide interaction sites for dimeric Dnm1 recruited from the cytoplasm. Dnm1 dimer binding could occur at the periphery or on the lateral face of one or multiple Mdv1 β-propeller domains. Alternatively, each Mdv1 dimer could bind a single Dnm1 dimer, as suggested by the ~1:1 Mdv1–Dnm1 stoichiometry of complexes assembled in vitro (Lackner et al., 2009). Previous studies identified residues in the Mdv1 β-propeller important for Dnm1 interaction (Cerveny and Jensen, 2003; Naylor et al., 2006); however, it is not known whether these residues make direct contact with Dnm1. Identification of such contact sites and/or structures of protein complexes will be necessary to model Mdv1–Dnm1 binding and determine how this interaction positions Dnm1 dimers to facilitate assembly into spirals. Although the overall length of the native Mdv1 CC is optimized for fission complex assembly and function, our experiments of the ΔHR mdv1 variants indicate that maintaining the length of this CC is not essential for Mdv1 function.

In addition to providing structural stability, Mdv1 dimerization via the CC is critical for the accurate assembly of functional Dnm1 fission complexes. The fraction of monomeric mdv1^{CC7} protein that localizes to mitochondria is sometimes sufficient to recruit and promote the assembly of Dnm1 puncta that resemble fission complexes (Fig. 4 C). However, the morphology of these structures is often qualitatively different from those observed in WT cells, as is their distribution along the mitochondrial tubule. Unlike WT Mdv1, which coassembles with Dnm1 during formation of a functional fission complex,

Published December 13, 2010

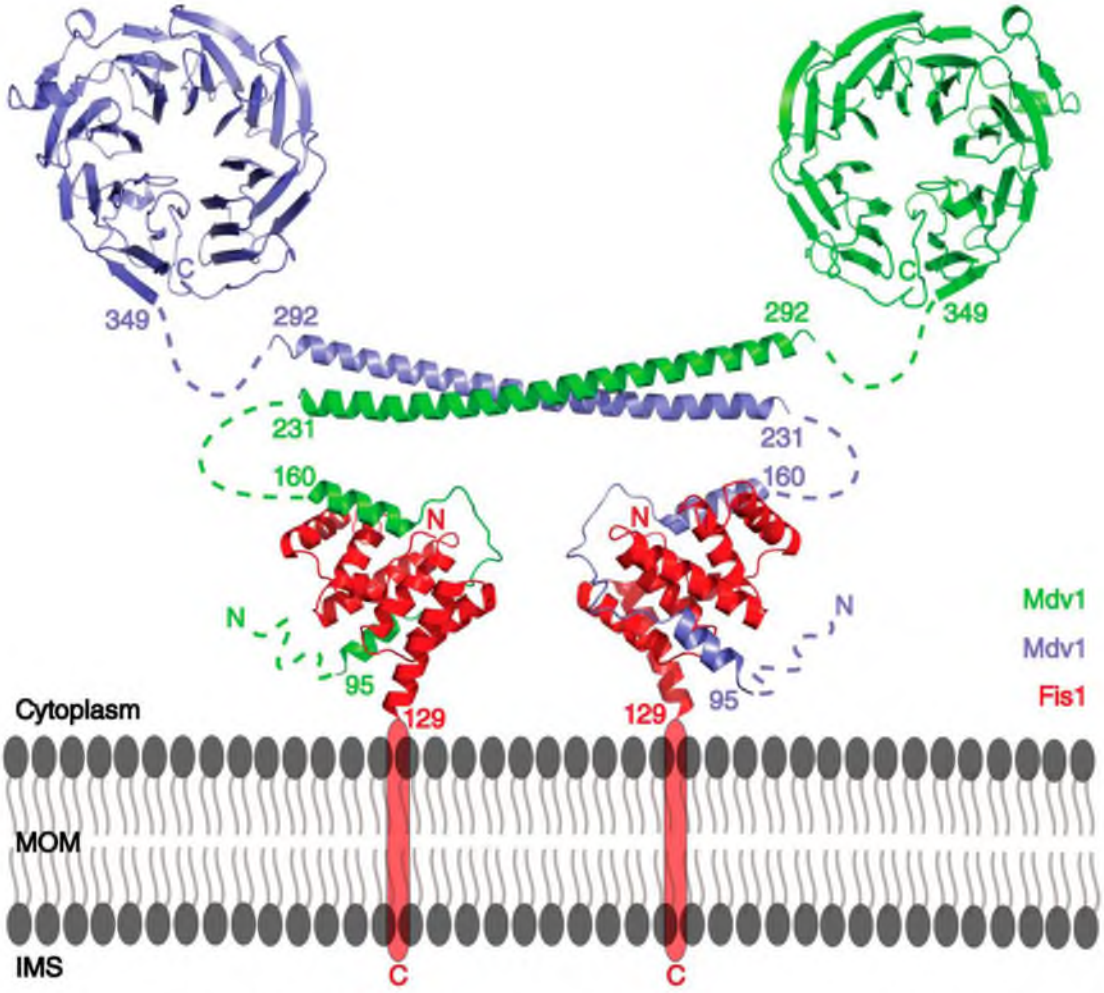

Figure 8. **Molecular architecture of the mitochondrial dynamin-related receptor.** A structural model of the Mdv1 dimer (green/purple) bound to two Fis1 cytoplasmic domains (red) anchored in the outer mitochondrial membrane (gray). The model was generated from crystal structures of the Fis1 cytoplasmic domain in complex with a fission adaptor NTE (Protein Data Bank [PDB] accession no. 2PQR) and the Mdv1 antiparallel CC (PDB accession no. 2XU6). The C-terminal WD40 domain of Mdv1 is shown as a homology model based on the known structure of the Cdc4 WD40 repeat (PDB 1NEX). Loops of variable length and unknown structure connect these two regions to the central CC dimer.

mdv1^{CC7} fails to assemble and form visible puncta in vivo (Fig. 4 D). This last observation is consistent with the idea that a scaffolding function of dimeric Mdv1 is necessary for its inclusion in the Dnm1 polymer as it assembles. The scaffolding model is also supported by our finding that restoring Mdv1 dimerization using a heterologous antiparallel CC rescues mdv1^{HR2} oligomerization and mitochondrial fission defects.

Surprisingly, the rescue provided by mdv1^{HR2} was incomplete, owing to a reduction in the interaction of the chimeric protein with Fis1 (Fig. 6). This result complements our previous finding that an E250G CC substitution stabilizes complex formation between Mdv1 and both WT and mutant Fis1 proteins (Karren et al., 2005). Glu250 lies at heptad position g in the native CC (Fig. S2) and likely participates in an electrostatic interaction that stabilizes a protein–protein interface. In additional experiments, we have shown that mdv1^{E250G} and mdv1^{E250A} substitutions suppress fission defects caused by a mutant Fis1 protein equally well (unpublished data). The E to G substitution is predicted to increase helix flexibility in addition to disrupting a side chain interaction. The E to A substitution should not increase helix flexibility but could also disrupt a side chain interaction. The simplest explanation for these combined findings is that Mdv1 Glu250 negatively regulates Fis1 binding via an Mdv1 self-interaction or interaction with another protein. According to this scenario, both the E to G and E to A substitutions would disrupt this interaction, generating a form of Mdv1 that is constitutively available for partner binding. Because the exact nature of this interaction remains to be determined, it is

Published December 13, 2010

not depicted in Fig. 8. A simple binding interface between Fis1 and Mdv1 seems unlikely, as the purified Fis1 cytoplasmic domain is not able to bind the purified Mdv1 CC in vitro (unpublished data).

Fis1–Mdv1 is the only membrane-anchored receptor complex known to function with a dynamin-related GTPase in a membrane fission event. Our experiments provide the first structural model for the presentation of binding sites recognized by the Dnm1 GTPase as it transitions from the cytoplasm to the mitochondrial outer membrane. Although the Fis1–Mdv1 complex is uniformly distributed on the membrane, assembly of Dnm1 and Mdv1 into fission complexes is restricted to discrete sites along the length of the mitochondrial tubule. Thus, post-translational modifications and/or induced conformation changes in the Fis1–Mdv1 complex seem essential to regulate Dnm1 access to the Mdv1 β-propellers. Alternatively, additional factors may act in vivo to stabilize Dnm1 assembly at specific locations and limit its propagation laterally on the membrane. Our results provide a framework for understanding how adaptors act as scaffolds to orient and stabilize the assembly of dynamins on membranes.

Materials and methods

Protein production

Mdv1 residues 231–299 (Mdv1-CC) were fused to the C terminus of MBP via a linker containing 10xHis and the PreScission protease cleavage site (MBP-10xHis-PPCS-CC$^{231–299}$). This construct was expressed in BL21(DE3) codon$^+$ (RIPL; Agilent Technologies) *E. coli* grown in autoinduction medium (Studier, 2005). Overnight cultures, grown in PA-0.5G, were diluted (1:1,000) in ZYP-5052 (MBP-CC) or PASM-5052 (MBP-CC^{SeMet}) and grown at 37°C for 8 h (Studier, 2005). Cultures were transferred to 23°C and grown for an additional 12–36 h before harvesting. All purification steps were performed at 4°C. Proteins were purified by affinity chromatography on amylose resin (New England Biolabs, Inc.) followed by cleavage with PreScission protease (GE Healthcare). After cleavage, Mdv1-CC contained two heterologous N-terminal residues (Gly-Pro). Protein was further purified by mono-Q anion exchange chromatography (GE Healthcare). Residual MBP and uncleaved protein were removed by additional nickel Sepharose (GE Healthcare) and amylose affinity chromatography. Purified Mdv1-CC was dialyzed in CD/ES buffer (50 mM Na-phosphate, pH 7.4, and 150 mM NaCl) or crystallization buffer (20 mM Tris-Cl, pH 7.5, and 100 mM NaCl) and concentrated to 1–10 mg/ml using Centriprep centrifugal concentrators (YM-3; 3 kD NMWL; Millipore).

CD and ES analysis

CD analysis was performed on a CD spectrometer (410; Aviv Biomedical, Inc.). Wavelength scans (200–260 nm) were performed at 23°C on 10 µM protein samples in 50 mM sodium phosphate, pH 7.4, and 150 mM NaCl using a 1-mm path length cuvette with a 5-s averaging time. ES analysis of Mdv1-CC was performed at 4°C using a centrifuge (Optima XL-A; Beckman Coulter) at initial protein subunit concentrations of 335.0, 168.0, and 84.0 µM (monomer) in a buffer containing 50 mM sodium phosphate, pH 7.4, and 150 mM NaCl. Centrifugation was performed at 20,000 rpm (Fig. 1 C) and 25,000 rpm. Resulting equilibrium datasets were globally fit to a single ideal species model with a floating molecular mass using the nonlinear least-squares algorithms in HeteroAnalysis software (Cole, 2004). Protein partial-specific volumes and solvent densities were calculated with the program SEDNTERP (version 1.09; Laue et al., 1992).

Crystallization and structure determination

The protein crystallized in several conditions of the Crystal Screen HT (Hampton Research). After optimization, Mdv1-CC^{SeMet} (10 mg/ml in 20 mM Tris-Cl, pH 7.5, and 100 mM NaCl) was crystallized in 2 µl/2 µl vapor diffusion experiments against a well solution containing 16% PEG 3350, 0.1 M Bis-Tris-Propane, pH 7.5, and 0.4 M NaCl. Flat-plate crystals were cryoprotected in 20% PEG 3350, 0.1 M BTP, pH 7.5, 0.4 M NaCl, and 25% glycerol and flash frozen in liquid nitrogen. Peak and inflection data were collected on beamline (version 7.1; SSRL) and processed with HKL2000 (Otwinowski and Minor, 1997) to a final Rmerge of 5.3% to 2.6 Å. The selenium sites were identified with SOLVE (Terwilliger and Berendzen, 1999), and solvent flattening and preliminary model building with RESOLVE (Terwilliger and Berendzen, 1999) resulted in 60% of the residues correctly positioned. Final model building and validation was performed in COOT (Emsley and Cowtan, 2004). Refinement with REFMAC5 (Murshudov et al., 1997) within the CCP4 suite (Collaborative Computational Project 4, 1994) resulted in a final R_{factor}/R_{merge} of 27.1%/31.1% and a model with good geometric statistics (Table S2).

Yeast strains and plasmids

Yeast strains used in this study include JSY5740 (*MATa leu2Δ1 his3Δ200 trp1Δ63 ura3-52 lys2Δ202*), JSY8612 (*MATa leu2Δ1 his3Δ200 trp1Δ63 ura3-52 lys2Δ202 mdv1::HIS3 caf4::KanMX*; also referred to as the adaptor Δ strain), JSY9465 (*MATa leu2Δ1 his3Δ200 trp1Δ63 ura3-52 lys2Δ202 mdv1::HIS3 caf4::KanMX dnm1::GFP-DNM1*), JSY9135 (*MATa leu2Δ1 his3Δ200 trp1Δ63 ura3-52 lys2Δ202 mdv1::HIS3 caf4::KanMX dnm1::HIS3*), JSY9541 (*MATa leu2Δ1 his3Δ200 trp1Δ63 ura3-52 lys2Δ202 mdv1::HIS3 caf4::KanMX fis1::HIS3*), and JSY7674 (*MATa leu2Δ1 his3Δ200 trp1Δ63 ura3-52 fis1-3 mdv1::HIS3*).

A list of plasmids used in this study is provided in Table S1. To construct *pMAL-c2x-mdv1-CC*, DNA sequences encoding residues 231–299 of *MDV1* were PCR amplified with a forward primer that introduced an EcoRI site, 10xHis, a PreScission Protease cleavage site, and a reverse primer that introduced three stop codons and a HindIII site. The resulting fragment was cloned into the EcoRI and HindIII sites of the *pMAL-c2x* vector (New England Biolabs, Inc.). The *pMAL-c2x-mdv1-CC^{SeMet}* construct was made by site-directed mutagenesis (QuikChange kit; Agilent Technologies) of *pMAL-c2x-mdv1-CC* to change leucine codons to methionine codons at positions encoding residues 248 and 281 in the full-length Mdv1 protein. Construction of *pRS416MET25-MDV1* was described previously (Karren et al., 2005). For *pRS416MET25-mdv1^{CC7}*, sequential site-directed mutagenesis of a *pRS416MET25-MDV1* template was used to introduce sequences encoding the substitutions L233E, L237E, I251E, I254E, L268E, I272E, and I275E. For *pRS415MET25-GFP-MDV1*, pRS415MET25-*GFP-mdv1^{CC7}*, and *pRS415MET25-GFP-mdv1^{HR2}*, PCR-amplified *MDV1*, *mdv1^{CC7}*, and *mdv1^{HR2}* sequences were cloned into the BamHI and SalI sites of *pRS415MET25-GFP*. *pRS415MET25-mdv1^{HR2}* was created using the following five steps: (1) sited-directed mutagenesis was used to introduce two silent restriction endonuclease sites into *MDV1* at nucleotides 628–633 (XmaI) and nucleotides 901–906 (XhoI) in the *pRS416MET25-MDV1* vector, (2) an existing XhoI site in the multiple-cloning site of *pRS416MET25-MDV1* was removed by site-directed mutagenesis, (3) A $_{yeast}$*MDV1*-$_{mouse}$*MFN1* CC chimeric sequence was synthesized by MR. GENE. The nucleotide sequence of the synthesized *MDV1-MFN1* CC chimera was *XmaI-MDV1(634–687)-MFN1(2022–2202)-MDV1 (883–900)-XhoI*, (4) the CC chimera provided in a vector was excised by XmaI and XhoI digestion and cloned into the same sites of the *pRS416MET25-MDV1* plasmid generated in step 1. To construct, *pRS416MET25-MDV1-13MYC*, *MDV1* was PCR amplified, digested with SpeI and SacII, and cloned into a vector that fused sequence encoding13MYC in frame at the C terminus of Mdv1. *pRS416MET25-mdv1^{CC7}-13MYC* and *pRS416MET25-mdv1^{HR2}-13MYC* were cloned by similar strategies. To create *pRS415MET25-MDV1-3HA*, *MDV1* was PCR amplified, digested, and cloned into the BamHI–XhoI sites of *pRS415MET25-CAF4-3HA*. In the resulting clone, the *CAF4* ORF was replaced by the *MDV1* ORF, and sequence encoding 3HA was fused in frame to the C terminus of Mdv1. A similar strategy was used to generate clones encoding C-terminal 3HA -agged forms of mdv1^{CC7}, mdv1^{HR2}, and mdv1^{E250G}. For *pRS416MET25-9MYC-FIS1*, *9MYC-FIS1* was excised from *pRS415MET25-9MYC-FIS1* (Karren et al., 2005) using SpeI and XhoI and cloned into *pRS416MET25*. To create *pRS416MET25-mdv1$^{\Delta 2HR}$* and *pRS416MET25-mdv1$^{\Delta 4HR}$*, DNA encoding mdv1$^{\Delta 2HR}$ (XmaI-634–708-ΔHR-730–836-ΔHR-855–900-XhoI) or mdv1$^{\Delta 4HR}$ (XmaI-634–708-ΔΔHR-751–813-ΔΔHR-855–900-XhoI) was synthesized and cloned by Integrated DNA Technologies, Inc. After digestion of the provided plasmids with XmaI and XhoI, the cloned fragments were ligated into silent XmaI and XhoI sites engineered on either side of the encoded Mdv1 CC in *pRS416MET25-MDV1*. *pRS415MET25-mdv1$^{\Delta 2HR}$-3HA*, *pRS415MET25-mdv1$^{\Delta 4HR}$-3HA*, *pRS415MET25-GFP-mdv1$^{\Delta 2HR}$*, and *pRS415MET25-GFP-mdv1$^{\Delta 4HR}$* were generated using strategies similar to those described for WT and mutant Mdv1 variants. For *pRS416MET25-ffRFP-mdv1^{CC7}*, a PCR-amplified fragment containing mdv1^{CC7} was digested with BamHI and SalI and ligated into *pRS416MET25-ffRFP*.

Published December 13, 2010

Fluorescence microscopy

Mitochondrial morphologies were scored in WT, adaptor Δ, and *fis1-3 mdv1::HIS3* strains as WT (more than two free tubule ends in the mother cell) or fission mutant (less than three free tubule ends in the mother cell). Localization of GFP fusions GFP-Mdv1, GFP-mdv1^{CC2}, GFP-mdv1^{HR2}, GFP-mdv1$^{\Delta 2HR}$, and GFP-mdv1$^{\Delta 4HR}$ were scored in WT or adaptor Δ strains expressing mitochondrial-targeted fast-folding RFP (mito-RFP). GFP-Dnm1 localization/puncta formation was analyzed in the adaptor Δ strain containing genomically integrated *GFP-DNM1*. Overnight cultures grown at 30°C in appropriate synthetic dextrose dropout media containing 0.1 mg/ml methionine were diluted to ∼0.2 OD_{600} and grown for 3–5 h (OD_{600}, 0.5–1.0). Under these conditions, the *MET25* (methionine repressible) promoter is leaky. The abundance of proteins expressed from the uninduced *MET25* promoter was about fourfold greater than that of endogenously expressed Mdv1 (Karren et al., 2005). For analysis of dominant-negative phenotypes, cells were diluted in medium lacking methionine and grown for 4 h before scoring. The steady-state abundance of proteins expressed from the *MET25* promoter after a 4-h induction were ∼3–4-fold higher than that of uninduced Mdv1 expressed from the same promoter (Fig. S4, A and B; Karren et al., 2005). For analysis in the *fis1-3 mdv1::HIS3* strain, cells grown overnight at 25°C were diluted in medium lacking methionine and grown for 2 h at 25 or 37°C before scoring. Phenotypes were analyzed in 100 cells in three or more independent experiments. Data reported are the means of all experiments ($n \geq 3$) with the indicated standard deviations. Images were acquired and processed as described previously (Amiott et al., 2009). Cells were visualized on an imaging microscope (Axioplan 2; Carl Zeiss, Inc.) with a 100× NA 1.4 oil immersion objective. Digital fluorescence and differential interference contrast (DIC) images of cells were acquired using a monochrome digital camera (AxioCam MRm; Carl Zeiss, Inc.). Z stacks of 0.2-µm slices were obtained and deconvolved using AxioVision software (version 4.6; Carl Zeiss, Inc.). Three-dimensional projections of mitochondria were generated with the transparency (voxel) setting and converted to a single image. Final images were processed and assembled using Photoshop and Illustrator (CS3; Adobe). Brightness and contrast were adjusted using only linear operations applied to the entire image.

Analysis of protein expression and targeting

Protein expression was analyzed in WCEs prepared by the alkaline extraction method (Kushnirov, 2000). To analyze subcellular localization of proteins, cells grown in the appropriate synthetic galactose dropout medium were spheroplasted and homogenized to produce WCE, which was subsequently subjected to differential sedimentation to isolate postmitochondrial supernatant and mitochondrial pellet enriched fractions (Kondo-Okamoto et al., 2003). Either 0.5 OD_{600} equivalents of alkaline extract or 50 µg protein of WCE, 50 µg postmitochondrial supernatant, and 25 µg mitochondrial pellet fractions were separated by SDS-PAGE and analyzed by Western blotting using anti-HA (1:2,000; University of Utah Core Facility), anti-PGK (1:2,000; Invitrogen), anti-porin (1:2,000; Invitrogen), and HRP-conjugated secondary goat anti–mouse antibody (1:10,000; Sigma-Aldrich). Proteins were detected by ECL (GE Healthcare). Steady-state abundance of HA-tagged WT and mutant Mdv1 proteins (Fig. S4, A and B) expressed from the *MET25* promoter was determined in adaptor Δ cells grown for 4 h after dilution in selective medium containing 0.1 mg/ml methionine or lacking methionine. Alkali protein extracts (0.25 OD_{600} cell equivalents) separated by SDS-PAGE were analyzed by Western blotting with anti-HA primary antibody and fluorescent secondary antibody followed by detection using a scanner (Odyssey; LI-COR Biosciences). The mean intensity of each HA-tagged protein band was normalized to a control 3PGK protein band in each lane. To determine fold induction of *MET25*-regulated protein expression, normalized HA signals from induced and uninduced samples were compared. Bars in uninduced and induced graphs represent the abundance of HA-tagged signal in each lane relative to WT. Error bars indicate the standard deviation from three independent experiments.

Co-IP assays

For Mdv1–Mdv1 and Mdv1–Fis1 interaction experiments, functional HA- and Myc-tagged Mdv1 and Fis1 proteins and variants were expressed in adaptor Δ cells or adaptor Δ cells lacking *FIS1* (*fis1Δ* adaptor Δ). coIPs were performed with anti–c-Myc agarose-conjugated beads (Sigma-Aldrich) as described previously (Karren et al., 2005; Bhar et al., 2006). In brief, 30 OD_{600} cell equivalents were harvested and lysed with glass beads in 500 µl IP buffer (0.5% Triton X-100, 150 mM NaCl, 1 mM EDTA, 50 mM Tris, pH 7.4, and 1:500 protease inhibitor cocktail set III [EMD]). After centrifugation at 18,000 *g* for 10 min, 400 µl supernatant was incubated with 40 µl anti–c-Myc–conjugated agarose beads (Sigma-Aldrich) for 1 h at 4°C. Agarose beads were collected, washed in IP buffer, and incubated in 60 µl SDS-PAGE sample buffer lacking r-mercaptoethanol at 60°C for 8 min to release bound proteins. After addition of 3.2 µl r-mercaptoethanol and boiling, samples were analyzed by SDS-PAGE and Western blotting with anti-Myc (Santa Cruz Biotechnology, Inc.), and anti-HA (University of Utah Core facility) antibodies. Immunoprecipitated proteins were detected using the appropriate HRP-conjugated secondary antibodies and ECL Plus (GE Healthcare) followed by exposure to film. In Fig. 6 B, detection was accomplished using fluorescent secondary antibody (IRDye 800 anti–mouse; LI-COR Biosciences), and signals were quantified using a scanner (Odyssey) and analysis software (Odyssey version 3.0; LI-COR Biosciences).

Mdv1–Dnm1 coIPs were performed using adaptor Δ cells expressing endogenous Dnm1 and plasmid-borne HA-tagged Mdv1 variants as described previously (Karren et al., 2005). 50 OD_{600} U of cells grown at 30°C were treated with 0.2 mg/ml zymolase for 60 min at 30°C. Cross-linking was performed with 2.5 mM dithiobis(succinimidyl propionate) (DSP; Thermo Fisher Scientific) for 30 min at 30°C. DSP was quenched by addition of 50 mM glycine (also present in all subsequent buffers). After homogenization, pellets were collected by spinning at 18,000 *g* for 10 min, solubilized for 10 min at 4°C in 500 µl IP buffer (1% Triton X-100, 150 mM NaCl, 30 mM Hepes-KOH, pH 7.4, and 1:500 protease inhibitor cocktail set III), and cleared by spinning for an additional 10 min at 18,000 *g*. 400 µl cleared supernatant was incubated with 40 µl anti-HA–conjugated agarose beads (Sigma-Aldrich) for 1 h at 4°C. Agarose beads were collected, washed in IP buffer, and bound proteins were released as described in the previous paragraph. Samples were analyzed by SDS-PAGE and ECL Western blotting with anti-HA and anti-Dnm1 antibodies (Otsuga et al., 1998).

Online supplemental material

Fig. S1 shows additional analysis of mdv1^{HR2} localization and function. Fig. S2 shows that Glu250 is exposed on one face of the dimeric antiparallel CC. Fig. S3 shows an additional analysis of mdv1^{D2HR} and mdv1^{D4HR} proteins. Fig. S4 shows dominant-negative effects of WT and mutant Mdv1 proteins. Table S1 shows plasmids used in this study. Table S2 shows x-ray data and model statistics. Online supplemental material is available at http://www.jcb.org/cgi/content/full/jcb.201005046/DC1.

We thank Jane Macfarlane for expertise in mutagenesis and plasmid construction, Steve Alam for advice regarding protein purification, and members of the Shaw laboratory for critical discussions.

Research support was provided by the National Institutes of Health (grants GM53466 to J.M. Shaw, GM59135 to C.P. Hill, and GM82545 to M.S. Kay). Support for sequencing, antibody, and oligonucleotide services at the University of Utah is provided by the National Institutes of Health Center for Cancer Research Resources (grant M01RR00064). Portions of this research were carried out at the Stanford Synchrotron Radiation Light Source (SSRL) Office of Basic Energy Sciences, a national user facility operated by Stanford University on behalf of the U.S. Department of Energy. The SSRL Structural Molecular Biology Program is supported by the Department of Energy, the Office of Biological and Environmental Research, and the National Institutes of Health, National Center for Research Resources, Biomedical Technology Program, and National Institute of General Medical Sciences.

Submitted: 11 May 2010
Accepted: 8 November 2010

References

Amiott, E.A., M.M. Cohen, Y. Saint-Georges, A.M. Weissman, and J.M. Shaw. 2009. A mutation associated with CMT2A neuropathy causes defects in Fzo1 GTP hydrolysis, ubiquitylation, and protein turnover. *Mol. Biol. Cell.* 20:5026–5035. doi:10.1091/mbc.E09-07-0622

Bhar, D., M.A. Karren, M. Babst, and J.M. Shaw. 2006. Dimeric Dnm1-G385D interacts with Mdv1 on mitochondria and can be stimulated to assemble into fission complexes containing Mdv1 and Fis1. *J. Biol. Chem.* 281:17312–17320. doi:10.1074/jbc.M513530200

Bleazard, W., J.M. McCaffery, E.J. King, S. Bale, A. Mozdy, Q. Tieu, J. Nunnari, and J.M. Shaw. 1999. The dynamin-related GTPase Dnm1 regulates mitochondrial fission in yeast. *Nat. Cell Biol.* 1:298–304. doi:10.1038/13014

Collaborative Computational Project 4. 1994. The CCP4 suite: programs for protein crystallography. *Acta Crystallogr. D. Biol. Crystallogr.* D50:760–763.

Cerveny, K.L., and R.E. Jensen. 2003. The WD-repeats of Net2p interact with Dnm1p and Fis1p to regulate division of mitochondria. *Mol. Biol. Cell.* 14:4126–4139. doi:10.1091/mbc.E03-02-0092

Published December 13, 2010

Cerveny, K.L., J.M. McCaffery, and R.E. Jensen. 2001. Division of mitochondria requires a novel DMN1-interacting protein, Net2p. *Mol. Biol. Cell.* 12:309–321.

Chen, H., and D.C. Chan. 2005. Emerging functions of mammalian mitochondrial fusion and fission. *Hum. Mol. Genet.* 2:R283–R289. doi:10.1093/hmg/ddi270

Cole, J.L. 2004. Analysis of heterogeneous interactions. *Methods Enzymol.* 384:212–232. doi:10.1016/S0076-6879(04)84013-8

Emsley, P., and K. Cowtan. 2004. Coot: model-building tools for molecular graphics. *Acta Crystallogr. D Biol. Crystallogr.* 60:2126–2132. doi:10.1107/S0907444904019158

Griffin, E.E., J. Graumann, and D.C. Chan. 2005. The WD40 protein Caf4p is a component of the mitochondrial fission machinery and recruits Dnm1p to mitochondria. *J. Cell Biol.* 170:237–248. doi:10.1083/jcb.200503148

Ingerman, E., E.M. Perkins, M. Marino, J.A. Mears, J.M. McCaffery, J.E. Hinshaw, and J. Nunnari. 2005. Dnm1 forms spirals that are structurally tailored to fit mitochondria. *J. Cell Biol.* 170:1021–1027. doi:10.1083/jcb.200506078

Kairen, M.A., E.M. Coonrod, T.K. Anderson, and J.M. Shaw. 2005. The role of Fis1p-Mdv1p interactions in mitochondrial fission complex assembly. *J. Cell Biol.* 171:291–301. doi:10.1083/jcb.200506158

Kondo-Okamoto, N., J.M. Shaw, and K. Okamoto. 2003. Mmm1p spans both the outer and inner mitochondrial membranes and contains distinct domains for targeting and foci formation. *J. Biol. Chem.* 278:48997–49005. doi:10.1074/jbc.M308436200

Koshiba, T., S.A. Detmer, J.T. Kaiser, H. Chen, J.M. McCaffery, and D.C. Chan. 2004. Structural basis of mitochondrial tethering by mitofusin complexes. *Science.* 305:858–862. doi:10.1126/science.1099793

Kushnirov, V.V. 2000. Rapid and reliable protein extraction from yeast. *Yeast.* 16:857–860. doi:10.1002/1097-0061(20000630)16:9<857::AID-YEA561>3.0.CO;2-B

Lackner, L.L., J.S. Horner, and J. Nunnari. 2009. Mechanistic analysis of a dynamin effector. *Science.* 325:874–877. doi:10.1126/science.1176921

Laue, T., B. Shah, T. Ridgeway, and S. Pelletier. 1992. Computer-aided interpretation of analytical sedimentation data for proteins. *In* Analytical Ultracentrifugation in Biochemistry and Polymer Science. Royal Society of Chemistry, Cambridge, England, UK. 90–125.

Mozdy, A.D., J.M. McCaffery, and J.M. Shaw. 2000. Dnm1p GTPase-mediated mitochondrial fission is a multi-step process requiring the novel integral membrane component Fis1p. *J. Cell Biol.* 151:367–380. doi:10.1083/jcb.151.2.367

Murshudov, G.N., A.A. Vagin, and E.J. Dodson. 1997. Refinement of macromolecular structures by the maximum-likelihood method. *Acta Crystallogr. D Biol. Crystallogr.* 53:240–255. doi:10.1107/S0907444996012255

Naylor, K., E. Ingerman, V. Okreglak, M. Marino, J.E. Hinshaw, and J. Nunnari. 2006. Mdv1 interacts with assembled dnm1 to promote mitochondrial division. *J. Biol. Chem.* 281:2177–2183. doi:10.1074/jbc.M507943200

Okamoto, K., and J.M. Shaw. 2005. Mitochondrial morphology and dynamics in yeast and multicellular eukaryotes. *Annu. Rev. Genet.* 39:503–536. doi:10.1146/annurev.genet.38.072902.093019

Otsuga, D., B.R. Keegan, E. Brisch, J.W. Thatcher, G.J. Hermann, W. Bleazard, and J.M. Shaw. 1998. The dynamin-related GTPase, Dnm1p, controls mitochondrial morphology in yeast. *J. Cell Biol.* 143:333–349. doi:10.1083/jcb.143.2.333

Otwinowski, Z., and W. Minor. 1997. Processing of x-ray diffraction data collected in oscillation mode. *In* Methods in Enzymology. Macromolecular Crystallography, part A. Vol. 276. C.W. Carter, Jr. and R.M. Sweet, editors. Academic Press, New York. 307–326.

Shaw, J.M., and J. Nunnari. 2002. Mitochondrial dynamics and division in budding yeast. *Trends Cell Biol.* 12:178–184. doi:10.1016/S0962-8924(01)02246-2

Studier, F.W. 2005. Protein production by auto-induction in high density shaking cultures. *Protein Expr. Purif.* 41:207–234. doi:10.1016/j.pep.2005.01.016

Suzuki, M., A. Neutzner, N. Tjandra, and R.J. Youle. 2005. Novel structure of the N terminus in yeast Fis1 correlates with a specialized function in mitochondrial fission. *J. Biol. Chem.* 280:21444–21452. doi:10.1074/jbc.M414092200

Terwilliger, T.C., and J. Berendzen. 1999. Automated MAD and MIR structure solution. *Acta Crystallogr. D Biol. Crystallogr.* 55:849–861. doi:10.1107/S0907444999000839

Tieu, Q., and J. Nunnari. 2000. Mdv1p is a WD repeat protein that interacts with the dynamin-related GTPase, Dnm1p, to trigger mitochondrial division. *J. Cell Biol.* 151:353–366. doi:10.1083/jcb.151.2.353

Tieu, Q., V. Okreglak, K. Naylor, and J. Nunnari. 2002. The WD repeat protein, Mdv1p, functions as a molecular adaptor by interacting with Dnm1p and Fis1p during mitochondrial fission. *J. Cell Biol.* 158:445–452. doi:10.1083/jcb.200205031

Wolf, E., P.S. Kim, and B. Berger. 1997. MultiCoil: a program for predicting two- and three-stranded coiled coils. *Protein Sci.* 6:1179–1189. doi:10.1002/pro.5560060606

Zhang, Y., and D.C. Chan. 2007. Structural basis for recruitment of mitochondrial fission complexes by Fis1. *Proc. Natl. Acad. Sci. USA.* 104:18526–18530. doi:10.1073/pnas.0706441104

Published December 13, 2010

Supplemental material JCB

Koirala et al., http://www.jcb.org/cgi/content/full/jcb.201005046/DC1

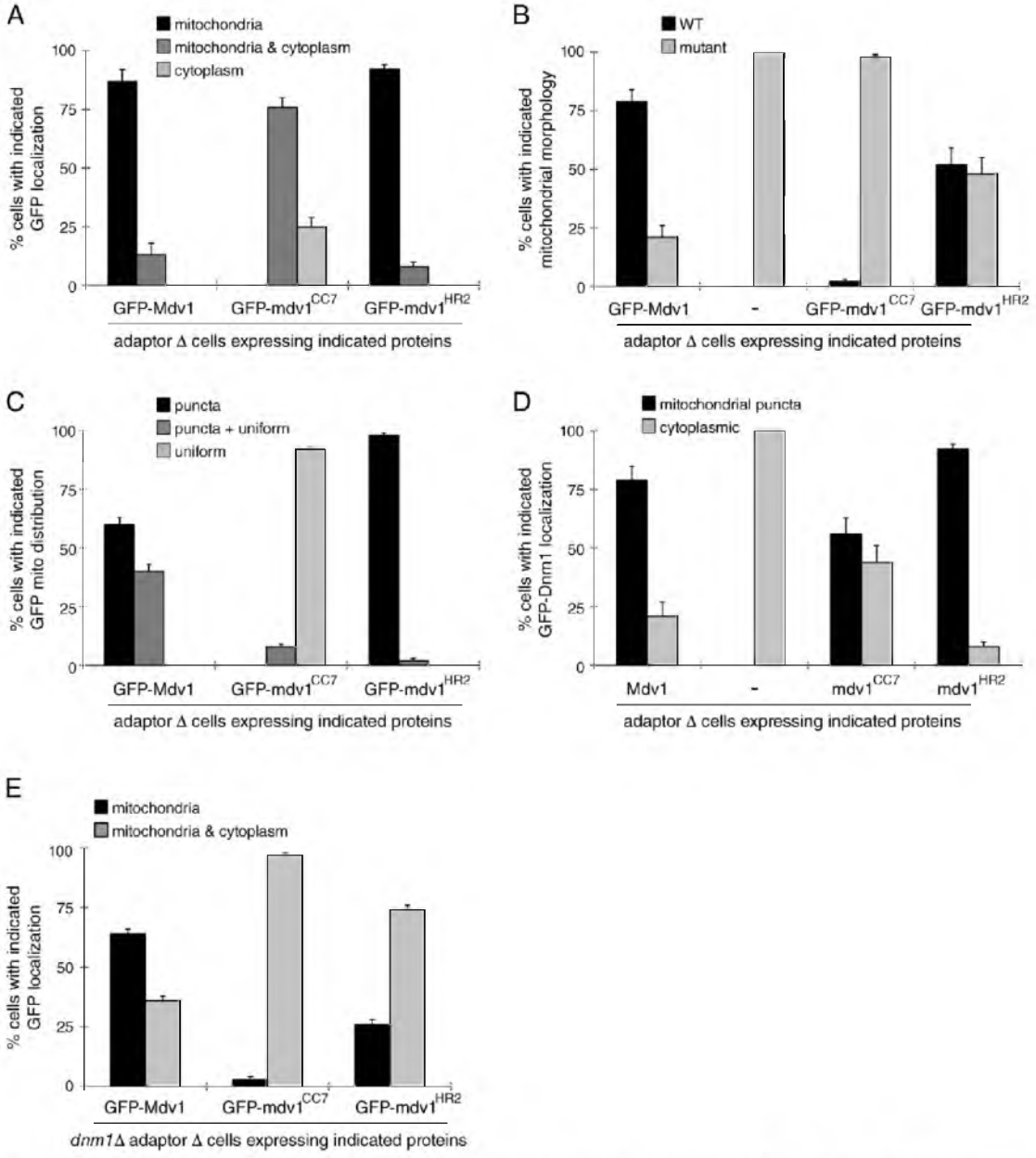

Figure S1. **Additional Analysis of mdv1^{HR2} localization and function.** (A) Subcellular localization of N-terminal GFP-tagged Mdv1, mdv1^{CC7}, and mdv1^{HR2} proteins in adaptor Δ cells. (B) Mitochondrial morphologies in adaptor Δ cells expressing GFP-tagged Mdv1, mdv1^{CC7}, and mdv1^{HR2} proteins. (C) Mitochondrial distribution of GFP-tagged Mdv1, mdv1^{CC7}, and mdv1^{HR2} proteins. (D) Localization of genomically expressed GFP-Dnm1 in cells expressing Mdv1, mdv1^{CC7}, or mdv1^{HR2}. (E) Subcellular localization of GFP-tagged Mdv1, mdv1^{CC7}, and mdv1^{HR2} proteins in *dnm1*Δ adaptor Δ cells. Error bars represent the mean and standard deviation of at least three independent experiments (n = 100).

Published December 13, 2010

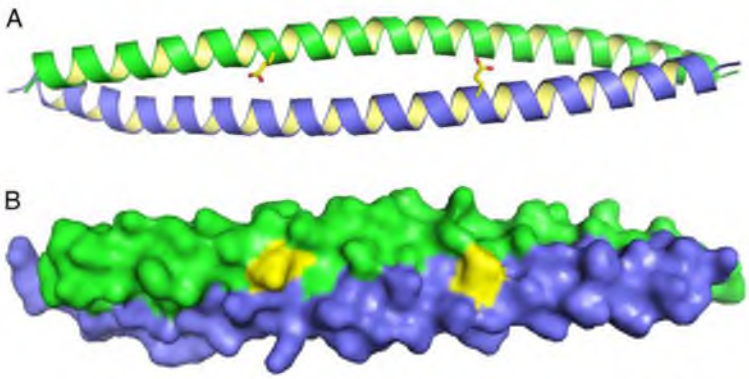

Figure S2. **Glu250 is exposed on one face of the dimeric antiparallel CC.** (A and B) Positions of E250 residues on the Mdv1 CC structure are shown as yellow side chains on the ribbon structure (A) and as yellow patches on the space-filling model (B). The different α-helices in the CC are shown in green and blue.

Published December 13, 2010

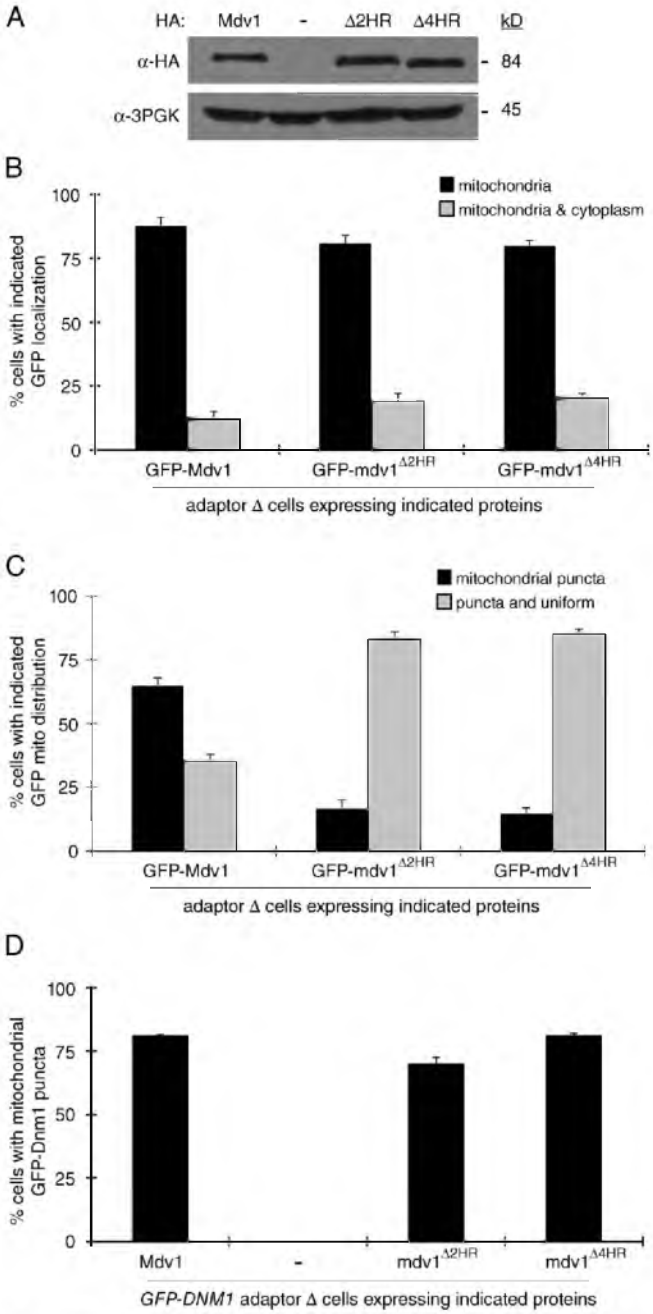

Figure S3. **Additional analysis of mdv1$^{\Delta 2HR}$ and mdv1$^{\Delta 4HR}$ proteins.** (A) Steady-state abundance of C-terminal HA-tagged Mdv1, mdv1$^{\Delta 2HR}$, and mdv1$^{\Delta 4HR}$ proteins expressed in adaptor Δ cells. WCEs separated by SDS-PAGE were immunoblotted with anti-HA and anti-3PGK antibodies. (B) Mitochondrial distribution of GFP-tagged WT and ΔHR mutant Mdv1 proteins. (C) Mitochondrial distribution of GFP-tagged Mdv1, mdv1$^{\Delta 2HR}$, and mdv1$^{\Delta 4HR}$ proteins imaged in adaptor Δ cells. (D) Localization of genomically expressed GFP-Dnm1 in cells expressing Mdv1, mdv1$^{\Delta 2HR}$, and mdv1$^{\Delta 4HR}$ proteins. Error bars represent the mean and standard deviation of at least three independent experiments (n = 100).

Published December 13, 2010

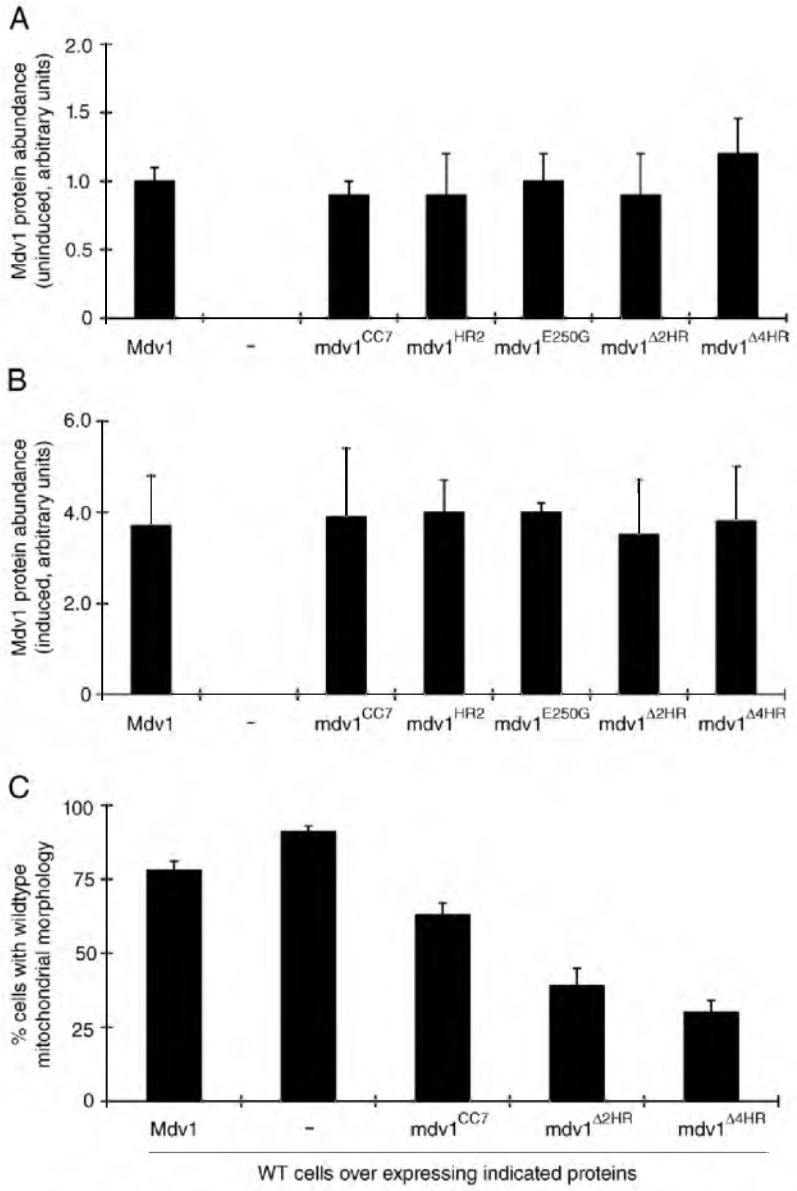

Figure S4. **Dominant-negative effects of WT and mutant Mdv1 proteins.** (A) Relative steady-state abundance of WT and mutant Mdv1 proteins expressed from the uninduced *MET25* promoter in adaptor Δ cells. (B) Relative steady-state abundance of WT and mutant proteins expressed from the induced *MET25* promoter in adaptor Δ cells. Quantification details for A and B are discussed in Materials and methods. (C) Mitochondrial morphology in WT cells expressing WT and mutant Mdv1 proteins from the *MET25* promoter after a 4-h induction. Error bars represent the mean and standard deviation of at least three independent experiments ($n = 100$).

Published December 13, 2010

Table S1. **Plasmids used in this study**

ID number	Plasmid	Protein expressed	Source
B493	*pRS415MET25*	None	ATCC 87322
B494	*pRS416MET25*	None	ATCC 87324
B824	*pRS415MET25-9MYC-FIS1*	9Myc-Fis1	Karren et al., 2005
B1642	*p414GPD-mt-ffRFP*	*N. crassa* ATP9(1–69) + fast-folding DsRed	Karren et al., 2005
B1808	*pRS415MET25-MDV1*	MDV1	Karren et al., 2005
B2053	*pRS416MET25-MDV1*	MDV1	Karren et al., 2005
B2054	*pRS416MET25-mdv1^{E250G}*	Mdv1^{E250G}	Karren et al., 2005
B2499	*pMAL-c2x-mdv1-CC*	10xHIS-PPCS-mdv1-CC	This study
B2620	*pRS416MET25-mdv1^{CC7}*	mdv1$^{L233E, L237E, I251E, I254E, L268E, I272E, I275E}$	This study
B2621	*pMAL-c2x-mdv1-CC^{SeMet}*	mdv1-CC$^{L248M, L281M}$	This study
B2683	*pRS415MET25-GFP-mdv1^{CC7}*	GFP-mdv1^{CC7}	This study
B2783	*pRS416MET25-mdv1^{HR2}*	Mdv1$^{1–229}$–*M. musculus* Mfn1$^{674–734}$–Mdv1$^{295–714}$	This study
B2798	*pRS416MET25-mdv1^{CC7}-13MYC*	mdv1^{CC7}-13MYC	This study
B2800	*pRS415MET25-mdv1^{HR2}-13MYC*	mdv1^{HR2}-13MYC	This study
B2821	*pRS415MET25-MDV1-3HA*	Mdv1-3HA	This study
B2832	*pRS416MET25-mdv1^{HR2}-3HA*	mdv1^{HR2}-3HA	This study
B2833	*pRS416MET25-mdv1^{HR2}-13MYC*	mdv1^{HR2}-13MYC	This study
B2837	*pRS416MET25-MDV1-13MYC*	Mdv1-13MYC	This study
B2839	*pRS415MET25-mdv1^{CC7}-3HA*	mdv1^{CC7}-3HA	This study
B2864	*pRS416MET25-9MYC-FIS1*	9MYC-Fis1	This study
B2882	*pRS415MET25-mdv1^{E250G}-3HA*	mdv1^{E250G}-3HA	This study
B2892	*pRS415MET25-GFP-mdv1^{HR2}*	GFP-mdv1^{HR2}	This study
B3003	*pRS416MET25-ffRFP-mdv1^{CC7}*	ffRFP-mdv1^{CC7}	This study
B3015	*pRS416MET25-mdv1$^{\Delta 2HR}$*	mdv1$^{\Delta 2HR}$	This study
B3016	*pRS416MET25-mdv1$^{\Delta 4HR}$*	mdv1$^{\Delta 4HR}$	This study
B3017	*pRS415MET25-mdv1$^{\Delta 2HR}$-3HA*	mdv1$^{\Delta 2HR}$-3HA	This study
B3018	*pRS415MET25-mdv1$^{\Delta 4HR}$-3HA*	mdv1$^{\Delta 4HR}$-3HA	This study
B3028	*pRS415MET25-GFP-mdv1$^{\Delta 2HR}$*	GFP-mdv1$^{\Delta 2HR}$	This study
B3029	*pRS415MET25-GFP-mdv1$^{\Delta 4HR}$*	GFP-mdv1$^{\Delta 4HR}$	This study

ATCC, American Type Culture Collection.

Table S2. **X-ray data and model statistics**

Space group $P4_12_12$	*SeMdv13* Se peak	*SeMdv13* Se inflection
Data collection		
Cell a =, c = (Å)	41.38, 227.38	41.35, 227.39
Resolution (Å) (high)	38–2.7 (2.79–2.7)	38–2.8 (2.9–2.8)
No. unique reflections	10,392	9,222
Rmerge	5.3 (27.9)	6.4 (21.1)
Completeness	99.2 (99.2)	98.8 (98.5)
I–SigI	10.0 (2.4)	10.2 (2.31)
Redundancy	1.8 (1.7)	1.8 (1.7)
Refinement		
R/Rfree	27.0/31.4	NA
No. protein atoms	1,067	NA
No. water atoms	21	NA
<B> protein	58.5	NA
<B> water	52.1	NA
Rms bond (Å)	0.014	NA
Rms angle (°)	1.5	NA

NA, not applicable.

Published December 13, 2010

Reference

Karren, M.A., E.M. Coonrod, T.K. Anderson, and J.M. Shaw. 2005. The role of Fis1p–Mdv1p interactions in mitochondrial fission complex assembly. *J. Cell Biol.* 171:291–301. doi:10.1083/jcb.200506158

CHAPTER 3

MULTIPLE ADAPTORS REGULATE MITOCHONDRIAL DYNAMIN GTPASE ASSEMBLY FOR MEMBRANE SCISSION

Authors

Sajjan Koirala, Qian Guo*, Raghav Kalia*, Debra Eckert, Adam Frost, Janet M. Shaw
* These authors have contributed equally to this work.
This chapter is currently under review at Developmental Cell.

Summary

Mitochondrial fission is mediated by the dynamin-related GTPases Dnm1/Drp1 (yeast/mammals), which form spirals around constricted sites on mitochondria. Additional membrane-associated adaptor proteins (Fis1, Mdv1, Mff and MiDs) are required to recruit these GTPases from the cytoplasm to the mitochondrial surface. Whether these adaptors participate in both membrane scission and GTPase recruitment is not known. Here we use a yeast strain lacking all fission proteins to identify the minimal combinations of GTPases and adaptors sufficient for mitochondrial fission. Although Fis1 is dispensable for fission, membrane-anchored Mdv1, Mff, or MiDs paired individually with their respective GTPases are sufficient to divide mitochondria. In addition to their role in Drp1 membrane recruitment, MiD proteins coassemble with Drp1 in vitro. The resulting heteropolymer adopts a dramatically different structure with a narrower diameter than Drp1 homopolymers assembled in isolation. This result provides the first demonstration that an adaptor protein alters the architecture of a mitochondrial dynamin GTPase polymer in a manner that could facilitate membrane constriction and severing activity.

Introduction

Dynamin-related proteins (DRPs) are self-assembling GTPases that regulate lipid remodeling events at different cellular membranes (Praefcke and McMahon, 2004). Two of these DRPs, Dnm1 (yeast) and Drp1 (human), play conserved roles in mitochondrial fission, which is important for biological processes including mitochondrial inheritance during cell division (Gorsich and Shaw, 2004; Taguchi et al., 2007), clearance of defective mitochondria via mitophagy (Gomes et al., 2011; Parone et al., 2008; Rambold

et al., 2011; Twig et al., 2008) and mammalian development (Ishihara et al., 2009; Wakabayashi et al., 2009).

In vivo, both the Dnm1 and Drp1 GTPases assemble from the cytoplasm into structures that encircle mitochondria at sites of future fission (Bleazard et al., 1999; Labrousse et al., 1999; Otsuga et al., 1998; Sesaki and Jensen, 1999). In vitro, addition of GTP to Dnm1-lipid tubules is sufficient to constrict synthetic liposomes (Ingerman et al., 2005; Mears et al., 2011). However, a recent study revealed that mitochondrial constriction in yeast and mammals occurs at sites where endoplasmic reticulum (ER) tubules circumscribe mitochondria (Friedman et al., 2011). This ER-mediated mitochondrial constriction occurs prior to Dnm1 or Drp1 recruitment, suggesting that DRPs act after the initial constriction event to complete membrane fission. Neither Dnm1 nor Drp1 has ever been shown to independently catalyze membrane scission *in vivo* or *in vitro.*

A variety of adaptor proteins localized to the outer mitochondrial membrane (OMM) play important, but poorly understood, roles in Dnm1/Drp1 recruitment and function. The membrane recruitment step is best understood in yeast, where Dnm1 binds to the fungal-specific adaptor Mdv1 (Cerveny et al., 2001; Tieu and Nunnari, 2000), which is in turn bound to the tail-anchored Fis1 protein (Mozdy et al., 2000). Fluorescence microscopy studies show that Mdv1 colocalizes with Dnm1 at sites of mitochondrial fission (Naylor et al., 2006). *In vitro*, Mdv1 interacts with the GTP-bound form of Dnm1 and stimulates Dnm1 self-assembly (Lackner et al., 2009).

Fis1 is conserved in humans (hFis1), but does not appear to recruit Drp1 to mitochondria. Instead, Drp1 recruitment is mediated by Mff, another tail-anchored

protein (Gandre-Babbe and van der Bliek, 2008; Otera et al., 2010). Two additional human proteins, the orthologs MiD49 and MiD51, are N-terminally anchored in the OMM and also play a role in Drp1 recruitment (Palmer et al., 2011; Zhao et al., 2011). Neither Mff or MiDs are related by sequence or predicted secondary structure to Mdv1. The Mff and MiD49/51 proteins form rings surrounding mitochondria, suggesting that they coassemble with Drp1 (Palmer et al., 2011); however, their specific roles in Drp1 assembly and membrane scission are not well understood. Thus, major unanswered questions remain regarding whether or not adaptor proteins participate in lipid remodeling and membrane scission and whether they act independently or in concert *in vivo*.

Here we use a yeast strain devoid of fission proteins to identify the minimal combination of DRPs and adaptors sufficient for mitochondrial fission. We provide new evidence that Fis1 is dispensable for mitochondrial membrane scission. We also demonstrate that Mdv1, Mff, or MiDs paired individually with their respective DRPs are interchangeable, in that each is sufficient to catalyze fission. Importantly, co-assembly of a MiD protein with Drp1 dramatically decreases the diameter of the Drp1 structures formed. This result provides a direct demonstration that an adaptor protein can alter the architecture of a DRP assembly in a manner that could facilitate their membrane constriction and severing ability.

Experimental Procedures

Yeast Strains and Growth Conditions

Yeast strains and plasmids used in this study are listed in Tables 3.1 and 3.2. Standard yeast and bacterial techniques were used for construction and growth of strains (Green and Sambrook, 2012; Guthrie and Fink., 2002).

Plasmid Construction

Plasmids used in this study are listed in Table 3.2. Plasmids B1642, B1808 and B2053 were described previously (Karren et al., 2005). To construct B1607 and B1816, DNA sequences encoding full length *FIS1* and human *DRP1* isoform 3 were PCR amplified and cloned into BamHI and SalI sites of the *pRS415MET25* and *pRS416MET25* vectors (Stratagene). To create B2729, DNA sequences encoding *TOM20 (1-51aa)* (Ramage et al., 1993)were PCR amplified and cloned into the XbaI and BamHI sites of B1808 (in-frame with the existing FL *MDV1* coding region). B2730 and B2731 were constructed by replacing BamHI-*MDV1*-SalI in B2729 with the indicated *MDV1* coding sequences. For B3090, a three-way ligation reaction was performed with the *pRS415MET25* vector (Stratagene) and PCR amplified fragments of monomeric GFP^{A207K} and yeast $Fis1^{131\text{-}155aa}$ to generate *pRS415MET25-BamHI-mOMGFP-BsiWI-*$Fis1^{131\text{-}155aa}$*-SalI-pRS415* vector. For B3162, the StarGate® cloning system (IBA Solutions for Life Sciences) was used to introduce *-PreScission Protease Cleavage Site-BamHI-hDRP1 isoform 3-* into the EcoRI and SalI sites of the *pYSG-IBA167* vector. For B3259, B3262 and B3294, the indicated coding sequences were exchanged for *hDRP1* using existing *BamHI* and *SalI* sites. For B3265, a two-step cloning protocol was used. First, the PCR amplified *CUP1* promoter sequence was introduced into the *SacII* and *SalI*

Table 3.1: Yeast Strains Used in Chapter 3

ID	Genotype
JSY5740	*MAT*a, *leu2Δ1, his3Δ200, trp1Δ63, ura3-52, lys2Δ202*
JSY9548	*MAT*a, *leu2Δ1, his3Δ200, trp1Δ63, ura3-52, lys2Δ202, dnm1::GFP-DNM1, caf4::KanMX*
JSY9612	*MAT*a, *can1, ade2, trp1, ura3, his3, leu2, pep4::HIS3, prb1::LEU2, bar1::HISG, lys2::GAL1/10-GAL4*
JSY9801	*MATα, leu2Δ1, his3Δ200, trp1Δ63, ura3-52, lys2Δ202, fis1::HIS3, caf4::KanMX, mdv1:: MET25-TOM20(1-51aa)-MDV1(1-714aa)*
JSY9802	*MATα, leu2Δ1, his3Δ200, trp1Δ63, ura3-52, lys2Δ202, fis1::HIS3, caf4::KanMX, mdv1:: MET25-TOM20(1-51aa)-MDV1(218-714aa)*
JSY9803	*MATα, leu2Δ1, his3Δ200, trp1Δ63, ura3-52, lys2Δ202, fis1::HIS3, caf4::KanMX, mdv1:: MET25-TOM20(1-51aa)-MDV1(317-714aa)*
JSY9804	*MATa, leu2Δ1, his3Δ200, trp1Δ63, ura3-52, lys2Δ202, fis1::HIS3, caf4::KanMX, dnm1::GFP-DNM1, mdv1:: MET25-TOM20(1-51aa)-MDV1(1-714aa)*
JSY9805	*MATa, leu2Δ1, his3Δ200, trp1Δ63, ura3-52, lys2Δ202, fis1::HIS3, caf4::KanMX, dnm1::GFP-DNM1, mdv1:: MET25-TOM20(1-51aa)-MDV1(218-714aa)*
JSY9806	*MATa, leu2Δ1, his3Δ200, trp1Δ63, ura3-52, lys2Δ202, fis1::HIS3, caf4::KanMX, dnm1::GFP-DNM1, mdv1:: MET25-TOM20(1-51aa)-MDV1(317-714aa)*
JSY9807	*MATα, leu2Δ1, his3Δ200, trp1Δ63, ura3-52, lys2Δ202, caf4::KanMX, mdv1:: MET25-MDV1*
JSY10005	*MATα, leu2Δ1, his3Δ200, trp1Δ63, ura3-52, lys2Δ202, dnm1::HIS3, fis1::HIS3, caf4::KanMX, mdv1:: MET25-hfis1(1-119aa)-yfis1(122-155aa)*
JSY10006	*MATα, leu2Δ1, his3Δ200, trp1Δ63, ura3-52, lys2Δ202, dnm1::HIS3, fis1::HIS3, caf4::KanMX, mdv1:: MET25-hmff(1-198aa)-yfis1(127-155aa)*
JSY10007	*MATα, leu2Δ1, his3Δ200, trp1Δ63, ura3-52, lys2Δ202, dnm1::HIS3, fis1::HIS3, caf4::KanMX, mdv1:: MET25-TOM20(1-51aa)-hMiD49(48-454aa)*
JSY10009	*MATα, leu2Δ1, his3Δ200, trp1Δ63, ura3-52, lys2Δ202, dnm1::HIS3, fis1::HIS3, caf4::KanMX, mdv1:: MET25-TOM20(1-51aa)-hMiD51(47-463aa)*

Table 3.2: Plasmids Used in Chapter 3

ID	Plasmid	Protein expressed
B1642	*p414GPD-mito-ffRFP*	*N. crassa* ATP9(1-69aa)+ff DsRed
B1816	*pRS416MET25-hDRP1*	hDrp1 (isoform 3)
B1808	*pRS415MET25-MDV1*	Mdv1
B2053	*pRS416MET25-MDV1*	Mdv1
B2729	*pRS415MET25-T20-mdv1-FL*	T20(1-51aa)-Mdv1(1-714aa)
B2731	*pRS415MET25-T20-mdv1-CCWD*	T20 (1-51aa)-Mdv1(218-714aa)
B2732	*pRS415MET25-T20-mdv1-WD*	T20(1-51aa)-Mdv1 (317-714aa)
B3090	*pRS415MET25-mOMGFP-yFis1*	mOMGFP-yFis1-TM (131-155aa)
B3162	*pYSG-IBA167-hDrp1*	Flag-Strep-PP-hDrp1 (isoform 3)
B3259	*pYSG-IBA167-hMiD49*	Flag-Strep-PP-hMiD49(48-454aa)
B3262	*pYSG-IBA167-hMff*	Flag-Strep-PP-hMff(1-198aa)
B3265	*pRS416CUP1-mGFP-hDrp1*	mGFP-hDrp1 (isoform 3)
B3294	*pYSG-IBA167-10xHis-hMiD49*	Flag-Strep-PP-His-hMiD49 (48-454aa)
B3357	*pMAL-c2x-hMff*	MBP-10xHIS-PP-hMff (1-198aa)

Abbreviations: h, human; y, yeast; PP, PreScission Protease Cleavage Site; T20, TOM20; mOMGFP, monomeric mitochondrial outer membrane GFP; aa, amino acids; TM, trans-membrane domain; FL, full length; CCWD, coiled coil + WD repeat; WD, WD repeat

sites of the *pRS416* vector (Strategene) to create *pRS416CUP1*. This cloning step also introduced *EagI* and *BamHI* sites upstream of the *SalI* site. Second, a three-way ligation reaction was performed with *pRS416CUP1* and PCR amplified fragments encoding monomeric GFP^{A207K} and human Drp1 using *EagI*, *BamHI* and *SalI* sites. B3265 contains the following order of genes and restriction sites: *pRS416 vector-SacII-CUP1-EagI-mGFP-BamHI-DRP1-SalI- pRS416 vector*. B3357 was created by cloning PCR amplified sequences encoding residues 1-198aa of human Mff into the *EcoRI* and *HinDIII* sites of pMAL-c2x vector (New England Biolabs).

Fluorescence Microscopy

Mitochondrial morphologies were quantified as described previously (Amiott et al., 2009; Koirala et al., 2010) in the indicated strains expressing mitochondrial-matrix targeted fast-folding RFP (mito-ffRFP also referred to as mito-RFP) or mitochondrial outer membrane-targeted GFP (mito-OMGFP). Unless noted in the text, Mdv1, Mff and MiD49/51 proteins were expressed from the *MET25* promoter and integrated at the *MDV1* locus. Dnm1 and GFP-Dnm1 were expressed from the native promoter and locus. Drp1 (variant 3) and GFP-Drp1 were expressed from the *MET25* and *CUP1* promoters, respectively, on pRS416.

Overnight cultures were grown at 30°C in the appropriate selective synthetic dextrose (SD) medium containing 100 µg/mL methionine were diluted to 0.2 OD_{600} in medium containing 10 µg/mL methionine and grown for 3-5 hours. Western blotting and imaging confirmed that DRP and adaptor proteins were stably expressed from the *MET25* and *CUP1* promoters under these conditions. For GFP-Dnm1 analysis, cells were grown as described above but continually diluted into SD medium lacking methionine (to

maintain an OD_{600} between 0.2 and 1.0) and scored at the indicated times. Mitochondrial phenotypes and formation of GFP-Dnm1 puncta were scored in 100 cells, and data are represented as the average and S.E.M. of at least three independent experiments. Images were acquired and processed as described (Koirala et al., 2010).

Time-lapse Imaging

For single-color time-lapse imaging, cells expressing mito-RFP were grown in selective synthetic dextrose medium and applied to concanavalin A (2 mg/ml, Sigma) treated Lab-tek II Chamber wells (Thermo Scientific) maintained at 30°C. Z-stacks (0.2 μm optical sections) of fields of cells were acquired every 7 seconds over a 20 minute time course using a 3-I Marianas Live Cell Imaging microscope workstation (Denver, CO), equipped with dual ultra-sensitive Cascade II 512B EMCCD cameras (Roper Scientific, RS) configured with a Roper Dual-cam and Sutter DG-4 Illuminator (Sutter Instruments) with a 100X, 1.45 NA Plan-Apochromat objective (Zeiss). Data were deconvolved and analyzed using SlideBook 4.2 software (Intelligent Imaging Innovations, Inc). Substacks containing fission events were isolated from the entire stack to minimize signal background and assembled in Photoshop (CS3, Adobe). Brightness and contrast were adjusted using only linear operations applied to the entire image. For quantification, only cells that underwent one or more fission or fusion event during the time-course were selected for analysis. The results were expressed as the number of fission or fusion events per cell per 20-minute interval.

For two-color time-lapse imaging, cells expressing GFP-Drp1, mito-RFP and the indicated mammalian adaptor (MiD49, MiD51 or Mff) were grown in selective synthetic dextrose medium and applied to a Microfluidic chamber Y04c (Cellasic Corp.). Injection

of cells and medium was controlled by an ONIX Microfluidic Perfusion System and ONIX FG Version 2.6 software (Cellasic Corp.). Z-stacks of cells (0.3 μm optical sections) were imaged every 30 seconds over an 30-minute time-course using an Observer Z1 microscope (Zeiss) equipped with HE GFP (set 38) and mRFP (set 63) shift free filter sets, an Axiocam MRm Rev.3 camera and a 100X, 1.4 NA Plan-Apochromat objective (Zeiss). GFP and DsRed channels were acquired sequentially using AxioVision 4.8 software (Zeiss), and data were deconvolved and analyzed using AxioVision 4.6 software (Zeiss). Substacks containing fission events were isolated and assembled as described above.

Protein Production

Human Drp1 (isoform 3; NP_005681.2), MiD49 (accession number Q96C03) and Mff (accession number Q9GZY8) constructs, each containing an N-terminal PreScission protease cleavage site and a FLAG®-One-STrEP tag (IBA), were expressed in JSY9612. Overnight cultures were diluted into selective SD medium containing 1 mM $CuSO_4$ to induce expression (final OD_{600} of 0.2) and grown in a Belco fermentor at 30°C for 24 hours. After harvesting, cell pellets were snap frozen in liquid nitrogen as small droplets and pulverized in a Freezer Mill (3 minutes x 15 cycles). All subsequent purification steps were performed at 4°C. Cell powders were dissolved in either high ionic strength lysis buffer (for hDrp1 – 100 mM Tris-Cl-pH-8.0, 500 mM NaCl, 1 mM DTT, 1 mM EDTA) or low ionic strength buffer (for MiD49 or Mff - 100 mM Tris-Cl-pH-8.0, 150 mM NaCl, 1 mM DTT, 1 mM EDTA) containing Protease Inhibitor Cocktail III (Calbiochem). The lysates were clarified by centrifugation at 30,000 x g for 1 hour, filtered (0.45 μm), loaded onto 5 mL StrepTrap HP column (GE Healthcare), washed

with 1 liter lysis buffer and cleaved in the column with PreScission protease (GE Healthcare) for 16 hours. Drp1 was dialyzed against 20 mM HEPES pH 7.4, 150 mM KCl, 2 mM $MgCl_2$, 1 mM DTT, 0.5 mM EDTA, snap frozen in liquid nitrogen and stored at -80°C. Mff and MiD49 were further purified by size exclusion chromatography (Sepharose 200, GE Healthcare), dialyzed against 20 mM HEPES pH 7.4, 150 mM KCl, 2 mM $MgCl_2$, 1 mM DTT, 0.5 mM EDTA and stored at 4°C. Equilibrium sedimentation analysis performed on purified protein indicated that Drp1 variant 3 is a dimer in high ionic strength buffer (MW_{obs}/MW_{cal} = 2.17), the cytoplasmic domain of Mff is a dimer ((MW_{obs}/MW_{cal} = 2.25) and the cytoplasmic domain of MiD49 is a monomer (MW_{obs}/MW_{cal} = 0.99).

Analytical Equilibrium Sedimentation

The purified Drp1, MiD49 and Mff proteins were each centrifuged at a minimum of three concentrations (see Figure S1 legend) and two speeds (Drp1, 8,000 and 10,000 rpm; MiD49, 8,000, 10,000 and 12,000 rpm; and Mff, 10,000 and 12,000 rpm) at 4°C until equilibrium was established. Data were globally fit to an ideal single species model with a floating molecular weight using nonlinear least squares analysis as implemented in HETEROANALYSIS (Cole, 2004). Representative data are shown for 10,000 rpm, with the MW fit and oligomeric state indicated. Buffers used for the analysis were Drp1 (20 mM Hepes 7.4, 500 mM KCl, 2 mM $MgCl_2$, 1 mM EDTA, 1 mM DTT), MiD49 (100 mM Tris-Cl 8.0, 150 mM NaCl, 1 mM EDTA, 1 mM TCEP), and Mff (50 mM Sodium Phosphate 7.4, 150 NaCl). Bottom panels show the residual differences between the data and the fit. Buffer densities and protein partial specific volumes were calculated with

SEDNTERP (version 1.09) (Laue et al., 1992). For Drp1, 11% of the sample was lost during centrifugation (either to self-assembly or aggregation).

GTPase Assay

Inorganic phosphate release was measured using the malachite green phosphate assay (POMG-25H; BioAssay Systems) as described by the manufacturer and in Leonard et al. (Leonard et al., 2005). For the time course analysis, Drp1 (0.6 μM) was assayed at 37°C in high (500 mM KCl) or low (50 mM KCl) ionic strength buffer containing 20 mM HEPES pH 7.4, 2 mM $MgCl_2$, 1 mM DTT, 100 μM GTP. Reactions were halted at the indicated times by diluting 20 μL in 25 mM EDTA (final concentration) in a microtiter plate. Although 25mM EDTA was sufficient to halt the reaction, we found that higher EDTA concentrations lowered the signal generated by the malachite reagent during the development step. Samples were incubated at room temperature with 20 μL Malachite Reagent (BioAssay Systems) and 60 μL water for 30 minutes and the absorbance at 600 nm was measured using a Modulus^{TM} Microplate Reader (Turner BioSystems). For the steady state kinetic analyis, GTP assays were performed at 37°C in reactions containing 0.6 μM Drp1, 20 mM HEPES pH 7.4, 50 mM KCl, 2 mM $MgCl_2$, 1 mM DTT containing variable GTP concentrations (0, 25, 50, 75, 100, 200, 300, 500, 1000, 1500 and 2000 μM). Fixed volumes were removed every 5 minutes for 70 minutes, quenched by EDTA and developed as described above. K_{cat} and $k_{0.5}$ were calculated in GraphPad Prism using nonlinear regression curve fitting. For time course analyses with adaptor proteins, GTPase assays were performed in reactions containing Drp1 (0.1 μM) plus or minus Mff (0.5 μM) or MiD49 (0.5 μM) at 37°C in 50 μM KCl, 20 mM HEPES pH 7.4, 2 mM $MgCl_2$, 1 mM DTT and 200 μM GTP. In all experiments, data shown are

the average and S.E.M. values obtained from triplicate samples analyzed at the same time. Each experiment was repeated three times.

Velocity Sedimentation and Flotation Assays

For the velocity sedimentation assay (Figure 5C), 1.25 μM Drp1 was incubated either in low ionic strength buffer (20 mM HEPES – pH 7.4, 50 mM KCl, 2 mM $MgCl_2$, 1 mM DTT) or high ionic strength buffer (20 mM HEPES – pH 7.4, 500 mM KCl, 2 mM $MgCl_2$, 1 mM DTT) for 1 hour at 37°C. The reactions were spun down at 40,000 rpm (TLA 100 rotor) in a Beckman Optima MAX Ultracentrifuge for 1 hour at 25°C. Supernatants were removed and pellet fractions were resuspended in an equal volume of buffer. Twenty-five microliter of total, supernatant and pellet fractions were separated on 10% SDS-PAGE gels and stained with Coomassie Brilliant Blue (CBB) dye. For the velocity sedimentation in Figure 7A, 1.25 μM $MiD49^{\Delta TM}$, 1.25 μM Drp1 or 1.25 μM of both proteins were dialyzed at 25°C into 20 mM HEPES – pH 7.4, 25 mM KCl, 2 mM $MgCl_2$, 1 mM DTT, 200 μM GMP-PCP for six hours. Samples were pelleted and processed for SDS-PAGE as described above.

Liposome Preparation

(POPC) 1-palmitoyl-2-oleoyl-*sn*-glycero-3-phosphocholine, (POPS) 1-palmitoyl-2-oleoyl-*sn*-glycero-3-phospho-L-serine, Cholesterol, (Rhodamine-PE) 1,2-dipalmitoyl-*sn*-glycero-3-phosphoethanolamine-N-(lissamine rhodamine B sulfonyl) (ammonium salt), (Ni^{2+}-NTA-DOGS) 1,2-dioleoyl-*sn*-glycero-3-[(N-(5-amino-1-carboxypentyl) iminodiacetic acid)succinyl] (nickel salt) and (DOPS) 1,2-dioleoyl-*sn*-glycero-3-phospho-L-serine were purchased from Avanti Polar Lipids in chloroform. 4 types of

mixtures were prepared: 1) POPC, POPS, Cholesterol, Rhodamine-PE were mixed in a molar ratio 44.4:37:18:5:0.007 (37%PS liposomes), 2) POPC, POPS, Cholesterol and Ni2+-NTA-DOGS were mixed in a molar ratio 44.4:31:18.5:6 (Nickel liposomes), 3) 100% DOPS (DOPS liposomes) and 4) POPC:Cholesterol were mixed in a molar ratio 80:20 (neutral liposomes). Chloroform was evaporated by gentle vortexing under a steady stream of Nitrogen gas to make a thin lipid film around the walls of glass vials. These films were dried under vacuum for 1 hour at room temperature. Dried lipid films were then resolubilized in absolute hexane. The hexane was also evaporated under streaming nitrogen while vortexing, followed by a second round of dessication for 3-4 hours at room temperature. Lipid films were suspended in aqueous buffer (20mM HEPES pH 7.5, 100mM KCl) by vortexing at room temperature. Aliquots from the liposome preparation were stored at -80°C.

Flotation Assays

Liposomes and proteins were mixed in a molar ratio 1000:1 (lipid:protein) in Beckman polycarbonate centrifuge tubes. After a 1-hour incubation at 4°C, the mixtures were homogenized with 300μL 2M sucrose in 20 mM Hepes 7.5, 100 mM KCl, 1 mM GMP-PCP (~1.5M final sucrose concentration). Two additional layers of 1M (150μL) and 0.5M (300μL) sucrose in the same buffer were carefully overlaid (in that order) on top of the homogenized mixture. The mixtures were spun using a TLS-55 rotor in a Beckman centrifuge for 1 hour at 54000 rpm (4°C). After the spin, the liposomes migrated to interfaces between individual sucrose layers and could be seen as turbid bands. The interfaces between individual sucrose layers were collected by pipetting and analyzed by 10% SDS-PAGE and CBB staining.

In Vitro Membrane Binding and Tubulation Reactions

For DRP1 tubulation reactions, DOPS liposomes were mixed with protein (1:1, mass:mass). After 1 hour, GMP-PCP was added and the sample was incubated for 4 hours at room temperature. The effects of GTP hydrolysis were analyzed in two ways. First, after adsorption of the lipid and protein mixtures to EM grids, the sample was washed in 1mM GTP before immediately blotting and staining. Second, a stock of 10mM GTP was added to lipid-protein mixtures to a final concentration of 1mM GTP for 30 minutes before applying to EM grids for staining.

For DRP1-MID49 co-polymerization, proteins were mixed 1:1 mass:mass, with or without liposomes and dialyzed overnight against 20mM HEPES, 25mM KCl, 200mM GMP-PCP, 20mM $MgCl_2$ and 1mM DTT.

Electron Microscopy

For negative stain EM, carbon coated copper grids were glow discharged for 15 seconds. Five mictoliter of the sample were added to the surface, blotted and stained with 1% Uranyl Acetate. Images were acquired using an FEI Tecnai T12 electron microscope equipped with a LaB6 filament and operated at 120kV. Magnifications of 21000X-42000X were recorded on a Gatan CCD.

Results

Requirements of Individual Yeast Proteins for Mitochondrial Fission

In WT yeast, opposing fission and fusion events maintain branched mitochondrial tubules positioned at the cell cortex. When fission is disrupted, fusion continues unopposed and cells contain mitochondrial nets or a single, interconnected

mitochondrion, which often collapses to one side of the cell (Bleazard et al., 1999; Otsuga et al., 1998). To determine the minimal protein requirements for fission, we generated a yeast 'tester' strain lacking Dnm1, the Mdv1 adaptor and Fis1. This strain also lacked a paralog of the Mdv1 adaptor, Caf4, which was previously shown to be dispensable for fission *in vivo* (Griffin et al., 2005). This tester strain exhibited severe mitochondrial fission defects but was viable, grew as well as WT on a variety of media, and did not show increased mitochondrial DNA loss (unpublished data). To identify the minimal set of proteins sufficient for fission, we expressed combinations of wildtype (WT) and mitochondrial membrane-tethered Dnm1 and Mdv1 in the tester strain. Immunoblotting of whole cell extracts confirmed that all proteins were stably expressed at levels similar to the wildtype proteins *in vivo* (unpublished results). Mitochondrial morphology was then quantified to assess the ability of different protein combinations to restore WT mitochondrial fission and morphology.

Expression of cytoplasmic Dnm1, or Dnm1 tethered to the outer mitochondrial membrane by its N- or C-terminus was unable to rescue mitochondrial fission defects in the tester strain (unpublished data). Pair wise combinations of cytoplasmic Dnm1 expressed with WT Fis1 or Mdv1 alone also failed to rescue mitochondrial morphology in this strain (unpublished results). By contrast, normal mitochondrial morphology was restored in 80% of the cells by expressing cytoplasmic Dnm1 together with WT Mdv1 and Fis1 (Figure 3.1B). To determine whether Fis1 was necessary for post Dnm1 recruitment steps in fission, we expressed cytoplasmic Dnm1 with full-length and truncated forms of Mdv1 tethered to the outer mitochondrial membrane by the Tom20

Figure 3.1. Fis1 is Dispensable for Mitochondrial Fission
(A) Domain structure of WT Mdv1 and Mdv1 constructs fused to the N-terminal transmembrane anchor of yeast TOM20 (T20). NTE (N-terminal extension), CC (coiled coil), and predicted β-propeller domains are shown. (B) Quantification of mitochondrial morphology in cells expressing the indicated fission proteins. All values are mean ± SEM, $n \geq 300$. A representative image of WT tubular mitochondria is shown in Figure 4C.

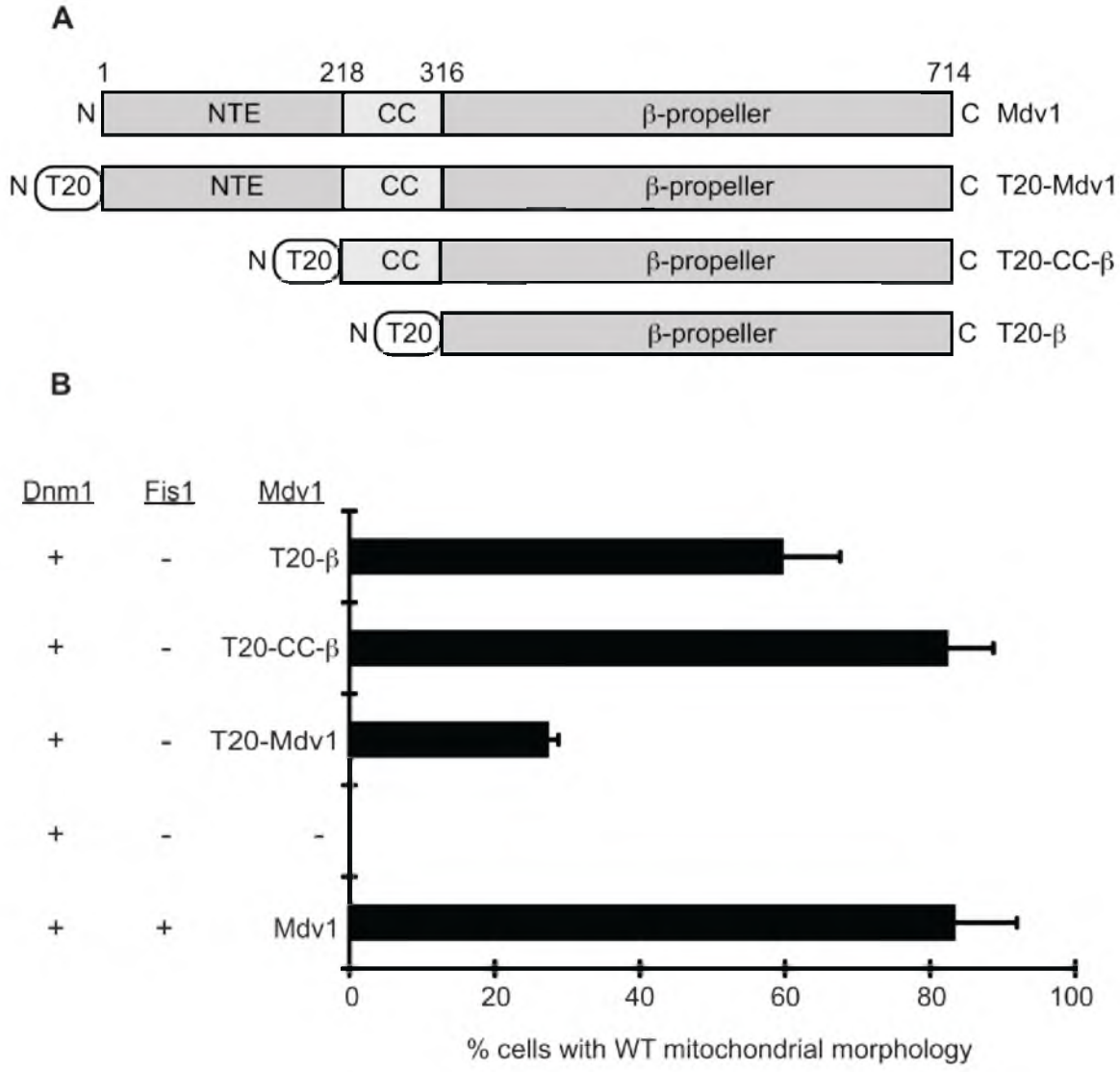
A
1
218
316
714
N
NTE
CC
β-propeller
C
Mdv1
N
T20
NTE
CC
β-propeller
C
T20-Mdv1
N
T20
CC
β-propeller
C
T20-CC-β
N
T20
β-propeller
C
T20-β
B
Dnm1
Fis1
Mdv1
+
-
T20-β
+
-
T20-CC-β
+
-
T20-Mdv1
+
-
-
+
+
Mdv1
0
20
40
60
80
100
% cells with WT mitochondrial morphology

membrane anchor (T20, Figure 3.1A). Mdv1 contains three domains, an N-terminal extension (NTE) that binds Fis1 (Tieu et al., 2002), a middle domain that dimerizes Mdv1 via an antiparallel coiled-coil (CC) (Koirala et al., 2010), and a predicted β-propeller domain that interacts with Dnm1 (Cerveny and Jensen, 2003; Tieu et al., 2002) (Figure 3.1A). Surprisingly, although WT mitochondrial morphology was restored in strains expressing Dnm1 plus all three tethered forms of Mdv1, the full-length construct was not the most efficient. The lack of a Fis1 binding partner for the NTE domain in the full-length Mdv1 construct may affect the conformation of the protein and be responsible for this effect. Consistent with this idea, the most efficient rescue occurred upon expression of the tethered Mdv1 coiled-coil plus β-propeller domain (lacking the NTE domain) (Figure 3.1B). The mitochondrial morphology rescue observed in these studies suggests that soluble Dnm1 and tethered forms of Mdv1 are sufficient to catalyze fission in the absence of Fis1.

Fis1 Is Not Essential for Dnm1 Assembly into Fission Complexes or Membrane Scission

When cells lack Mdv1 and Fis1, GFP-Dnm1 cannot be recruited to mitochondria and instead remains in the cytoplasm (unpublished results). When WT Mdv1 and Fis1 are present, GFP-Dnm1 assembles into punctate fission complexes distributed evenly along mitochondrial tubules (Figure 3.2A and B, top row). Consistent with their ability to rescue fission defects, all three forms of tethered Mdv1 were able to recruit GFP-Dnm1 to mitochondria in the absence of Fis1 (Figure 3.2A and B). The formation and distribution of GFP-Dnm1 complexes were similar to that observed in WT cells (Figure

Figure 3.2. Dnm1 Fission Complexes Assemble on Mitochondria in the Absence of Fis1

(A) Punctate GFP-Dnm1 fission complexes on mitochondria were quantified in strains expressing the indicated fission proteins. All values are mean ± SEM, n ≥ 300. (B) Representative images of GFP-Dnm1 puncta on mitochondria quantified in (A). Differential interference contrast (DIC), GFP-Dnm1, and merged mito-RFP (mitochondrial-matrix targeted dsRed) images are shown. Scale bar, 5 μm.

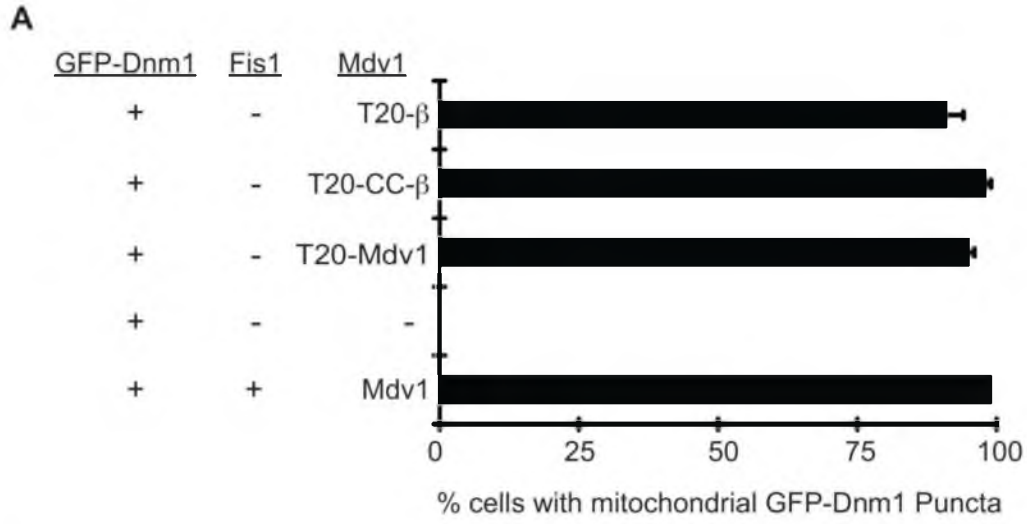
A
GFP-Dnm1
Fis1
Mdv1
+ - T20-β
+ - T20-CC-β
+ - T20-Mdv1
+ - -
+ + Mdv1
0
25
50
75
100
% cells with mitochondrial GFP-Dnm1 Puncta

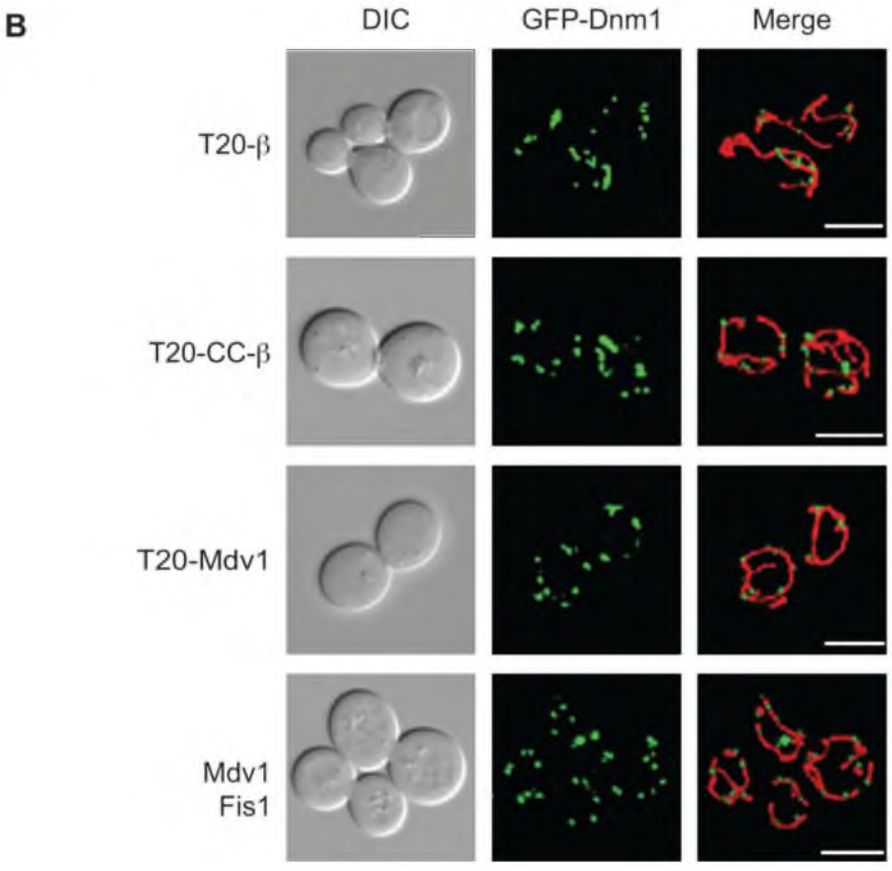
B
DIC
GFP-Dnm1
Merge
T20-β
T20-CC-β
T20-Mdv1
Mdv1
Fis1

3.2B), despite the fact that fission complexes formed by two of the tethered Mdv1 proteins (T20-Mdv1, T20β) were less functional than Mdv1 T20-CC-β (Figure 3.1B).

In vivo, yeast mitochondrial fission and fusion are coordinated, each process occurring approximately once every 2 minutes (Nunnari et al., 1997). Although the molecular basis of this coordination is unknown, the balance is critical for robust mitochondrial function (Twig and Shirihai, 2011). Quantification of fission and fusion events in time lapse imaging studies confirmed that these processes were balanced in our WT yeast strain (Figure 3.3A). We next determined whether the balance of fission and fusion was altered when fission occurred without Fis1 in the tester strain (Figure 3.3B). When cells expressed only cytoplasmic Dnm1, unopposed fusion formed interconnected mitochondria with few or no free tips. As a consequence, once the system achieved steady state, neither fission nor fusion was observed. By contrast, when cells expressed cytoplasmic Dnm1 and tethered forms of Mdv1, fission and fusion events were once again balanced. Representative images of fission and fusion events in these cells are shown in Figure 3.3C. Together, our results demonstrate that after Mdv1 and Dnm1 are recruited to the mitochondrial surface, Fis1 is not required for assembly of functional fission complexes and the subsequent membrane scission event. Moreover, a balance between fission and fusion is achieved in these strains.

Mff or MiDs Are Sufficient to Recruit Human Drp1 to Mitochondria and Catalyze Fission

The hFis1, Mff and MiD49/51 adaptors are all expressed in mammalian cells. As a consequence, it has been difficult to definitively determine whether these adaptors work individually or in concert to influence fission complex assembly or mitochondrial

Figure 3.3. Mitochondrial Fission and Fusion Events in Cells Lacking Fis1
Box-and-whisker plot showing the distribution of fission ($n \geq 10$ cells) and fusion ($n \geq 10$ cells) events in (A) WT and (B) strains expressing the indicated fission proteins. Total fission or fusion events per cell for a twenty-minute interval are indicated. (C) Representative mito-RFP labeled mitochondria are shown undergoing fission (top, arrow) and fusion (bottom, arrow) in cells expressing Dnm1 and tethered Mdv1 (T20-β).

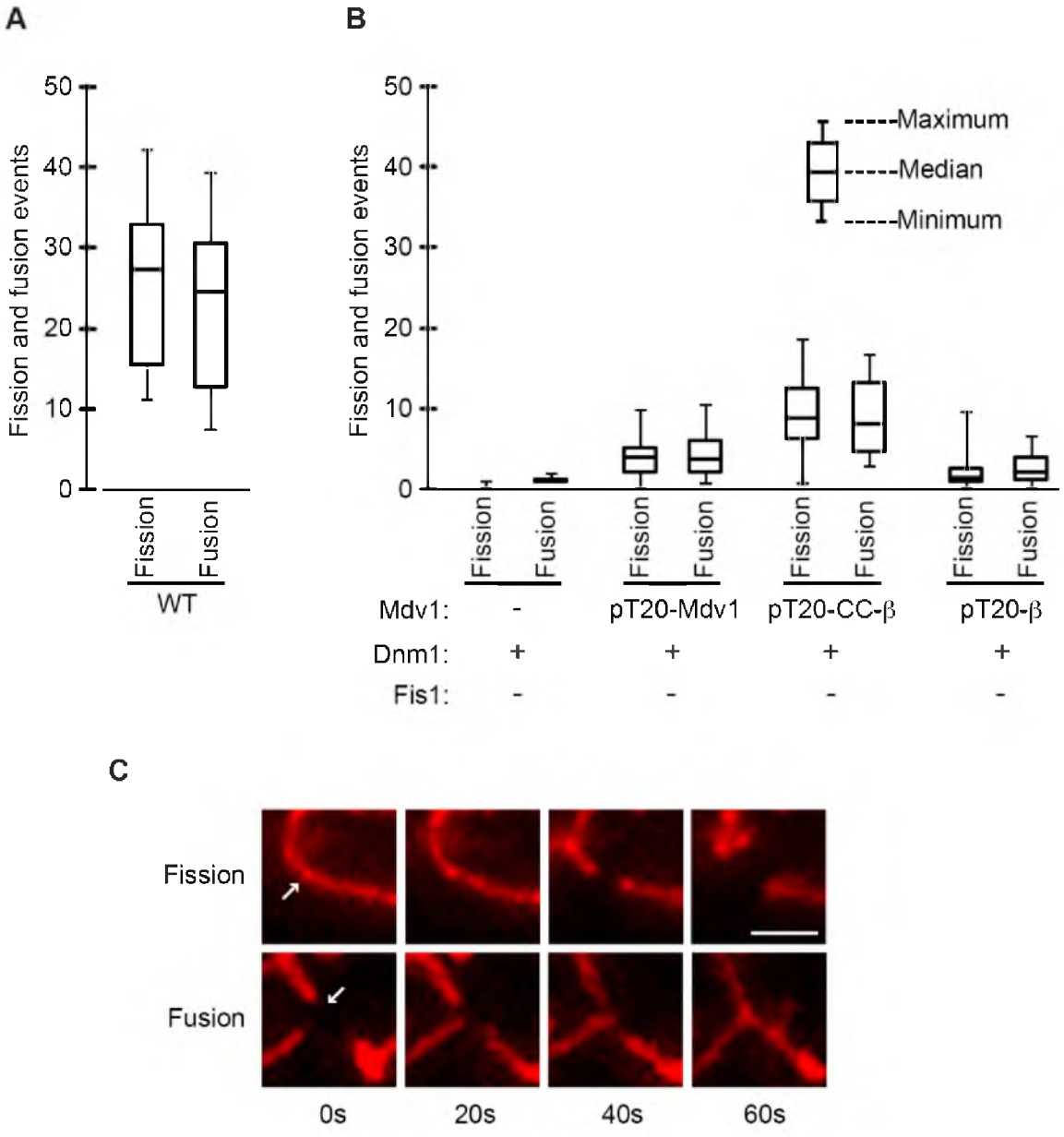
A
B
C
Fission and fusion events
50
40
30
20
10
0
Fission
Fusion
WT
-----Maximum
-----Median
-----Minimum
Mdv1: - pT20-Mdv1 pT20-CC-β pT20-β
Dnm1: + + + +
Fis1: - - - -
Fission
Fusion
0s
20s
40s
60s

division after Drp1 membrane recruitment. To address this issue, we individually expressed OMM tethered forms of each adaptor protein with soluble Drp1 (variant 3, NP_005681.2) in the yeast tester strain. To maintain their appropriate membrane topologies, the cytoplasmic domains of hFis1 and Mff were targeted using the yeast C-terminal Fis1 anchor (yTM) and the MiD proteins were targeted using the yeast N-terminal Tom20 anchor (T20) (Figure 3.4A).

In the absence of Drp1, expression of any of the three tethered forms shown in Figure 3.4A individually or in combination did not rescue fission defects (unpublished results). In addition, mitochondrial fission was not rescued by expression of Drp1 alone (unpublished results) or Drp1 with tethered hFis1 (Figure 3.4B). The latter result is consistent with a previous report that hFis1 is not essential for Drp1 recruitment in mammalian cells (Otera et al., 2010). By contrast, expression of soluble Drp1 with tethered Mff was sufficient to partially rescue mitochondrial fission and WT mitochondrial morphology *in vivo* (Figure 3.4B). Expressing tethered hFis1 in addition to Mff had little effect on this rescue. Thus, hFis1 does not appear to impact fission mediated by Drp1 and tethered Mff in this system.

We also examined mitochondrial fission rescue in a tester strain expressing Drp1 and MiD51 from the repressible *MET25* promoter. Prior to induction (Figure 3.4C, 0 hour.), approximately 79% of the cells in the population contained collapsed mitochondria and interconnected nets characteristic of a fission defect (Figure 3.4C, black). The remaining 21% contained WT tubular mitochondria (Figure 3.4C, grey) due to the fact that the *MET25* promoter is inefficiently repressed under these conditions and produces low levels of both Drp1 and MiD51 proteins. WT mitochondrial morphology

Figure 3.4. Mammalian Drp1 and Mitochondrial-Tethered Adaptor Proteins Rescue Mitochondrial Fission Defects in Yeast

(A) Domain structures of human Fis1 (hFis1) and Mff fused to the C-terminal outer membrane anchor of yeast Fis1 (yTM). Human MiD49 or MiD51 were targeted to the mitochondrial outer membrane via fusion to the N-terminal transmembrane anchor of yeast Tom20 (T20). (B) Quantification of mitochondrial morphology in cells expressing Mff plus the indicated fission proteins and mito-OMGFP. All values are mean ± SEM, n ≥ 300. (C) The graph shows quantification of mitochondrial morphologies observed in cells during induction of Drp1 and MiD51 from the *MET25* promoter. The merged DIC and mito-OMGFP images to the right of the graph are representative of the mitochondrial morphology categories scored. Scale bar, 5 μm. (D) Time-lapse images of GFP-Drp1 at fission sites in cells expressing Mff (top), MiD49 (middle) or MiD51 (bottom). Boxed regions mark fission sites imaged at 30 second intervals in each row. Scale bar, 2 μm.

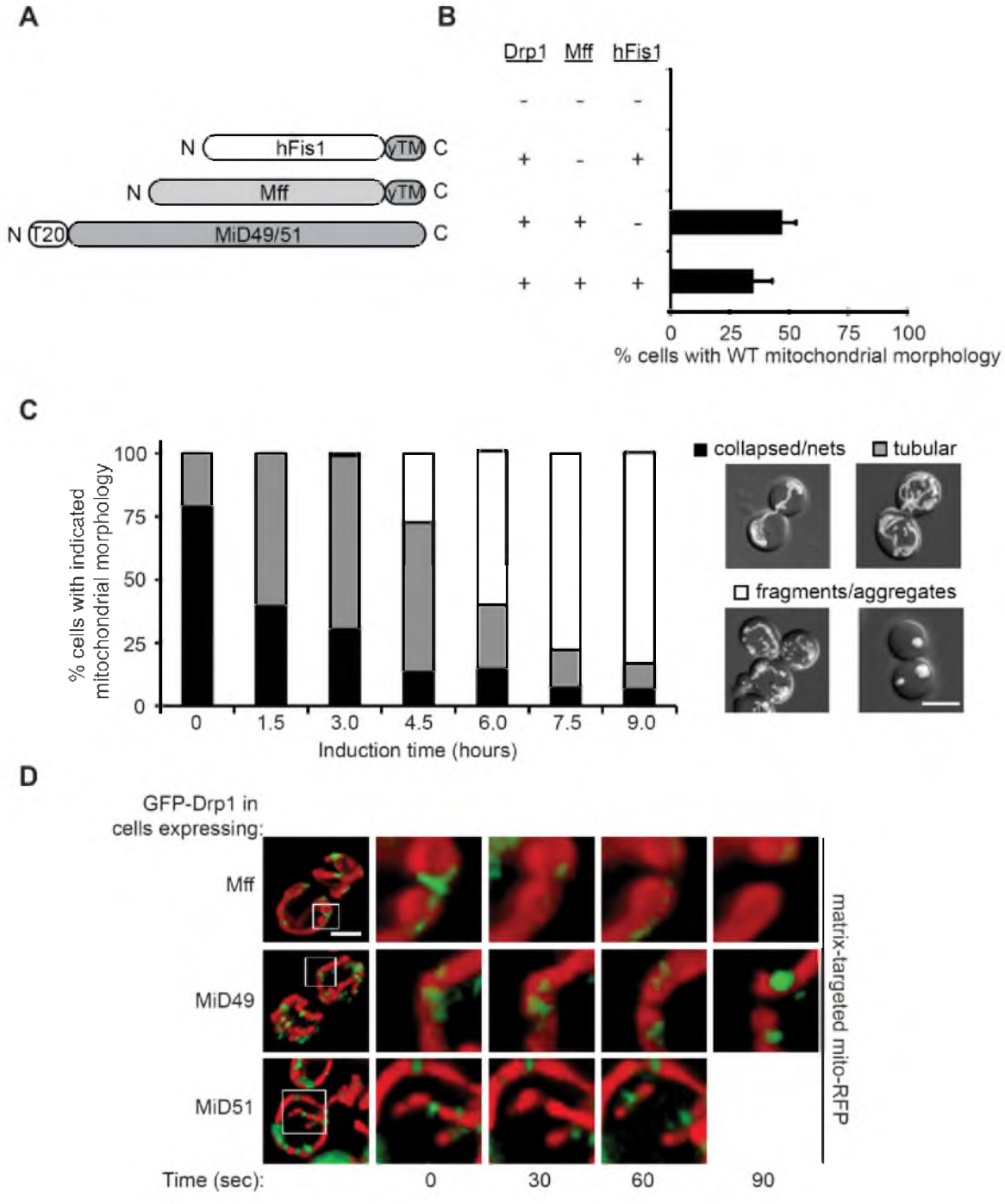
A
N hFis1 vTM C
N Mff vTM C
N T20 MiD49/51 C
B
Drp1 Mff hFis1
- - -
+ - +
+ + -
+ + +
0 25 50 75 100
% cells with WT mitochondrial morphology
C
% cells with indicated mitochondrial morphology
100
75
50
25
0
0 1.5 3.0 4.5 6.0 7.5 9.0
Induction time (hours)
collapsed/nets
tubular
fragments/aggregates
D
GFP-Drp1 in cells expressing:
Mff
MiD49
MiD51
matrix-targeted mito-RFP
Time (sec):
0 30 60 90

increased to 61% and 69% after 1.5 or 3.0 hours of MiD51 induction, respectively, suggesting that cytoplasmic Drp1 and tethered MiD51 are sufficient to catalyze fission in the yeast tester strain. Upon further induction (4.5-9 hours), the percentage of cells containing tubular mitochondrial morphology was reduced and the percentage of the population containing fragmented and aggregated mitochondrial membranes steadily increased from 27% to 83% (Figure 3.4C, white). This aggregated mitochondrial phenotype was also observed when MiD49 and MiD51 were over expressed in mammalian cells (Palmer et al., 2011). Similar results were obtained when the experiment was performed with MiD49 in place of MiD51 (unpublished results).

Time-lapse imaging studies confirmed that the mitochondrial morphology changes observed upon expression of Drp1 with either Mff, MiD49 or MiD51 was due to mitochondrial fission. In our tester strain expressing functional GFP-Drp1 and Mff, MiD49 or MiD51, green Drp1 puncta were observed on RFP-labeled mitochondrial tubules at sites where fission occurred (Figure 3.4D). Together, these results establish that Drp1 is able to function with multiple adaptors to catalyze mitochondrial membrane fission.

The Effect of Mff and MiD Adaptors on GTP Hydrolysis by Drp1

To determine whether mammalian adaptor proteins altered the kinetic properties of Drp1, we purified untagged versions of all three proteins (Drp1, Mff and MiD49). Analytical ultracentrifugation studies are consistent with Drp1 and Mff forming dimers, while MiD49 behaves as a monomer in solution (Figure 3.S1). As is characteristic of self-assembling GTPases in the dynamin family, Drp1 pelleted in low, but not high, ionic strength buffer in a standard sedimentation assay (Figure 3.5C). GTP-hydrolysis by Drp1

Figure 3.S1. Purification and Analytical Equilibrium Sedimentation Analysis of Drp1, MiD49 and Mff

(A) SDS-PAGE of the indicated purified proteins stained with Coomassie Brilliant Blue. Analytical equilibrium sedimentation analysis of (B) Drp1 (14.8 μM, 7.4 μM, 3.7 μM), (C) MiD49 (9.4 μM, 4.7 μM, 2.3 μM), and (D) Mff (130.0 μM, 65.1 μM, 32.6 μM). In (B-D), corresponding fits (MW_{obs}/M_{calc}) are indicated above each graph and residuals for the nonlinear least squared fits are shown below. See also Supplemental Experimental Procedures.

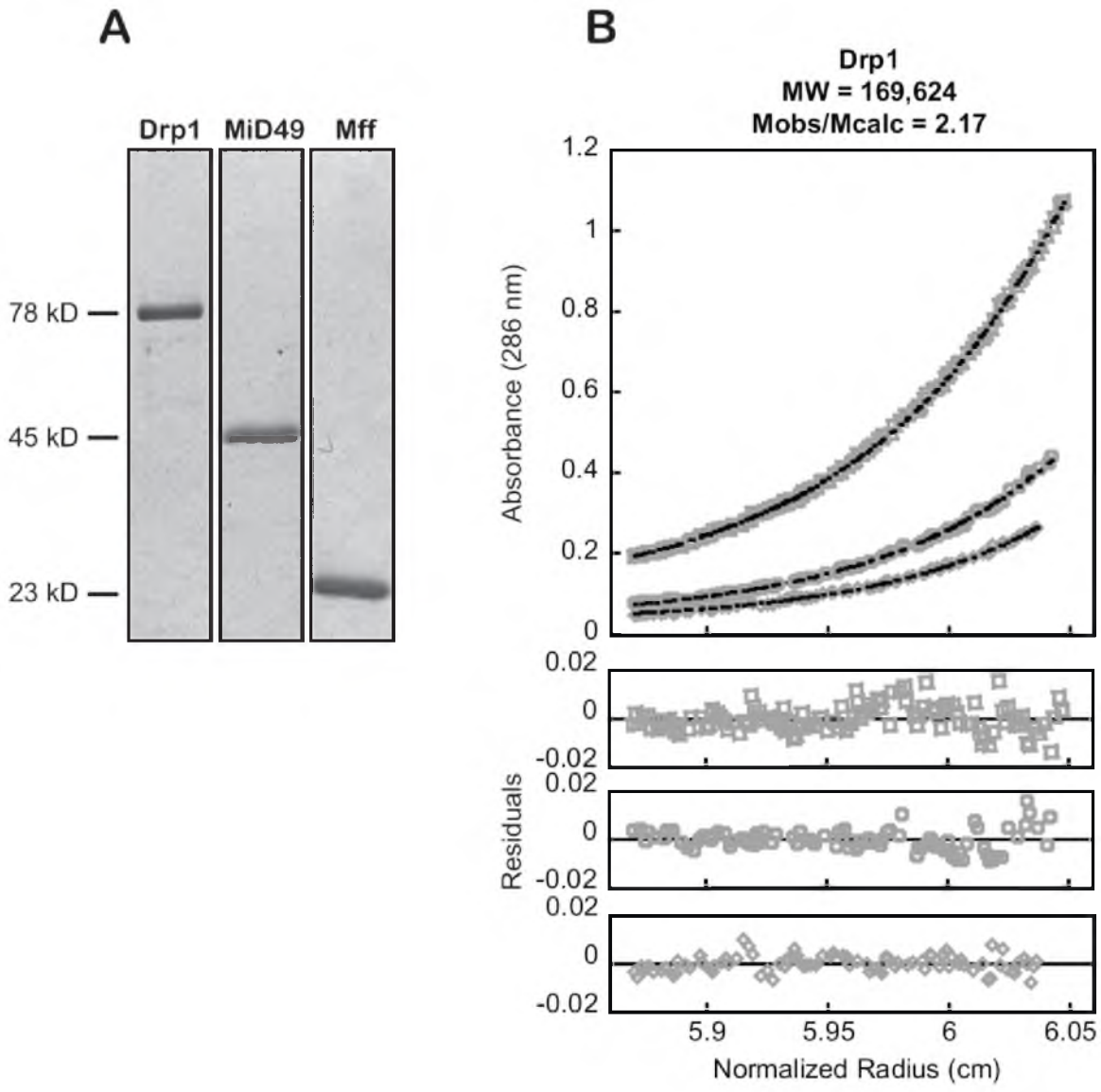
A
Drp1
MiD49
Mff
78 kD
45 kD
23 kD
B
Drp1
MW = 169,624
Mobs/Mcalc = 2.17
Absorbance (286 nm)
1.2
1
0.8
0.6
0.4
0.2
0
Residuals
0.02
0
-0.02
5.9
5.95
6
6.05
Normalized Radius (cm)

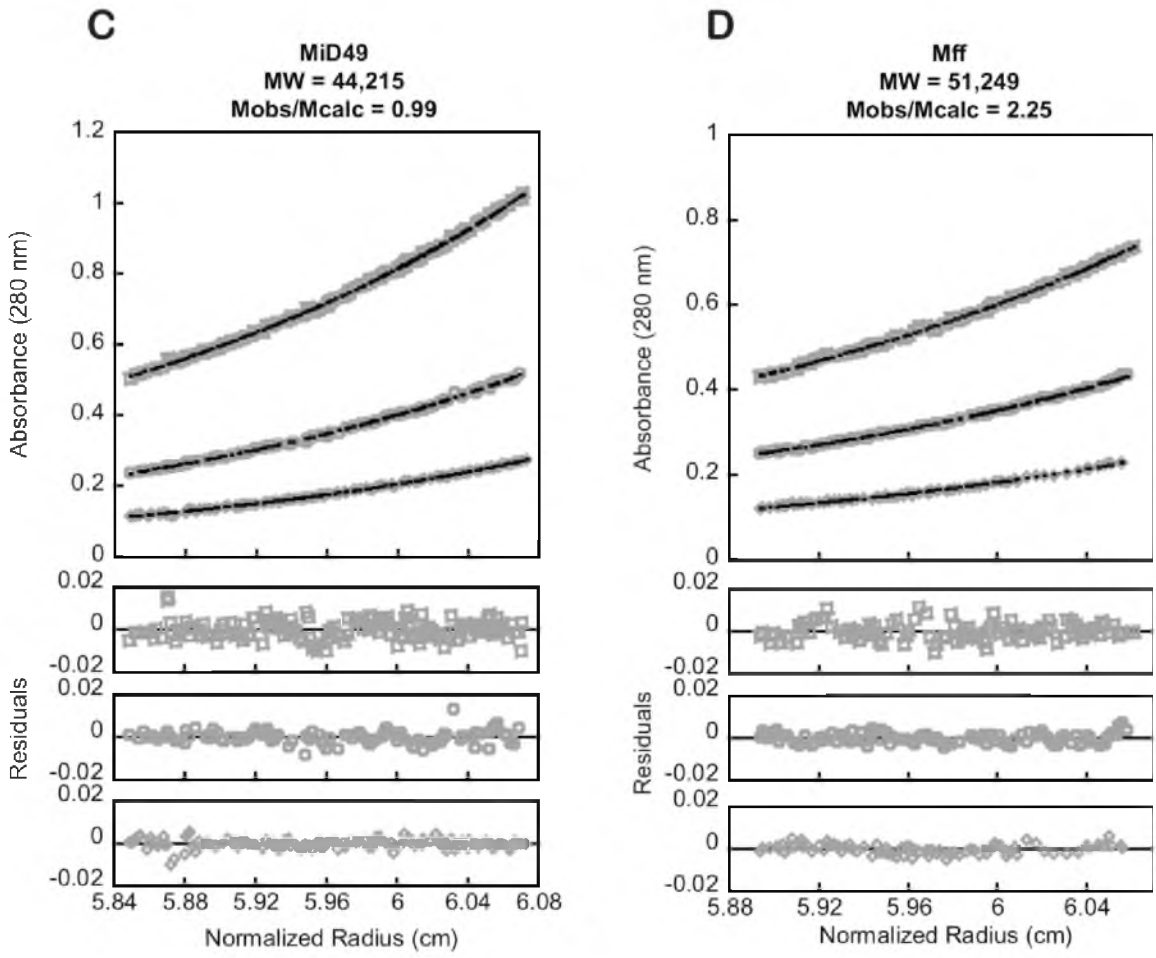
C
MiD49
MW = 44,215
Mobs/Mcalc = 0.99
Absorbance (280 nm)
Residuals
Normalized Radius (cm)
D
Mff
MW = 51,249
Mobs/Mcalc = 2.25
Absorbance (280 nm)
Residuals
Normalized Radius (cm)

Figure 3.5. Effects of Mff and MiD49 on Drp1 GTPase Activity
(A) Time course of GTP hydrolysis by Drp1 (0.6 μM) measured in 100 μM GTP, 37°C at high (500 mM KCl) and low (50 mM KCl) ionic strength. (B) Steady state kinetics of Drp1 (0.6 μM) GTP hydrolysis measured at low ionic strength (50 mM KCl), 37°C. (C) A Coomasie blue stained gel showing velocity sedimentation of Drp1 at high and low ionic strength. T, total; S, supernatant; P, pellet. (D) Drp1 kinetic parameters determined as described in (B) and the methods. k_{cat}, turnover number; V_{max}, maximal rate of hydrolysis; $K_{0.5}$, substrate concentration where velocity is one-half maximal. (E and F) GTP hydrolysis by Drp1 (0.1 μM) measured in 200 μM GTP, 50 mM KCl, 37°C in the presence and absence of the indicated adaptor proteins. Cytoplasmic domains of Mff (E) or MiD49 (F) purified from yeast were included at 0.5 μM. Similar results were obtained with Mff purified from yeast (shown here) and bacteria (unpublished data).

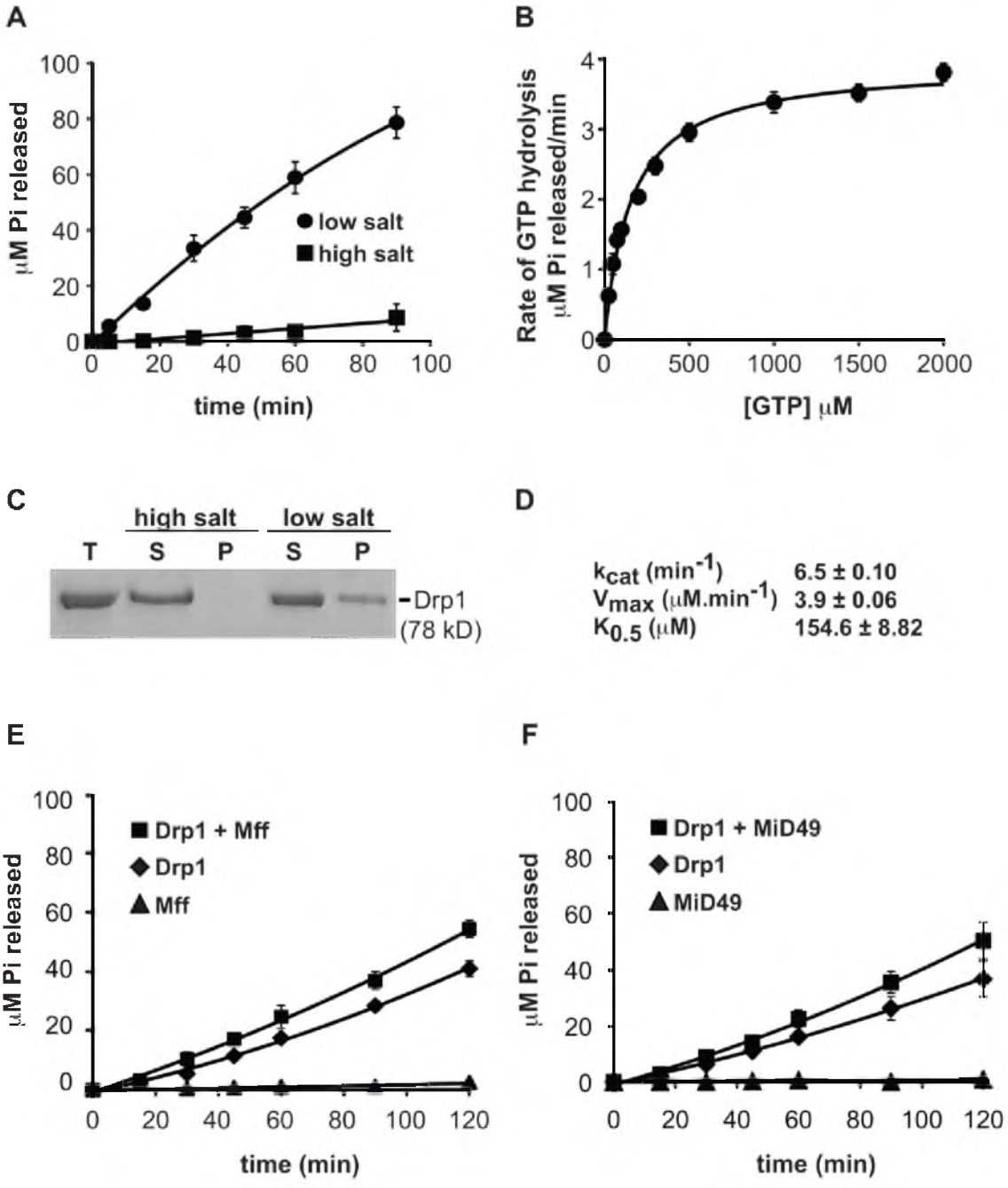
A
μM Pi released
time (min)
low salt
high salt
B
Rate of GTP hydrolysis
μM Pi released/min
[GTP] μM
C
high salt
low salt
T
S
P
S
P
Drp1
(78 kD)
D
kcat (min-1) 6.5 ± 0.10
Vmax (μM.min-1) 3.9 ± 0.06
K0.5 (μM) 154.6 ± 8.82
E
Drp1 + Mff
Drp1
Mff
μM Pi released
time (min)
F
Drp1 + MiD49
Drp1
MiD49
μM Pi released
time (min)

also increased up to 15 fold in low ionic strength buffer, indicating that self-assembly stimulated GTP hydrolysis (Figure 3.5A). Under assembly-stimulated conditions (low ionic strength, Figure 3.5B and D), the catalytic activity of Drp1 (k_{cat} = 6.5/min) was similar to that reported for the yeast mitochondrial dynamin Dnm1 (Lackner et al., 2009). However, the Drp1 catalytic activity shown here is 7.6 times greater than that reported previously for a CBP-Drp1 fusion protein (CBP, calmodulin-binding peptide) (Chang et al., 2010). It is possible that the N-terminal CBP tag on Drp1 or the bacterial expression system used to purify the CBP-Drp1 fusion protein contributed to the lower activity observed in the Chang et al. study. Importantly, the addition of Mff or MiD49 only modestly increased the assembly-driven GTP hydrolysis activity of Drp1 (Figure 3.5E and F). Thus, these adaptors do not act as classical effectors to enhance GTP hydrolysis by Drp1.

MiD49 Coassembles With Drp1 and Reduces Polymer Diameter

We used negative staining transmission electron microscopy (TEM) to analyze the structures formed by Drp1 *in vitro*. At low temperature, apo-Drp1 (without nucleotide) did not assemble into well-ordered structures (Figure 3.6A). When the non-hydrolyzable analog GMP-PCP was added, Drp1 assembled into rings with an average external diameter of 33.5 ± 4.1 nm (Figure 3.6B and G). Raising the temperature to 25°C in the presence of GMP-PCP, produced Drp1 spirals (34.4 ± 6.4 nm) that often excluded DOPS containing lipids present in the reaction (Figure 3.6C and asterisk). Less frequently, Drp1 was able to deform DOPS lipids in the presence of GMP-PCP at 25°C, forming tubes with ordered striations along their length (Figure 3.6D). Interestingly, the diameter of these Drp1 tubes was significantly smaller (64.7 ± 7.2 nm) than that reported

Figure 3.6. Drp1 Self-Assembly Induces Lipid Tubulation and Constriction *In Vitro*
(A-C) Transmission electron micrographs of negatively-stained Drp1 assemblies. (A) Drp1 protomers do not assemble in the absence of nucleotide at 4°C. (B) Drp1 assembles into limited rings in the presence of GMP-PCP at low temperature (white arrow). (C) At 25°C, Drp1 forms spirals or stacks of rings in the presence of GMP-PCP that exclude PS-containing lipids (asterisk). (D) Drp1 assembles around DOPS liposomes in the presence of GMP-PCP at 25°C. Drp1-decorated lipid tubes assembled in the presence of GMP-PCP were imaged after treatment with (E) 1mM GTP for 10 seconds or (F) 30 minutes. (G) Average external diameters of Drp1 structures in B-F (white arrowheads). For all measurements, n = 50. Bars are 50 nm.

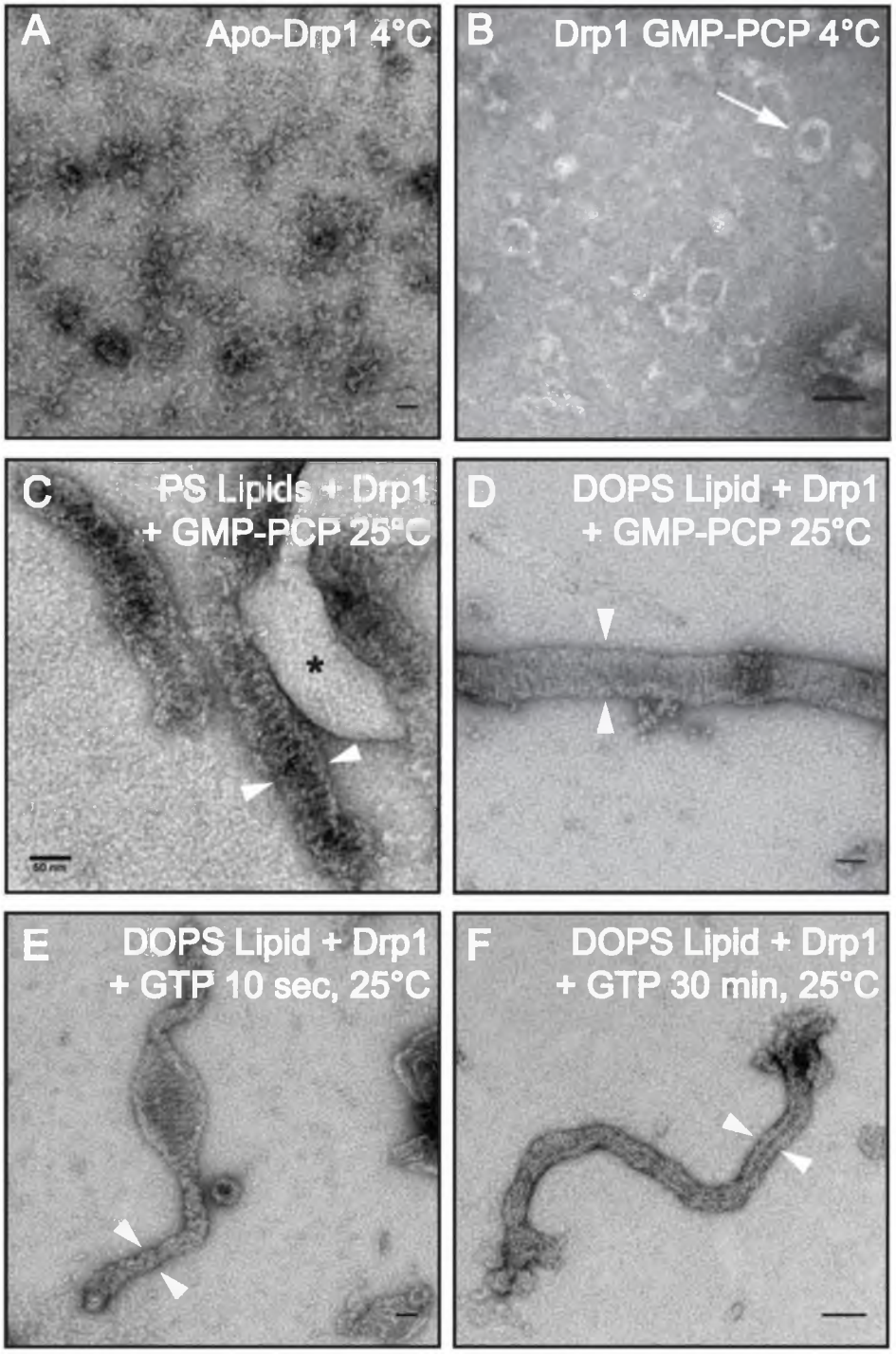

G

Structure	External diameter (nm)
Drp1 rings	33.5 +/- 4.1
Drp1 ring stacks	34.4 +/- 6.4
DOPS + Drp1 + GMP-PCP	64.7 +/- 7.2
DOPS + Drp1 + GTP	30.7 +/- 4.9

previously for Dnm1 assembled on lipids (109-121 nm, (Ingerman et al., 2005; Mears et al., 2011)). Constriction of these structures occurred upon exposure to GTP (Figure 3.6E and G), generating polymers with an average diameter of 30.7 ± 4.9 nm (Figure 3.6F and G).

We also analyzed the interaction of Drp1 with MiD49. In the presence of GMP-PCP, Drp1 self-assembles and pellets in a sedimentation assay (Figure 3.7A). Although the cytoplasmic domain of MiD49 alone (MiD49$^{\Delta TM}$) remains in the supernatant fraction, the adaptor sediments in the presence of Drp1, consistent with the idea that the two proteins bind to each other and may coassemble (Figure 3.7A). These findings were confirmed using a flotation assay (in the presence of GMP-PCP). His-tagged MiD49$^{\Delta TM}$ alone (His-MiD49$^{\Delta TM}$) was able to bind and float with liposomes containing nickel-modified lipids after centrifugation in a sucrose step gradient (Figure 3.7B, top, lane 1). This fractionation pattern was dependent upon the presence of nickel (Ni-NTA) lipids and did not occur when membranes lacking the Ni-NTA moiety were substituted in the experiment (Figure 3.7B, bottom, lane 1). Although Drp1 has a weak affinity for the Ni-NTA liposomes on its own (Figure 3.7B, top, lane 4), the fraction of Drp1 bound to these liposomes visibly increased in the presence of the MiD49 adaptor (Figure 3.7B, top, lane 7). In control experiments, MiD49 and Drp1 (alone or in combination) did not float with electrostatically-neutral lipids (Figure 3.7B, bottom, lanes 6 and 9).

Negative stain TEM revealed a dramatic effect of MiD49 on Drp1 polymer formation. At 25°C in the presence of GMP-PCP, Drp1 plus MiD49 formed extended, uniform polymers with distinct striations (Figure 3.7C, top). These polymers had an average external diameter of 14.9 ± 1.5 nm, which is less than half the diameter of ring

Figure 3.7. MiD49 Copolymerizes with Drp1 and Decreases Polymer Diameter
(A) MiD49$^{\Delta TM}$ (lacking the transmembrane domain) cosediments with Drp1. (B) DO DGS-NTA(Ni)-containing liposomes (top panel) decorated with His-tagged MiD49$^{\Delta TM}$ promote flotation of Drp1 in a sucrose step gradient. Charge-neutral liposomes (POPC/Cholesterol, bottom panel) bind His-tagged MiD49$^{\Delta TM}$ poorly and do not promote Drp1 flotation. As depicted in the cartoon gradient at the right, protein-bound liposomes float to the top of the 0.5 M sucrose layer. (C) Top, in the presence of MiD49$^{\Delta TM}$, Drp1 forms ordered polymers (arrows) with a diameter of 14.9 ± 1.5 nm. Bottom, periodicity (~5 nm) measured along the length of the Drp1:MiD49 polymers. (D) Effect of Drp1:MiD49 (molar:molar) ratios on polymer assembly. Decreasing MiD49 concentration reduces formation of narrow (14.9 nm) polymers (white arrowheads) and increases the diameter of larger (34.4 nm) polymers (black arrowheads).

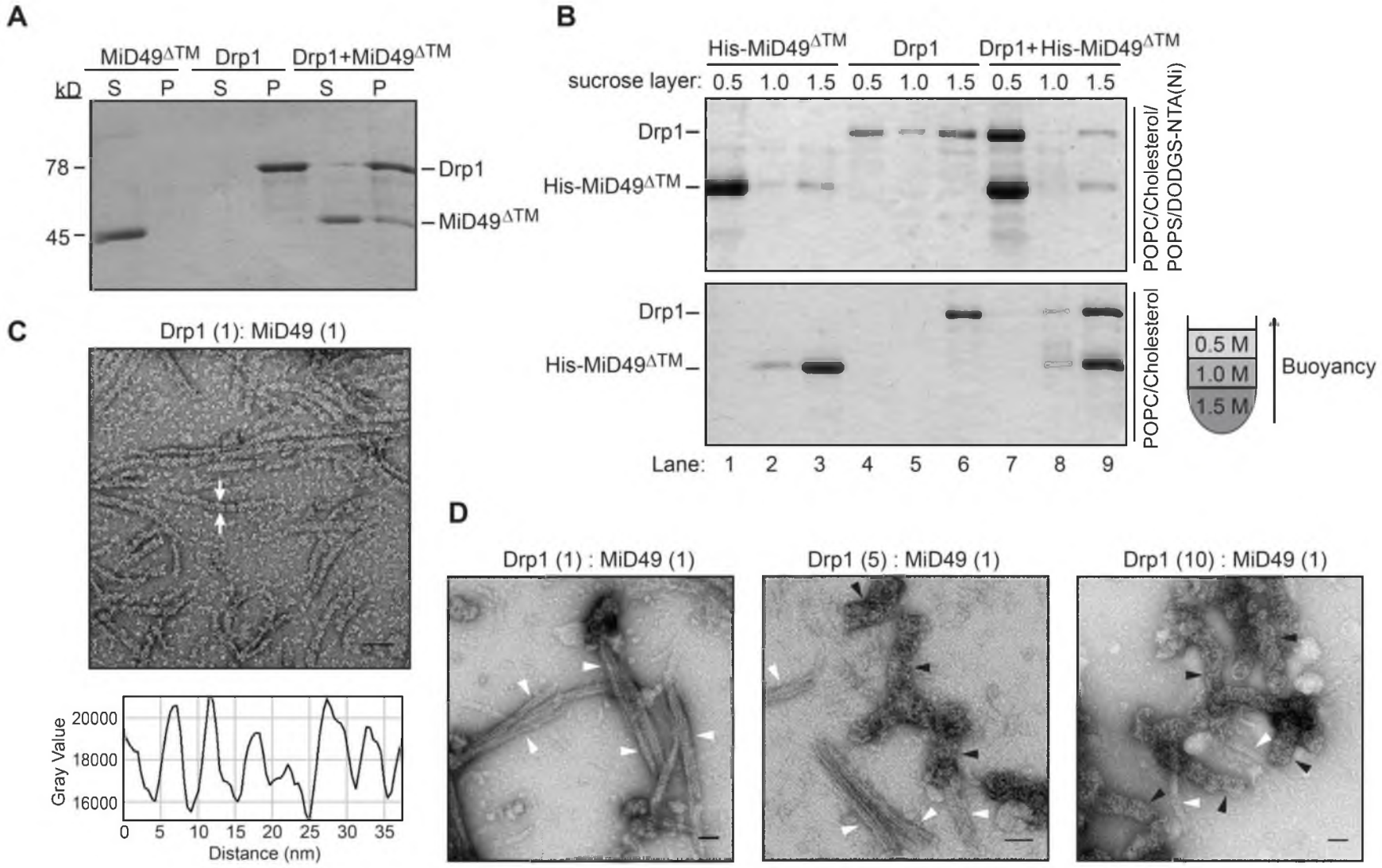
A
MiD49ΔTM
Drp1
Drp1+MiD49ΔTM
kD
S
P
S
P
S
P
78
45
Drp1
MiD49ΔTM
B
His-MiD49ΔTM
Drp1
Drp1+His-MiD49ΔTM
sucrose layer: 0.5 1.0 1.5 0.5 1.0 1.5 0.5 1.0 1.5
Drp1
His-MiD49ΔTM
POPC/Cholesterol/
POPS/DODGS-NTA(Ni)
Drp1
His-MiD49ΔTM
POPC/Cholesterol
0.5 M
1.0 M
1.5 M
Buoyancy
Lane: 1 2 3 4 5 6 7 8 9
C
Drp1 (1): MiD49 (1)
Gray Value
20000
18000
16000
0 5 10 15 20 25 30 35
Distance (nm)
D
Drp1 (1) : MiD49 (1)
Drp1 (5) : MiD49 (1)
Drp1 (10) : MiD49 (1)

stacks formed by Drp1 alone (34.4 ± 6.4 nm, Figure 3.6G). Measurement of pixel intensity along the length of these structures revealed a highly regular ~5 nm periodicity (Figure 3.7C, bottom). In control studies, MiD49 did not reproducibly assemble into visible structures in the presence or absence of GTP or GTP analogs (unpublished results).

To further investigate the nature of these narrower polymers, we examined assembly in the presence of different Drp1:MiD49 (molar:molar) ratios. Incubation of Drp1 and MiD49 at a 1:1 ratio in the presence of GMP-PCP produced mainly polymers with the smaller average diameter (Figure 3.7D, white arrowheads,14.9 ± 1.5 nm). These polymers often associated laterally into bundles. When a ratio of Drp1:MiD49 of 5:1 or 10:1 was examined, fewer narrow polymers were observed (Figure 3.7D, white arrowheads), with a concomitant increase in polymers of larger diameter (black arrowheads). Both the appearance and the diameter of the latter spirals were similar to those formed by Drp1 alone (Figure 3.6C). These data are consistent with the idea that coassembly of MiD49 with Drp1 is stoichiometric, and suggests that MiD49 copolymerizes with Drp1 rather than simply nucleating assembly of a Drp1 homopolymer.

Discussion

The adaptor proteins studied here were originally shown to mediate the recruitment of the Dnm1 or Drp1 GTPases to mitochondria, however, their post-recruitment roles in mitochondrial fission were not clear. In this study, we demonstrate that individual adaptor-GTPase pairs act after recruitment to catalyze membrane division

in vivo. In the case of Drp1, coassembly with one of these adaptors increases the order, and dramatically decreases the diameter of the polymers formed.

The identification of Fis1 and Dnm1/Drp1 in yeast and mammals initially suggested that the basic molecular machinery for mitochondrial fission was conserved during evolution. While the role of yeast Fis1 in Mdv1-Dnm1 recruitment to mitochondria has never been questioned, data supporting a function for mammalian Fis1 in Drp1 recruitment was contradictory. This issue was recently resolved by the demonstration that it is human Mff, rather than Fis1, that acts as the mitochondrial receptor for Drp1 (Otera et al., 2010). Soon after MiD49 and MiD51 were also reported to mediate Drp1 mitochondrial recruitment (Palmer et al., 2011; Zhao et al., 2011). We show here that yeast Fis1 is dispensable for fission when the Mdv1 adaptor is membrane-tethered, allowing Dnm1 recruitment to mitochondria. Moreover, expression of human Fis1 and Drp1 in yeast was not sufficient to rescue mitochondrial fission defects. Thus, Fis1 has not been conserved throughout evolution because of an essential role in Dnm1/Drp1-mediated membrane scission. What, then, is the conserved function of Fis1? Although mitochondrial fission proteins have also been implicated in peroxisome division and mitophagy in yeast and mammals (Koch et al., 2003; Kuravi et al., 2006; Li and Gould, 2003), Fis1 appears to be dispensable for peroxisome fission in human cells (Otera et al., 2010) and for mitophagy in yeast (Mendl et al., 2011; Okamoto et al., 2009). In addition, it was recently suggested that mammalian Fis1 directly interacts with MiD51 (also called MIEF1) to negatively regulate fission (Zhao et al., 2011). Further studies are clearly necessary to determine whether Fis1 has a conserved function(s) in organelle division.

Our findings show unambiguously that a single type of adaptor protein is sufficient for mitochondrial membrane scission by human Drp1. Why, then, do mammalian cells simultaneously express Mff, MiD49 and MiD51? Studies to date have not identified significant differences in the mitochondrial fission events mediated by these different adaptors (Otera et al., 2010; Palmer et al., 2011; Zhao et al., 2011). However, the assays used in these studies (morphological quantification and fixed time-point analysis) would fail to detect significant temporal, spatial or mechanistic differences in Drp1 recruitment, assembly and/or membrane scission that are specific to each adaptor. In addition, the physiological circumstances (i.e. apoptosis, mitophagy) in which each adaptor is activated might differ. Documented posttranslational modifications of Drp1 including phosphorylation (Cereghetti et al., 2008; Chang and Blackstone, 2007; Cribbs and Strack, 2007; Han et al., 2008; Kim et al., 2011; Taguchi et al., 2007), sumoylation (Braschi et al., 2009; Figueroa-Romero et al., 2009; Wasiak et al., 2007; Zunino et al., 2009), nitrosylation (Cho et al., 2009) and ubiquitination (Horn et al., 2011; Karbowski et al., 2007; Nakamura et al., 2006; Wang et al., 2011; Yonashiro et al., 2006) could also influence the identity of the adaptor used for fission (as could posttranslational modifications of the adaptors themselves) . Finally, it is possible that multiple adaptors work together with Drp1 at a single division site. Such cooperation has been documented for the paralogous adaptors Mdv1 and Caf4 in yeast (Guo et al., submitted) and it seems likely that the MiD49 and MiD51 paralogs will also have the capacity to function with Drp1 at the same fission site in mammals.

Distances of $\leq$ 1 nm between opposing lipid bilayers are thought to be necessary for initiation of inner leaflet hemifusion and subsequent membrane scission (Bashkirov et

al., 2008; Hernandez et al., 2012). Taking into account the diameter of a lipid bilayer (~ 5 nm) (Leforestier et al., 2012; Wang et al., 2006), and the fact that mitochondria have a double membrane, the average external diameter we measured for Drp1-lipid tubules (30.7 nm, Figure 3.6G) would not produce a lumenal distance small enough to initiate fission of both the inner and outer mitochondrial membranes. This problem could be overcome by coassembling MiD49 with Drp1, as the ~15 nm average external diameter of the Drp1:MiD49 copolymer is sufficiently narrow to drive fission. Like the copolymers formed by coincubation of dynamin-1 with endophilin (Sundborger et al., 2011) or amphiphysin (Takei et al., 1999), the MiD49:Drp1 copolymers shown here also change the structural properties of a dynamin GTPase polymer. In the case of N-BAR proteins and dynamin-1, the hybrid coat has a different diameter and different pitch. A detailed understanding of how MiD49 alters structural features of the Drp1 polymer, and the functional consequences of the hybrid assembly for the fission process requires further study.

Our findings clarify the individual functions of mitochondrial adaptors and challenge the notion that these proteins act solely to recruit and stimulate assembly of the DRPs Dnm1 and Drp1 on the correct cellular membrane. Instead, coassembly of adaptors with DRPs may work generally to change the physical properties of the resulting polymers in a manner that promotes or regulates membrane scission. For example, coassembly could prevent promiscuous fission by altering contacts between adjacent turns of the DRP helix, thereby inhibiting mechanochemical conformational changes that lead to constriction and fission. Such an inhibited state may be regulatory, delaying constriction until a signaling event or another factor is recruited. Alternatively, as shown

here, the copolymer may have different geometric properties and be able to form a more compact state that promotes membrane constriction and fission. Regardless of the mechanism, we suggest that the ability to modulate polymer geometry will be a common function of mitochondrial dynamin adaptors.

Acknowledgements

We thank Jane Macfarlane for expertise in mutagenesis and plasmid construction, Sarah Saffran for assistance with the initial GTPase assays, Mike Ryan and Alex van der Bliek for providing MiD and Mff plasmids and antibodies, Michael McCaffery for use of the John Hopkins University Integrated Imaging Facility and Beverly Wendland for the use of her lab space while working at the JHU facility. We are grateful to Michael Kay, Tim Formosa and members of the Shaw and Frost laboratories for stimulating discussions. This work was supported by NIH grants GM53466 and GM84970 to J.M.S. D.M.E. and the University of Utah Protein Interaction Core Facility are supported by NIH grant GM82545.

References

Amiott, E.A., Cohen, M.M., Saint-Georges, Y., Weissman, A.M., and Shaw, J.M. (2009). A mutation associated with CMT2A neuropathy causes defects in Fzo1 GTP hydrolysis, ubiquitylation, and protein turnover. Mol Biol Cell *20*, 5026-5035.

Bashkirov, P.V., Akimov, S.A., Evseev, A.I., Schmid, S.L., Zimmerberg, J., and Frolov, V.A. (2008). GTPase cycle of dynamin is coupled to membrane squeeze and release, leading to spontaneous fission. Cell *135*, 1276-1286.

Bleazard, W., McCaffery, J.M., King, E.J., Bale, S., Mozdy, A., Tieu, Q., Nunnari, J., and Shaw, J.M. (1999). The dynamin-related GTPase Dnm1 regulates mitochondrial fission in yeast. Nature Cell Biology *1*, 298-304.

Braschi, E., Zunino, R., and McBride, H.M. (2009). MAPL is a new mitochondrial SUMO E3 ligase that regulates mitochondrial fission. EMBO Reports *10*, 748-754.

Cereghetti, G.M., Stangherlin, A., Martins de Brito, O., Chang, C.R., Blackstone, C., Bernardi, P., and Scorrano, L. (2008). Dephosphorylation by calcineurin regulates translocation of Drp1 to mitochondria. Proceedings of the National Academy of Sciences of the United States of America *105*, 15803-15808.

Cerveny, K.L., and Jensen, R.E. (2003). The WD-repeats of Net2p interact with Dnm1p and Fis1p to regulate division of mitochondria. Mol Biol Cell *14*, 4126-4139.

Cerveny, K.L., McCaffery, J.M., and Jensen, R.E. (2001). Division of mitochondria requires a novel DMN1-interacting protein, Net2p. Mol Biol Cell *12*, 309-321.

Chang, C.R., and Blackstone, C. (2007). Cyclic AMP-dependent protein kinase phosphorylation of Drp1 regulates its GTPase activity and mitochondrial morphology. The Journal of Biological Chemistry *282*, 21583-21587.

Chang, C.R., Manlandro, C.M., Arnoult, D., Stadler, J., Posey, A.E., Hill, R.B., and Blackstone, C. (2010). A lethal de novo mutation in the middle domain of the dynamin-related GTPase Drp1 impairs higher order assembly and mitochondrial division. The Journal of Biological Chemistry *285*, 32494-32503.

Cho, D.H., Nakamura, T., Fang, J., Cieplak, P., Godzik, A., Gu, Z., and Lipton, S.A. (2009). S-nitrosylation of Drp1 mediates beta-amyloid-related mitochondrial fission and neuronal injury. Science *324*, 102-105.

Cole, J.L. (2004). Analysis of heterogeneous interactions. Methods in Enzymology *384*, 212-232.

Cribbs, J.T., and Strack, S. (2007). Reversible phosphorylation of Drp1 by cyclic AMP-dependent protein kinase and calcineurin regulates mitochondrial fission and cell death. EMBO Reports *8*, 939-944.

Figueroa-Romero, C., Iniguez-Lluhi, J.A., Stadler, J., Chang, C.R., Arnoult, D., Keller, P.J., Hong, Y., Blackstone, C., and Feldman, E.L. (2009). SUMOylation of the mitochondrial fission protein Drp1 occurs at multiple nonconsensus sites within the B domain and is linked to its activity cycle. FASEB journal : official publication of the Federation of American Societies for Experimental Biology *23*, 3917-3927.

Friedman, J.R., Lackner, L.L., West, M., DiBenedetto, J.R., Nunnari, J., and Voeltz, G.K. (2011). ER Tubules Mark Sites of Mitochondrial Division. Science *334*, 358-362.

Gandre-Babbe, S., and van der Bliek, A.M. (2008). The novel tail-anchored membrane protein Mff controls mitochondrial and peroxisomal fission in mammalian cells. Mol Biol Cell *19*, 2402-2412.

Gomes, L.C., Di Benedetto, G., and Scorrano, L. (2011). During autophagy mitochondria elongate, are spared from degradation and sustain cell viability. Nature Cell Biology *13*, 589-598.

Gorsich, S.W., and Shaw, J.M. (2004). Importance of mitochondrial dynamics during meiosis and sporulation. Mol Biol Cell *15*, 4369-4381.

Green, M., and Sambrook, J. (2012). Molecular Cloning: A Laboratory Manual (Fourth Edition) (Cold Spring Harbor Laboratory Press).

Griffin, E.E., Graumann, J., and Chan, D.C. (2005). The WD40 protein Caf4p is a component of the mitochondrial fission machinery and recruits Dnm1p to mitochondria. J Cell Biol *170*, 237-248.

Guthrie, C., and Fink., G. (2002). Guide to yeast genetics and molecular biology. Methods Enzymol *Vol. 350. San Diego: Academic Press, Inc.*

Han, X.J., Lu, Y.F., Li, S.A., Kaitsuka, T., Sato, Y., Tomizawa, K., Nairn, A.C., Takei, K., Matsui, H., and Matsushita, M. (2008). CaM kinase I alpha-induced phosphorylation of Drp1 regulates mitochondrial morphology. The Journal of Cell Biology *182*, 573-585.

Hernandez, J.M., Stein, A., Behrmann, E., Riedel, D., Cypionka, A., Farsi, Z., Walla, P.J., Raunser, S., and Jahn, R. (2012). Membrane fusion intermediates via directional and full assembly of the SNARE complex. Science *336*, 1581-1584.

Horn, S.R., Thomenius, M.J., Johnson, E.S., Freel, C.D., Wu, J.Q., Coloff, J.L., Yang, C.S., Tang, W., An, J., Ilkayeva, O.R., *et al.* (2011). Regulation of mitochondrial morphology by APC/CCdh1-mediated control of Drp1 stability. Molecular Biology of the Cell *22*, 1207-1216.

Ingerman, E., Perkins, E.M., Marino, M., Mears, J.A., McCaffery, J.M., Hinshaw, J.E., and Nunnari, J. (2005). Dnm1 forms spirals that are structurally tailored to fit mitochondria. The Journal of Cell Biology *170*, 1021-1027.

Ishihara, N., Nomura, M., Jofuku, A., Kato, H., Suzuki, S.O., Masuda, K., Otera, H., Nakanishi, Y., Nonaka, I., Goto, Y.-i., *et al.* (2009). Mitochondrial fission factor Drp1 is essential for embryonic development and synapse formation in mice. Nature Cell Biology *11*, 958-966.

Karbowski, M., Neutzner, A., and Youle, R.J. (2007). The mitochondrial E3 ubiquitin ligase MARCH5 is required for Drp1 dependent mitochondrial division. The Journal of Cell Biology *178*, 71-84.

Karren, M.A., Coonrod, E.M., Anderson, T.K., and Shaw, J.M. (2005). The role of Fis1p-Mdv1p interactions in mitochondrial fission complex assembly. J Cell Biol *171*, 291-301.

Kim, H., Scimia, M.C., Wilkinson, D., Trelles, R.D., Wood, M.R., Bowtell, D., Dillin, A., Mercola, M., and Ronai, Z.A. (2011). Fine-tuning of Drp1/Fis1 availability by AKAP121/Siah2 regulates mitochondrial adaptation to hypoxia. Mol Cell *44*, 532-544.

Koch, A., Thiemann, M., Grabenbauer, M., Yoon, Y., McNiven, M.A., and Schrader, M. (2003). Dynamin-like protein 1 is involved in peroxisomal fission. J Biol Chem *278*, 8597-8605.

Koirala, S., Bui, H.T., Schubert, H.L., Eckert, D.M., Hill, C.P., Kay, M.S., and Shaw, J.M. (2010). Molecular architecture of a dynamin adaptor: implications for assembly of mitochondrial fission complexes. J Cell Biol *191*, 1127-1139.

Kuravi, K., Nagotu, S., Krikken, A.M., Sjollema, K., Deckers, M., Erdmann, R., Veenhuis, M., and van der Klei, I.J. (2006). Dynamin-related proteins Vps1p and Dnm1p control peroxisome abundance in Saccharomyces cerevisiae. J Cell Sci *119*, 3994-4001.

Labrousse, A.M., Zappaterra, M.D., Rube, D.A., and van der Bliek, A.M. (1999). C. elegans dynamin-related protein DRP-1 controls severing of the mitochondrial outer membrane. Mol Cell *4*, 815-826.

Lackner, L.L., Horner, J.S., and Nunnari, J. (2009). Mechanistic analysis of a dynamin effector. Science *325*, 874-877.

Laue, T., Shah, B., Ridgeway, T., and Pelletier, S. (1992). Computer-aided interpretation of analytical sedimentation data for proteins. In Analytical Ultracentrifugation in Biochemistry and Polymer Science (Royal Society of Chemistry, Cambridge, England, UK).

Leforestier, A., Lemercier, N., and Livolant, F. (2012). Contribution of cryoelectron microscopy of vitreous sections to the understanding of biological membrane structure. Proceedings of the National Academy of Sciences of the United States of America *109*, 8959-8964.

Leonard, M., Song, B.D., Ramachandran, R., and Schmid, S.L. (2005). Robust colorimetric assays for dynamin's basal and stimulated GTPase activities. Methods Enzymol *404*, 490-503.

Li, X., and Gould, S.J. (2003). The dynamin-like GTPase DLP1 is essential for peroxisome division and is recruited to peroxisomes in part by PEX11. J Biol Chem *278*, 17012-17020.

Mears, J.A., Lackner, L.L., Fang, S., Ingerman, E., Nunnari, J., and Hinshaw, J.E. (2011). Conformational changes in Dnm1 support a contractile mechanism for mitochondrial fission. Nat Struct Mol Biol *18*, 20-26.

Mendl, N., Occhipinti, A., Muller, M., Wild, P., Dikic, I., and Reichert, A.S. (2011). Mitophagy in yeast is independent of mitochondrial fission and requires the stress response gene WHI2. Journal of Cell Science *124*, 1339-1350.

Mozdy, A.D., McCaffery, J.M., and Shaw, J.M. (2000). Dnm1p GTPase-mediated mitochondrial fission is a multi-step process requiring the novel integral membrane component Fis1p. J Cell Biol *151*, 367-380.

Nakamura, N., Kimura, Y., Tokuda, M., Honda, S., and Hirose, S. (2006). MARCH-V is a novel mitofusin 2- and Drp1-binding protein able to change mitochondrial morphology. EMBO Reports *7*, 1019-1022.

Naylor, K., Ingerman, E., Okreglak, V., Marino, M., Hinshaw, J.E., and Nunnari, J. (2006). Mdv1 interacts with assembled dnm1 to promote mitochondrial division. J Biol Chem *281*, 2177-2183.

Nunnari, J., Marshall, W.F., Straight, A., Murray, A., Sedat, J.W., and Walter, P. (1997). Mitochondrial transmission during mating in Saccharomyces cerevisiae is determined by mitochondrial fusion and fission and the intramitochondrial segregation of mitochondrial DNA. Molecular Biology of the Cell *8*, 1233-1242.

Okamoto, K., Kondo-Okamoto, N., and Ohsumi, Y. (2009). Mitochondria-anchored receptor Atg32 mediates degradation of mitochondria via selective autophagy. Developmental Cell *17*, 87-97.

Otera, H., Wang, C., Cleland, M.M., Setoguchi, K., Yokota, S., Youle, R.J., and Mihara, K. (2010). Mff is an essential factor for mitochondrial recruitment of Drp1 during mitochondrial fission in mammalian cells. J Cell Biol *191*, 1141-1158.

Otsuga, D., Keegan, B.R., Brisch, E., Thatcher, J.W., Hermann, G.J., Bleazard, W., and Shaw, J.M. (1998). The dynamin-related GTPase, Dnm1p, controls mitochondrial morphology in yeast. J Cell Biol *143*, 333-349.

Palmer, C.S., Osellame, L.D., Laine, D., Koutsopoulos, O.S., Frazier, A.E., and Ryan, M.T. (2011). MiD49 and MiD51, new components of the mitochondrial fission machinery. EMBO Reports *12*, 565-573.

Parone, P.A., Da Cruz, S., Tondera, D., Mattenberger, Y., James, D.I., Maechler, P., Barja, F., and Martinou, J.C. (2008). Preventing mitochondrial fission impairs mitochondrial function and leads to loss of mitochondrial DNA. PloS One *3*, e3257.

Praefcke, G.J., and McMahon, H.T. (2004). The dynamin superfamily: universal membrane tubulation and fission molecules? Nature reviews Molecular Cell Biology *5*, 133-147.

Ramage, L., Junne, T., Hahne, K., Lithgow, T., and Schatz, G. (1993). Functional cooperation of mitochondrial protein import receptors in yeast. The EMBO Journal *12*, 4115-4123.

Rambold, A.S., Kostelecky, B., Elia, N., and Lippincott-Schwartz, J. (2011). Tubular network formation protects mitochondria from autophagosomal degradation during nutrient starvation. Proceedings of the National Academy of Sciences of the United States of America *108*, 10190-10195.

Sesaki, H., and Jensen, R.E. (1999). Division versus fusion: Dnm1p and Fzo1p antagonistically regulate mitochondrial shape. J Cell Biol *147*, 699-706.

Sundborger, A., Soderblom, C., Vorontsova, O., Evergren, E., Hinshaw, J.E., and Shupliakov, O. (2011). An endophilin-dynamin complex promotes budding of clathrin-coated vesicles during synaptic vesicle recycling. Journal of Cell Science *124*, 133-143.

Taguchi, N., Ishihara, N., Jofuku, A., Oka, T., and Mihara, K. (2007). Mitotic phosphorylation of dynamin-related GTPase Drp1 participates in mitochondrial fission. The Journal of Biological Chemistry *282*, 11521-11529.

Takei, K., Slepnev, V.I., Haucke, V., and De Camilli, P. (1999). Functional partnership between amphiphysin and dynamin in clathrin-mediated endocytosis. Nature Cell Biology *1*, 33-39.

Tieu, Q., and Nunnari, J. (2000). Mdv1p Is a WD Repeat Protein that Interacts with the Dynamin-related GTPase, Dnm1p, to Trigger Mitochondrial Division. J Cell Biol *151*, 353-366.

Tieu, Q., Okreglak, V., Naylor, K., and Nunnari, J. (2002). The WD repeat protein, Mdv1p, functions as a molecular adaptor by interacting with Dnm1p and Fis1p during mitochondrial fission. The Journal of Cell Biology *158*, 445-452.

Twig, G., Elorza, A., Molina, A.J., Mohamed, H., Wikstrom, J.D., Walzer, G., Stiles, L., Haigh, S.E., Katz, S., Las, G., *et al.* (2008). Fission and selective fusion govern mitochondrial segregation and elimination by autophagy. EMBO J *27*, 433-446.

Twig, G., and Shirihai, O.S. (2011). The interplay between mitochondrial dynamics and mitophagy. Antioxidants & Redox Signaling *14*, 1939-1951.

Wakabayashi, J., Zhang, Z., Wakabayashi, N., Tamura, Y., Fukaya, M., Kensler, T.W., Iijima, M., and Sesaki, H. (2009). The dynamin-related GTPase Drp1 is required for embryonic and brain development in mice. The Journal of Cell Biology *186*, 805-816.

Wang, H., Song, P., Du, L., Tian, W., Yue, W., Liu, M., Li, D., Wang, B., Zhu, Y., Cao, C., *et al.* (2011). Parkin ubiquitinates Drp1 for proteasome-dependent degradation: implication of dysregulated mitochondrial dynamics in Parkinson disease. The Journal of Biological Chemistry *286*, 11649-11658.

Wang, L., Bose, P.S., and Sigworth, F.J. (2006). Using cryo-EM to measure the dipole potential of a lipid membrane. Proceedings of the National Academy of Sciences of the United States of America *103*, 18528-18533.

Wasiak, S., Zunino, R., and McBride, H.M. (2007). Bax/Bak promote sumoylation of DRP1 and its stable association with mitochondria during apoptotic cell death. The Journal of Cell Biology *177*, 439-450.

Yonashiro, R., Ishido, S., Kyo, S., Fukuda, T., Goto, E., Matsuki, Y., Ohmura-Hoshino, M., Sada, K., Hotta, H., Yamamura, H., *et al.* (2006). A novel mitochondrial ubiquitin ligase plays a critical role in mitochondrial dynamics. The EMBO Journal *25*, 3618-3626.

Zhao, J., Liu, T., Jin, S., Wang, X., Qu, M., Uhlen, P., Tomilin, N., Shupliakov, O., Lendahl, U., and Nister, M. (2011). Human MIEF1 recruits Drp1 to mitochondrial outer membranes and promotes mitochondrial fusion rather than fission. EMBO J *30*, 2762-2778.

Zunino, R., Braschi, E., Xu, L., and McBride, H.M. (2009). Translocation of SenP5 from the nucleoli to the mitochondria modulates DRP1-dependent fission during mitosis. The Journal of Biological Chemistry *284*, 17783-17795.

CHAPTER 4

DISCUSSION

Overview

In this dissertation, I present two studies that advance understanding of how yeast and mammalian adaptor proteins regulate mitochondrial fission DRP activity. Chapter 2 studies establish the importance of Mdv1 CC-mediated dimerization in Dnm1 assembly and function. The crystal structure of the Mdv1 CC provides insight into the molecular architecture of the Fis1-Mdv1 complex and its role in positioning the Dnm1 GTPase for assembly on the membrane (Figure 1.4). In addition, my studies reveal that the length and amino acid sequence of the antiparallel Mdv1 CC is optimized for efficient Dnm1 assembly and function in mitochondrial membrane scission.

In Chapter 3, I analyzed the relative contributions of yeast and mammalian adaptors to fission using a novel yeast tester strain. These studies advance the field by showing that: 1) yFis1 is dispensable for mitochondrial fission as long as Mdv1 is artificially recruited (tethered) to the mitochondrial outer membrane, 2) yFis1 does not regulate Dnm1 assembly or fission function *in vivo*, 3) yFis1 does not contribute to the equilibrium of balanced fission and fusion, 4) hMff, hMiD49 and hMiD51 work independently and interchangeably to recruit and assist hDrp1 in mitochondrial membrane fission, 5) hFis1 is not a mitochondrial fission adaptor for hDrp1, and 6) hMiD49 alters hDrp1 assembly properties *in vitro*.

In the Appendix, I include a study that dissects the role of the Mdv1 paralog, Caf4, in yeast mitochondrial fission (Guo et al., 2012). This project was led by my colleague and fellow graduate student Qian Guo. In particular, I contributed to the fixed-time point analysis showing that Mdv1 and Caf4 colocalize in fission complexes on mitochondrial tubules. Complementary time-lapse imaging studies were used to confirm

the colocalization and demonstrate that bona fide mitochondrial fission events occurred at sites containing both adaptors. Similar imaging experiments showed for the first time that Caf4 alone mediates mitochondrial fission when Mdv1 is absent. This study further demonstrates that unlike Mdv1, Caf4 function in mitochondrial fission is very sensitive to protein concentration. Caf4 generates highly interconnected mitochondria when over expressed, indicative of a dominant-negative effect on mitochondrial scission. Together our findings demonstrate that Caf4 is a functional fission adaptor, although the functions of Caf4 and Mdv1 are not equivalent.

Together, my thesis studies further our general understandings of how the mitochondrial fission adaptors have structurally diversified in the course of evolution yet functionally converged to assist the mitochondrial fission DRPs in membrane scission reactions. As described below, my thesis studies have also raised new questions for future study.

Dispensability of Fis1 and Caf4 in Mitochondrial Fission

Yeast has two paralogous fission adaptors Mdv1 and Caf4 (Figure 1.3). Although we were able to show that Caf4 can function as an adaptor on its own, we were unable to identify physiological conditions where Caf4 was necessary or beneficial to cell survival or fitness. Nevertheless, it remains possible that Caf4 has one or more physiological roles that contribute to organismal fitness. First, phylogenetic analysis carried out by Qian Guo indicates that Caf4 has been conserved in all but one related yeast species since it was created by an ancient gene duplication event. Second, the increased rate of amino acid substitution and low sequence identity (30%, Table 1.2) of Caf4 relative to Mdv1 supports the idea that the functions of the two proteins have, or are in the process of,

diverging. It may be that the fitness advantage conferred by Caf4 is so small that we simply cannot measure it using the available methods. Since the physiology and/or growth of other yeast species shown in the phylogenetic analysis may differ from *S. cerevisiae*, it may be worthwhile to examine how loss of Caf4 affects fitness in these other yeasts.

Although I was able to show that yeast Fis1 is dispensable for mitochondrial fission when Mdv1 is tethered to mitochondria, under normal circumstances, Fis1 is essential for both Mdv1 and Dnm1 recruitment to the outer mitochondrial membrane. However, the need for Fis1 function in mammals is much less clear. The fact that Fis1 orthologs are present in all eukaryotic kingdoms suggests that there is a conserved function for Fis1. Interestingly, when Fis1 sequences of yeast and human are aligned, there is only around 22% amino acid sequence identity between them (Table 1.2). Study by Stojanovski et al., 2004, showed that cytoplasmic domains of hFis1 and yFis1p are not functionally interchangeable *in vivo*. Structural studies also reveal differences at the N-terminus of yeast and human Fis1 (Suzuki et al., 2003; Suzuki et al., 2005). Together these facts suggest that the Fis1 sequences might have diverged, possibly to accommodate different cellular functions in different organisms. Consistent with this idea, a recent finding indicates that hFis1 functions in transmitting the apoptotic signal from the mitochondria to the ER via a physical interaction with Bap31 at the ER. This interaction was shown to be required for the recruitment and activation of apoptotic factor, procaspase-8 (Iwasawa et al., 2011). In addition, an unpublished fis1 knockout study in mice indicates that Fis1 is important for embryonic development (David Chan, personal communication).

In the course of my studies, I observed that a GFP tagged yFis1 transmembrane domain localizes to small membranous vesicles throughout the yeast cytoplasm (Sajjan Koirala). Although this construct predominantly colocalized with mitochondrial and peroxisomal markers, there were additional cellular bodies that were decorated with GFP-yFis1™ proteins. The identity and function of these novel membranous structures is not known. It may be that the Fis1 transmembrane domain can be targeted to more than one membrane trafficking pathway that moves in and out of mitochondria (Soubannier et al., 2012). Future studies should explore whether localization of GFP-Fis1-TM to various subcellular membranous compartments has any physiological significance.

Mysteries of the Mdv1 Coiled Coil Domain

The glutamate residue at position 250 of the Mdv1 CC has been shown to be important for yFis1 interaction (Karren et al., 2005). When I started working on the Mdv1 CC project, no structural information was available to explain how a residue in the Mdv1 CC could influence the Fis1-Mdv1 interaction. To address this issue, I purified the Mdv1 CC domain and determined whether the Mdv1 CC domain interacted with the purified cytoplasmic TPR domain of yFis1. Surprisingly, in contrast to the genetic interaction identified by Karren et al., (2005) no physical interaction between the Mdv1 CC domain and the Fis1-TPR domain were detected (Koirala et al., 2010). Several factors could explain this negative result. First, it is possible that the Mdv1 CC does not directly interact with the Fis1-TPR domain. Second, the interaction between these two domains may depend upon other domains of Mdv1. Our CC study, discussed in chapter 2, supports the latter notion that the Mdv1-E250G mediated suppression of *fis1-3* is via an indirect interaction. In this suppression model, parts of the NTE make contacts with the

Mdv1 CC that is disrupted by the E250G mutation. This allows the Mdv1 NTE to make robust interactions with Fis1 (Karren et al., 2005). Further studies tested the validity of this model. When I truncated the Mdv1 CC by several heptad repeats from either end of the CC including the E250 residue, the suppression of *fis1-3* was still observed. These results indicate that the E250 mediated suppression of *fis1-3* is by a long distance indirect interaction and not by a residue specific interactions (Koirala et al., 2010). Consistent with this model, a new co-crystal structure of the Fis1-TPR and Mdv1 NTE-CC showed that: 1) the NTE of Mdv1 folds back to make interactions with the Mdv1-CC domain that do not include residue E250 and 2) the Mdv1-NTE interaction with the Fis1-TPR is not at the concave surface where the temperature sensitive mutations in *fis1-3* lie (Zhang et al., 2012). Together these findings have explained the molecular mechanism of the Mdv1-E250G mediated suppression of *fis1-3 ts* mutation.

The studies presented in Chapter 2 of this dissertation highlight the importance of the Mdv1 CC in: 1) Fis1 and Dnm1 interactions, 2) Dnm1 assembly and 3) mitochondrial fission. The CC domain swap and truncation studies indicated that the Mdv1 CC domain is not critical for mitochondrial fission but greatly enhances Dnm1 mediated fission. Consistent with this interpretation, the Mdv1 tethering studies in Chapter 3 indicated that mitochondrial fission can be achieved even without the Mdv1 CC. However, for optimal fission, the Mdv1 CC is required (Figure 3.1). Surprisingly, in the same study, tethered full length Mdv1 had very poor mitochondrial fission activity (Figure 3.1). This may be because, in the absence of Fis1, the NTE domain of Mdv1 may not fold properly and may interact non-productively with the Mdv1 CC or β-propeller domains (Zhang et al., 2012). Together, the domain specific studies in Chapter 2 and 3 show that the Mdv1 β-propeller

domain is the only domain in Mdv1 that is critical for Dnm1-mediated mitochondrial fission but the Mdv1 CC domain enhances the efficiency of Dnm1-mediated mitochondrial fission, possibly by helping Dnm1 to assemble correctly into functional fission complexes.

Multiple Adaptors Regulate Human Dynamin-Related GTPase

Although hFis1 has long been implicated in human mitochondrial fission, the role of hFis1 in mitochondrial fission remained unclear, as no human Mdv1 orthologs that might bind hFis1 had been identified (Chan, 2006; Okamoto and Shaw, 2005; Zhao et al., 2012). In recent years, new human mitochondrial adaptors, including Mff, MiD49 and MiD51, were identified that are structurally predicted to be very different from Mdv1 (Figure 1.3 and Table 1.2) (Otera et al., 2010; Palmer et al., 2011; Zhao et al., 2011). By testing pair wise functions of these mammalian adaptors with Drp1 in the yeast tester strain, I provided direct evidence that each adaptor can independently recruit Drp1 and complete mitochondrial fission.

In the future, it will be important to determine whether these adaptors can also work together at the same fission site, and whether there are mechanistic and/or functional differences in fission mediated by hMff-hDrp1 versus hMiD49/51-hDrp1. Since these newly discovered adaptors are ubiquitously expressed, understanding the cellular signals that modulate these parallel fission machineries in the same and different cells and tissues will be critical. Interestingly, Mff is conserved in all metazoans but the MiDs are found only in vertebrates. Thus, differences in mitochondrial functions in vertebrates and invertebrates may provide clues regarding the specific functions of Mff and MiDs.

Whether or not such differences are identified, the regulation of each type of fission should be explored. It is well established that hDrp1 is posttranslationally modified by phosphorylation, sumoylation, ubiquitination, and S-nitrosylation (Chang and Blackstone, 2010). One or more of these Drp1 posttranslational modifications could regulate the binding to a specific adaptor(s) under different physiological circumstances. In addition, it will also be important to determine if these mitochondrial fission adaptors compete with each other for Drp1 binding and, if so, whether this competition is important for regulation of mitochondrial dynamics. Finally, there is one report that the MiD51 adaptor functions in mitochondrial fusion (Zhao et al., 2011). If this is the case, the molecular events that determine whether these adaptors carry out fission or fusion will have to be identified and characterized.

The field is now in the position to understand the molecular details of hMff-hDrp1, hMiD49-hDrp1, and hMiD51-hDrp1 interactions by solving the co-crystal or cryo-EM structures of these complexes. These studies will help us understand how the same molecule can use a variety of unrelated adaptors to promote self-assembly and lipid remodeling. hDrp1 is a GTPase. Studies that are focused on whether/how these adaptors regulate hDrp1 GTPase activity will have to take into account the posttranslational modifications of these proteins, as these modifications are likely to play a role in providing specificity to adaptor-Drp1 interactions.

Lastly, the discovery that the ER marks and constricts mitochondrial tubules prior to adaptor and Dnm1/Drp1 recruitment has raised a variety of new questions (Friedman et al., 2011). It is speculated that the constrictions created by the ER on the mitochondrial tubule are not sufficient for mitochondrial fission. This implies that the mitochondrial

fission DRPs are necessary for further constriction and fission of the compartment. *In vitro*, yeast Mdv1 has been implicated in modulating Dnm1 self-assembly, and indirectly, assembly stimulated GTPase activity (Lackner et al., 2009). Do the mammalian adaptors also regulate Drp1 GTPase assembly and activity? As discussed in Chapter 3, the MiD49 adaptor regulates hDrp1 assemblies *in vitro* and dramatically changes their shape. A mechanistic understanding of how these adaptors assist the GTPase in membrane constriction and fission requires *in vitro* assays that recapitulate coassembly of adaptors and DRPs on liposomes and reconstitute fission. With the purified proteins in hand, the field is now much closer to the development of such assays.

References

Chan, D.C. (2006). Mitochondrial fusion and fission in mammals. Annu Rev Cell Dev Biol *22*, 79-99.

Chang, C.R., and Blackstone, C. (2010). Dynamic regulation of mitochondrial fission through modification of the dynamin-related protein Drp1. Annals of the New York Academy of Sciences *1201*, 34-39.

Friedman, J.R., Lackner, L.L., West, M., DiBenedetto, J.R., Nunnari, J., and Voeltz, G.K. (2011). ER tubules mark sites of mitochondrial division. Science *334*, 358-362.

Iwasawa, R., Mahul-Mellier, A.L., Datler, C., Pazarentzos, E., and Grimm, S. (2011). Fis1 and Bap31 bridge the mitochondria-ER interface to establish a platform for apoptosis induction. EMBO J *30*, 556-568.

Karren, M.A., Coonrod, E.M., Anderson, T.K., and Shaw, J.M. (2005). The role of Fis1p-Mdv1p interactions in mitochondrial fission complex assembly. J Cell Biol *171*, 291-301.

Koirala, S., Bui, H.T., Schubert, H.L., Eckert, D.M., Hill, C.P., Kay, M.S., and Shaw, J.M. (2010). Molecular architecture of a dynamin adaptor: implications for assembly of mitochondrial fission complexes. J Cell Biol *191*, 1127-1139.

Lackner, L.L., Horner, J.S., and Nunnari, J. (2009). Mechanistic analysis of a dynamin effector. Science *325*, 874-877.

Okamoto, K., and Shaw, J.M. (2005). Mitochondrial morphology and dynamics in yeast and multicellular eukaryotes. Annu Rev Genet *39*, 503-536.

Otera, H., Wang, C., Cleland, M.M., Setoguchi, K., Yokota, S., Youle, R.J., and Mihara, K. (2010). Mff is an essential factor for mitochondrial recruitment of Drp1 during mitochondrial fission in mammalian cells. J Cell Biol *191*, 1141-1158.

Palmer, C.S., Osellame, L.D., Laine, D., Koutsopoulos, O.S., Frazier, A.E., and Ryan, M.T. (2011). MiD49 and MiD51, new components of the mitochondrial fission machinery. EMBO Reports *12*, 565-573.

Soubannier, V., McLelland, G.L., Zunino, R., Braschi, E., Rippstein, P., Fon, E.A., and McBride, H.M. (2012). A vesicular transport pathway shuttles cargo from mitochondria to lysosomes. Current Biology *22*, 135-141.

Suzuki, M., Jeong, S.Y., Karbowski, M., Youle, R.J., and Tjandra, N. (2003). The solution structure of human mitochondria fission protein Fis1 reveals a novel TPR-like helix bundle. J Mol Biol *334*, 445-458.

Suzuki, M., Neutzner, A., Tjandra, N., and Youle, R.J. (2005). Novel structure of the N terminus in yeast Fis1 correlates with a specialized function in mitochondrial fission. J Biol Chem *280*, 21444-21452.

Zhang, Y., Chan, N.C., Ngo, H.B., Gristick, H., and Chan, D.C. (2012). Crystal structure of mitochondrial fission complex reveals scaffolding function for mitochondrial division 1 (Mdv1) coiled coil. J Biol Chem *287*, 9855-9861.

Zhao, J., Lendahl, U., and Nister, M. (2012). Regulation of mitochondrial dynamics: convergences and divergences between yeast and vertebrates. Cell Mol Life Sci *69*,1-26.

Zhao, J., Liu, T., Jin, S., Wang, X., Qu, M., Uhlen, P., Tomilin, N., Shupliakov, O., Lendahl, U., and Nister, M. (2011). Human MIEF1 recruits Drp1 to mitochondrial outer membranes and promotes mitochondrial fusion rather than fission. EMBO J *30*, 2762-2778.

APPENDIX A

THE MITOCHONDRIAL FISSION ADAPTORS CAF4 AND MDV1 ARE NOT FUNCTIONALLY EQUIVALENT

Authors

Qian Guo, Sajjan Koirala, Edward M. Perkins, J. Michael McCaffery, Janet M. Shaw
This chapter is accepted for publication in PLOS ONE journal.

Introduction

An ancient genome wide duplication in the lineage including the budding yeast *Saccharomyces cerevisiae* played an important role in the evolution of this singled celled eukaryote (Kellis et al., 2004; Wolfe and Shields, 1997). After this event, duplicated genes (paralogs) experienced accelerated evolution, most often involving one member of the gene pair. Of the 5885 existing *S. cerevisiae* genes, 450 are paralog pairs (Goffeau et al., 1996; Musso et al., 2007). For many of these, it remains unclear whether one of the genes has acquired a new function, maintains a redundant function, or has developed a specialized function within the same cellular process.

Mitochondrial fission is one cellular process that utilizes paralogous genes. Yeast mitochondrial membranes form tubular structures that undergo frequent fission and fusion events (Nunnari et al., 1997; Okamoto and Shaw, 2005). When fission is blocked, ongoing fusion creates a single, interconnected mitochondrial net (Bleazard et al., 1999; Otsuga et al., 1998; Sesaki and Jensen, 1999). A previous study demonstrated that defects in mitochondrial fission have a negative fitness cost in yeast, since these abnormal nets are inefficiently partitioned into newly formed daughter cells during meiotic division, and the resulting spores are inviable (Gorsich and Shaw, 2004). Successful mitochondrial fission requires an adaptor protein called Mdv1 (Cerveny et al., 2001; Tieu and Nunnari, 2000), which bridges the interaction between the cytoplasmic dynamin-related GTPase Dnm1 and the mitochondrial outer membrane-anchored protein Fis1 (Cerveny and Jensen, 2003; Mozdy et al., 2000; Tieu et al., 2002). On the membrane, Mdv1 promotes the assembly of Dnm1 into spirals that often surround the mitochondrial tubule (Ingerman et al., 2005; Legesse-Miller et al., 2003). A subset of these structures are

located at sites on mitochondria that ultimately divide (Legesse-Miller et al., 2003; Schauss et al., 2006).

An Mdv1 paralog called Caf4 was identified in a directed proteomics screen (Griffin et al., 2005). Like Mdv1, the Caf4 adaptor is composed of three domains, an N-terminal extension (NTE), a coiled-coil (CC) and C-terminal WD40 repeats predicted to form a β-propeller (Figure. AI.1A). The NTE domains of Mdv1 or Caf4 form a clamp around the Fis1 TPR-like domain, which mediates adaptor localization to the mitochondrial surface (Zhang and Chan, 2007). The Mdv1 and Caf4 WD40/β-propeller domains interact with, and recruit, Dnm1 to the membrane (Cerveny and Jensen, 2003; Griffin et al., 2005; Tieu et al., 2002). Structural studies reveal that Mdv1 dimerizes via an antiparallel coiled-coil (Koirala et al., 2010; Zhang et al., 2012), and Caf4 is thought to dimerize by a similar mechanism. Caf4 and Mdv1 also interact in vivo (Griffin et al., 2005), though whether this occurs via coiled-coil formation between the two proteins is unclear.

Yeast cells lacking Mdv1 exhibit severe mitochondrial morphology defects, establishing an essential role for this adaptor in fission (Cerveny et al., 2001; Tieu and Nunnari, 2000). By contrast, loss of Caf4 function enhances mitochondrial fission defects when Mdv1 is absent, but does not cause obvious fission defects on its own (Griffin et al., 2005). Although Caf4 can function to recruit Dnm1 to mitochondria in vivo, it has not been shown to directly participate in membrane scission. Moreover, it is not clear whether there is functional divergence between the two adaptor proteins.

In this study, we directly test the function of Caf4 in mitochondrial fission. We show that Caf4 is a bona fide fission adaptor that assembles at sites of mitochondrial

division. Although Caf4 can function alone as an adaptor, complexes containing both Caf4 and Mdv1 exhibit no obvious defects in mitochondrial fission. Genomic swapping studies indicate that Caf4 cannot substitute for Mdv1 *in vivo*. Moreover, over expression of Caf4 (but not Mdv1) from a regulated promoter induces dominant negative fission defects. When combined with phylogenetic analysis, these findings establish that Caf4 mitochondrial fission activity has diverged from that of Mdv1.

Materials and Methods

Growth Conditions, Strains and Plasmids

Yeast strains and plasmids used in this study are listed below. Unless noted in the Figure legend, standard rich or synthetic dropout media were used for growth, transformation and genetic manipulation of *S. cerevisiae* (Guthrie and Fink, 1991) and *E. coli* (Maniatis et al., 1982). Standard synthetic dextrose medium contains 0.6 mM methionine and cysteine.

The *CAF4* gene encodes two potential initiation codons that could result in methionine at positions 1 and 17 of the predicted protein. To determine whether this 16 amino acid difference at the N-terminus affected Caf4 function, we expressed proteins initiated from each methionine codon under control of the *MET25* promoter. Because we observed no difference in steady-state abundance or fission function of the two proteins (data not shown), the longer version was used for all constructs described in this study.

Plasmids pRS414-*GPD-mt-ffRFP* and pRS416-*MET25-MDV1* were described previously (Karren et al., 2005; Koirala et al., 2010). pRS414-*GPD-mt-mCherry* was generated by PCR amplification of the mCherry open reading frame that was cloned into the EcoRI and XhoI sites of pRS414-*GPD*-mt after digestion and removal of *ffRFP* by

the same enzymes. pRS416-*MET25-CAF4* was generated by PCR amplification of the *CAF4* open reading frame that was cloned into the BamHI and SalI sites of pRS416-*MET25*. To construct pRS415-*MET25-GFP-CAF4*, the PCR amplified *CAF4* open reading frame was cloned into the BamHI and SalI sites of pRS416-*MET25-GFP*. To construct pRS415-*MET25-GFP-MDV1*, the PCR amplified *MDV1* open reading frame was cloned into the BamHI and SalI sites of pRS416-*MET15-GFP*. To construct pRS416-*MET25-ffRFP-MDV1*, the PCR amplified *ffRFP* coding region was cloned into the SpeI and BamHI sites of pRS416-*MET25-MDV1*. To construct pRS416-*MET25-RFP-CAF4*, PCR amplified *CAF4* was cloned into the BamHI and SalI sites of pRS-*MET25-RFP*.

Western Blotting and Protein Quantification

Protein expression and abundance was analyzed in yeast whole cell extracts prepared by the alkaline extraction method (Kushnirov, 2000). 0.25 OD_{600} equivalents of extract was separated by SDS-PAGE and analyzed by Western blotting using the following primary antibodies: anti-yeast actin (1:5000, J. Cooper, Washington University Saint Louis), α-3-PGK (1: 5000, Invitrogen), anti-Mdv1 (1:1000, J. Nunnari, U. C. Davis) and anti-Caf4 (1:250, generated against bacterially expressed, 6His-Caf4 amino acids 175-659). Primary antibodies were detected using fluorescent secondary anti-goat, anti-rabbit or anti-mouse IRDye 800 (LiCor). Fluorescent signals were quantified using an Odyssey scanner and Odyssey 3.0 analysis software (LiCor). In Figure AI.2B, anti-Caf4 or anti-Mdv1 signals were first normalized to anti-actin signals. The abundance of each protein was subsequently normalized to its abundance in 2.0 mM methionine. In

Figure AI.3B, anti-Caf4 or anti-Mdv1 signals were normalized to anti-3-PGK. In all experiments, data are represented as the mean and SD of three independent experiments.

Quantification of Mitochondrial Morphology

Mitochondrial morphology was scored in WT and mutant cells expressing fast folding matrix-targeted red fluorescent protein (mt-ffRFP). Strains were grown at 30°C in selective dextrose synthetic medium and scored in log phase (0.2-0.8 OD_{600}). Basal expression levels of Mdv1 and Caf4 proteins from the *MET25* promoter under these conditions result in an approximately five-fold increase over endogenous Mdv1 or Caf4 protein levels with no adverse effects on mitochondrial morphology or fission (Karren et al., 2005)(data not shown). For the methionine titration experiments in Figure AI.2A, *caf4*Δ *mdv1*Δ (adaptor null JSY8612 cells) expressing the indicated Caf4 and Mdv1 proteins from the *MET25* promoter were grown in selective dextrose medium at 30°C overnight. Cultures were diluted to 0.2 OD_{600} in selective dextrose medium lacking cysteine and containing the indicated concentrations of methionine to suppress expression from the *MET25* promoter. Cultures were grown for 3 hours prior to scoring. Mitochondrial phenotypes were scored in 100 cells, and data are represented as the average and SD of three independent experiments.

Colocalization Studies

Log phase *caf4*Δ *mdv1*Δ cells expressing GFP- or RFP-labeled Mdv1 and Caf4 were grown in standard selective dextrose medium, fixed in 4% formaldehyde (Fisher Scientific) for five minutes at room temperature and washed three times with phosphate buffered saline (PBS, 137mM NaCl, 2.7mM KCl, 4.3mM Na_2HPO_4, 1.47mM KH_2PO_4,

pH 7.4). Cells were imaged on a Nikon fluorescence microscope using a 100X oil immersion objective, EGFP and DsRed filters and a Coolsnap HQ digital camera (Phototmetrics). Z-stacks (0.2 μm optical sections) were acquired and processed using the DeltaVisionRT system and accompanying DeltaVision software (Applied Precision, Issaquah, WA). Colocalization of GFP and RFP signals was determined in three dimensions using the Orthogonal View function of the DeltaVision software. The number of GFP puncta colocalized with RFP puncta was quantified and normalized to the total number of RFP puncta in each cell (n=10 cells). Bars and error bars represent the average and SD of three independent experiments.

Time-lapse Imaging

For dual-color time-lapse imaging, log phase *caf4*Δ *mdv1*Δ cells expressing GFP-Caf4 and mitochondrial targeted RFP were grown in standard selective synthetic dextrose medium and applied to concanavalin A (2 mg/ml, Sigma) treated Lab-tek II Chamber wells (Thermo Scientific) maintained at 30°C. Z-stacks (0.2 μm optical sections) of fields of cells were acquired every 7 seconds over a 20 minute time course using a 3-I Marianas Live Cell Imaging microscope workstation (Denver, CO), equipped with dual ultra-sensitive Cascade II 512B EMCCD cameras (Roper Scientific, RS) configured with a Roper Dual-cam and Sutter DG-4 Illuminator (Sutter Instruments) for simultaneous two-channel TIRF/fluorescence acquisition with a 100X, 1.45 NA Plan-Apochromat objective (Zeiss). Data were deconvolved and analyzed using SlideBook 4.2 software (Intelligent Imaging Innovations, Inc). Substacks containing fission events were isolated from the entire stack to minimize signal background and assembled in Photoshop (CS3, Adobe).

Brightness and contrast were adjusted using only linear operations applied to the entire image.

Three-color time-lapse imaging was carried out as described above with the following changes. Log phase *caf4*Δ *mdv1*Δ cells expressing integrated Cerulean-Caf4 and EYFP-Mdv1 from the *MET25* promoter (JSY9774) and plasmid-borne mt-mCherry were grown overnight at 30°C in selective synthetic dextrose medium. Cultures were diluted to 0.3 OD_{600} in medium lacking cysteine and containing 1.0 mM methionine 3 hours before imaging. Z-stacks (0.2 µm optical sections) of fields of cells were acquired every 10 seconds over a 25-minute time course using a CerFP/EYFP/mCherry filter set (Semrock) and dual Cascade II 512B EMCCD cameras and Sutter DG-4 illuminator (Sutter Instruments) for imaging EYFP, mCherry, and Cerulean signals.

Phylogenetic Analysis

Blast (NCBI) was used to identify homologs of Caf4 and Mdv1. The genomic sequences of homologs were identified via the Saccharomyces Genome Database and GOLD (Genomes OnLine Database). Predicted protein sequences used to generate this tree were obtained from: YKR036C (*S. cerevisiae CAF4*), YJL112W (*S. cerevisiae MDV1*), PORF 13363 (*S. paradoxus CAF4*), PORF 11728 (*S. paradoxus MDV1*), PROF 13800 (*S. mikatae CAF4*), Contig 2819.8 (*S. mikatae MDV1*), PROF 15127 (*S. bayanus CAF4*), PROF 12617 (*S. bayanus MDV1*), Contig 1606.5 (*S. kudriavzevii CAF4*), GS115 (*P. pastoris ortholog*), KLTH0E15576p (*L. thermotolerans ortholog*), Af293 (*A. fumigatus ortholog*). Amino acid sequences were aligned using ClustalW2 (European Bioinformatics Institute) and indels were removed. PhyML (European Bioinformatics Institute) was used to calculate and assemble the phylogenetic tree.

Table A.1: Plasmids Used in this Study

Strain ID	Plasmid	Protein Expressed	Reference
B493	pRS415-*MET25*	None	ATCC 87322
B494	pRS416-*MET25*	None	ATCC 87324
B1642	pRS414-*GPD-mt-ffRFP*	*N. crassa* ATP9 (1-69) + fast folding DsRed (RFP)	Karren et al., 2005
B2053	pRS416-*MET25-MDV1*	Mdv1	Karren et al., 2005
B2212	pRS416-*MET25-CAF4*	Caf4	This Study
B2290	pRS415-*MET25-GFP-CAF4*	GFP-Caf4	This Study
B2291	pRS416-*MET25-ffRFP-MDV1*	RFP-Mdv1	This Study
B2384	pRS415-*MET25-GFP-MDV1*	GFP-Mdv1	This Study
B2408	pRS416-*MET25-ffRFP-CAF4*	RFP-Caf4	This Study
B3002	p414-*GPD-mt-mCherry*	*N. crassa* ATP9 (1-69) + mCherry	This Study

Table A.2: Yeast Strains Used in this Study

Strain ID	Mating type	Genotype	Reference
JSY5740	*MAT**a***	*ura3-52 leu2Δ1 his3Δ200 trp1Δ63*	Koirala et al., 2010
JSY8612	*MAT**a***	*ura3-52 leu2Δ1, his3Δ200, trp1Δ63, caf4::KanMx, mdv1::HIS3*	Koirala et al., 2010
JSY8614	*MAT**a***	*ura3-52 leu2Δ1 his3Δ200 trp1Δ63 caf4::KanMx*	This Study
JSY8616	*MAT**a***	*ura3-52 leu2Δ1 his3Δ200 trp1Δ63 mdv1::HIS3*	This Study
JSY9774	*MAT**a***	*ura3-52 leu2Δ1 his3Δ200 trp1Δ63 lys2Δ202 caf4::KanMX mdv1::MET-EYFP-MDV1 ho::MET25-Cerulean-CAF4*	This Study
JSY9886	*MAT**a***	*ura3-52 leu2Δ1 his3Δ200 trp1Δ63 lys2Δ202 caf4::KanMX mdv1::CAF4*	This Study
JSY9903	*MAT**a***	*ura3-52 leu2Δ1 his3Δ200 trp1Δ63 caf4::MDV1, mdv1::HIS3*	This Study

Results

Caf4 is Present at Mitochondrial Fission Sites and is Sufficient for Fission

A genome wide analysis of yeast protein expression showed that the abundance of Caf4 is one sixth that of Mdv1 (Ghaemmaghami et al., 2003). This finding raised the possibility that lower expression of Caf4 relative to Mdv1 was responsible for the functional differences observed for the two fission adaptors. We tested this idea by examining the effect of increasing Caf4 expression on mitochondrial fission in vivo. As shown in Figure A.1B, 100% of wildtype (WT, *CAF4 MDV1*) cells expressing Caf4 and Mdv1 had branched, tubular mitochondria, while cells lacking both adaptors had severe fission defects (*caf4*Δ *mdv1*Δ, 3% cells with WT morphology). Similar to previous reports (Griffin et al., 2005), an *mdv1*Δ strain expressing endogenous Caf4 exhibited significant fission defects (*CAF4 mdv1*Δ, 29% cells with WT morphology), and a *caf4*Δ strain expressing endogenous Mdv1 exhibited essentially no fission defects (*caf4*Δ *MDV1*, 95% cells with WT morphology). Importantly, when Caf4 expression was induced from the *MET25* promoter on a plasmid in the *caf4*Δ *mdv1*Δ strain, the population of cells with WT mitochondrial morphology increased to 51%. This increased rescue of fission defects was correlated with a 5.4-fold increase over native Caf4 expression (data not shown).

Time-lapse imaging studies confirmed that Caf4 in these cells was mediating mitochondrial fission when Mdv1 was absent. By epifluorescence microscopy, Dnm1-containing fission complexes appear as puncta that colocalize with mitochondrial tubules

Figure A.1. Caf4 Functions Independently as a Mitochondrial Fission Adaptor.
(**A**) Domain structure of the Caf4 fission adaptor, including the N-terminal extension (NTE), predicted coiled-coil (CC), and WD40 repeats predicted to form a β-propeller (WD40 repeats/ β-propeller). (**B**) Quantification of mitochondrial morphology in the indicated strains (n=100 cells). Bars and error bars are the mean and SD of three independent experiments. (**C**) Time-lapse imaging of a mitochondrial fission event

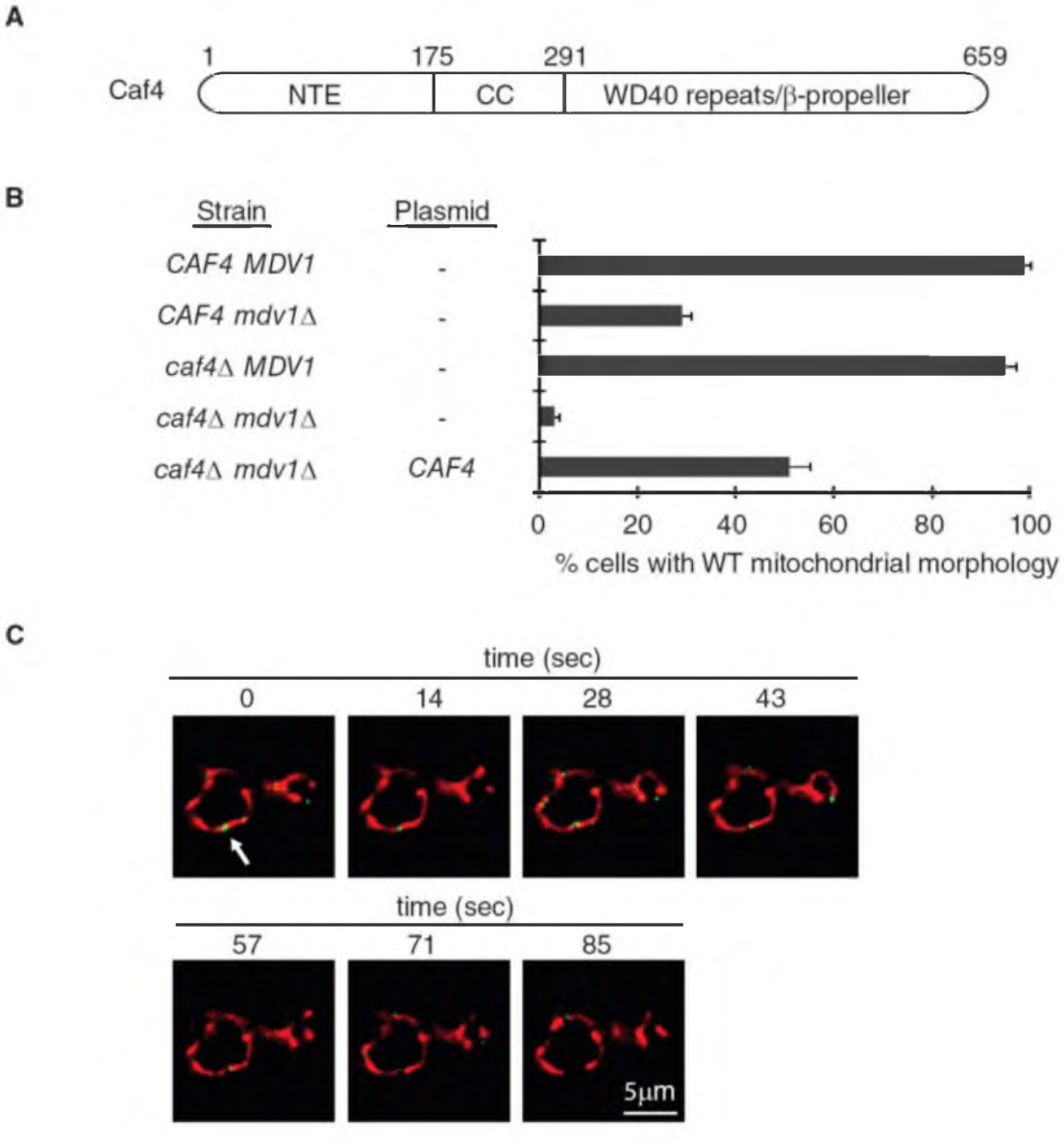
A
1
175
291
659
Caf4
NTE
CC
WD40 repeats/β-propeller
B
Strain
Plasmid
CAF4 MDV1
-
CAF4 mdv1Δ
-
caf4Δ MDV1
-
caf4Δ mdv1Δ
-
caf4Δ mdv1Δ
CAF4
0
20
40
60
80
100
% cells with WT mitochondrial morphology
C
time (sec)
0
14
28
43
time (sec)
57
71
85
5μm

(Otsuga et al., 1998). Mdv1 or Caf4 also appear in these puncta after coassembly with Dnm1 (Cerveny et al., 2001; Griffin et al., 2005; Tieu and Nunnari, 2000). In *mdv1*Δ *caf4*Δ cells expressing GFP-Caf4 protein, green Caf4 puncta mediated by GFP-Caf4 expressed in a *caf4Δ mdv1Δ* strain. Mitochondria are labeled with mt-RFP. Scale bar: 5 μm. were observed on mt-RFP labeled mitochondrial tubules at sites where fission occurred (Figure A.1C arrow, a representative example is shown). Together, these results indicate that Caf4 can function independently as a fission adaptor in yeast.

The Caf4 and Mdv1 Adaptors Are not Functionally Equivalent

Although Caf4 can carry out fission in the absence of Mdv1, the two adaptors may not be functionally equivalent. To test this possibility, Caf4 and Mdv1 were expressed from the MET25 promoter in a caf4Δ mdv1Δ strain, and the abundance of each adaptor was increased by reducing the methionine concentration in the medium. WT mitochondrial morphology increased from 41% to 80% (Figure A.2A) when Mdv1 steady state abundance was raised 4.2-fold by removing methionine from the medium (Figure A.2B). By contrast, raising Caf4 steady-state abundance 1.3-fold (1.0 mM methionine, Figure A.2B) initially increased WT mitochondrial morphology from 49% to 57% (Figure A.2A). Further induction to 2.6-fold Caf4 over expression (0.0 mM methionine) reduced the rescue to 29%, indicating that increasing Caf4 expression had a dominant negative effect on mitochondrial fission. Although we did not observe dominant-negative fission defects by increasing Mdv1 expression 4.2-fold (0.0 mM methionine) in these studies, we were able to induce dominant-negative defects by over expressing Mdv1 from the inducible *GAL1* promoter (~20-fold induction, data not shown) (Cerveny and Jensen, 2003). These different effects of Caf4 and Mdv1 over expression on mitochondrial

Figure A.2. Caf4 and Mdv1 Are not Functionally Equivalent.
(**A**) Quantification of mitochondrial morphology in a *caf4Δ mdv1Δ* strain expressing Caf4 or Mdv1 from the repressible *MET25* promoter in media containing different methionine concentrations (n=100 cells). (**B**) Protein abundance of Caf4 or Mdv1 expressed from the repressible *MET25* promoter in difference methionine concentrations. The abundance of each protein was subsequently normalized to its abundance in 2.0 mM methionine. Bars and error bars are the mean and SD of three independent experiments.

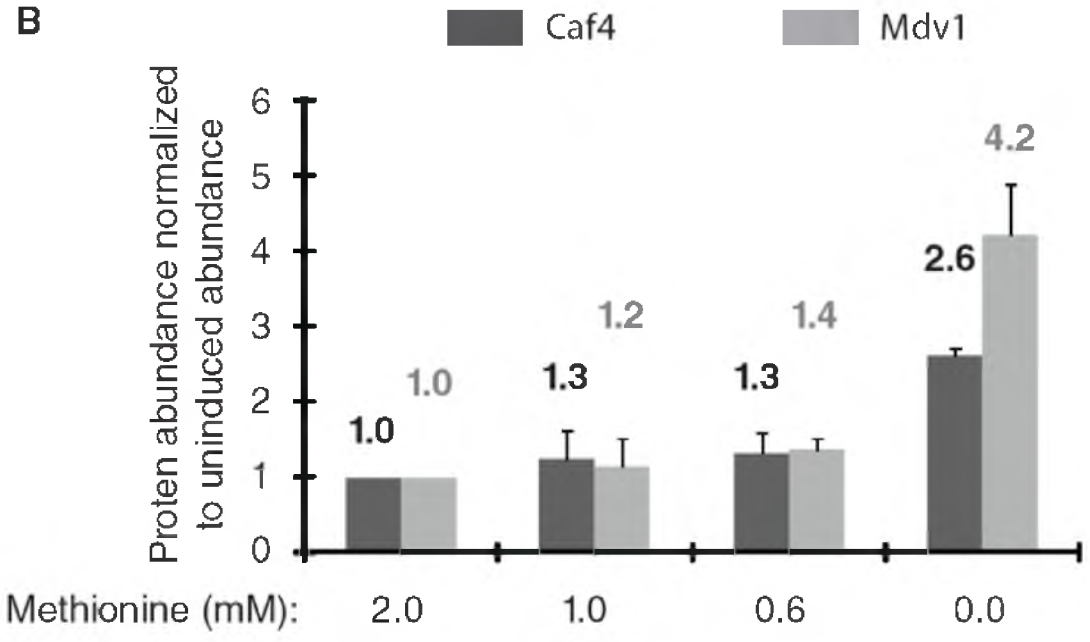
B
Caf4
Mdv1
Proten abundance normalized to uninduced abundance
0
1
2
3
4
5
6
1.0
1.0
1.3
1.2
1.3
1.4
2.6
4.2
Methionine (mM):
2.0
1.0
0.6
0.0

A

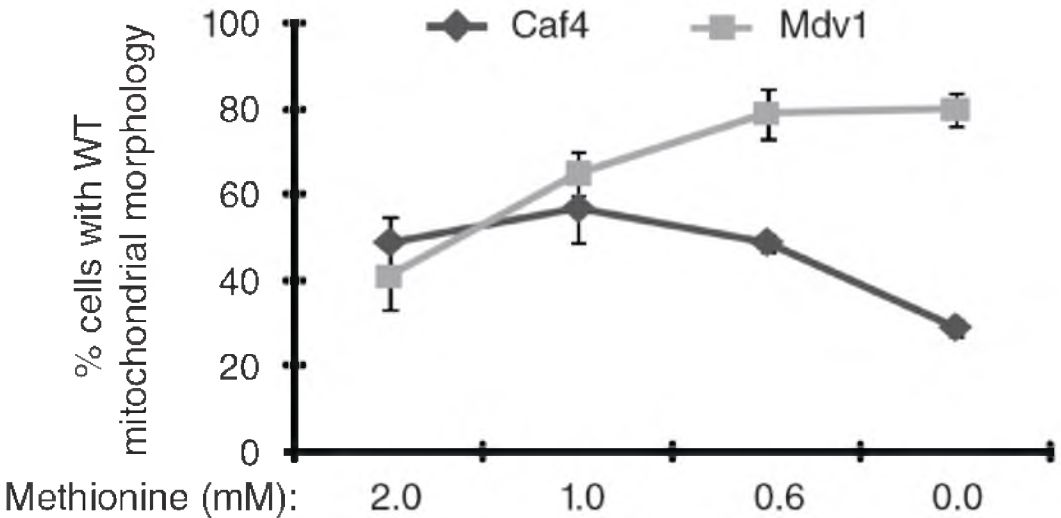
Caf4
Mdv1
% cells with WT mitochondrial morphology
100
80
60
40
20
0
Methionine (mM):
2.0
1.0
0.6
0.0

fission support the idea that the fission adaptor functions of the two proteins are not equivalent.

We also tested whether expression of Caf4 from the native *MDV1* promoter and locus was sufficient to replace Mdv1 function. Mitochondrial morphology was WT in cells expressing only Mdv1 from its native locus (Figure A.3A). When Caf4 alone was expressed from the *MDV1* promoter, Caf4 abundance increased 1.6-fold over the endogenous level (Figure A.3B) but mitochondrial fission remained defective (Figure A.3A, 20% WT morphology). (Note that this 1.6-fold increase is lower than the level of Caf4 expression shown to cause dominant negative fission defects in Figure A.2). Thus, Caf4 expressed from the *MDV1* locus is not able to support WT levels of mitochondrial fission. By contrast, we observed a 0.6-fold decrease in expression of Mdv1 from the *CAF4* promoter with a corresponding decrease in WT mitochondrial morphology. We also noted a reproducible 1.3-fold increase in Caf4 expression from its native locus when the *MDV1* coding region was deleted. However, Mdv1 abundance did not change significantly when *CAF4* was absent. Thus, regulatory circuits that control expression from the *CAF4* gene may be able to sense and respond to changes in cellular Mdv1 abundance.

Caf4 and Mdv1 Can Work Together at a Mitochondrial Fission Site

Mdv1 self-assembles via dimerization of an internal coiled-coil (Koirala et al., 2010; Zhang et al., 2012) and, based on structural predictions and two hybrid assays, Caf4 is predicted to behave in a similar manner. Caf4 and Mdv1 can also interact with one another (Griffin et al., 2005). However, it is not known whether Caf4 and Mdv1 can

Figure A.3. Caf4 Causes Dominant-negative Fission Defects when Expressed from the *MDV1* Promoter at the *MDV1* Locus.
(**A**) Quantification of mitochondrial morphology in the indicated strains (n=100 cells). (**B**) Steady-state abundance of Caf4 and Mdv1 in strains shown in (**A**). Owing to the use of different antibodies, the abundance of Caf4 and Mdv1 in the same and different strains should not be compared to one another. Bars and error bars are the mean and SD of three independent experiments.

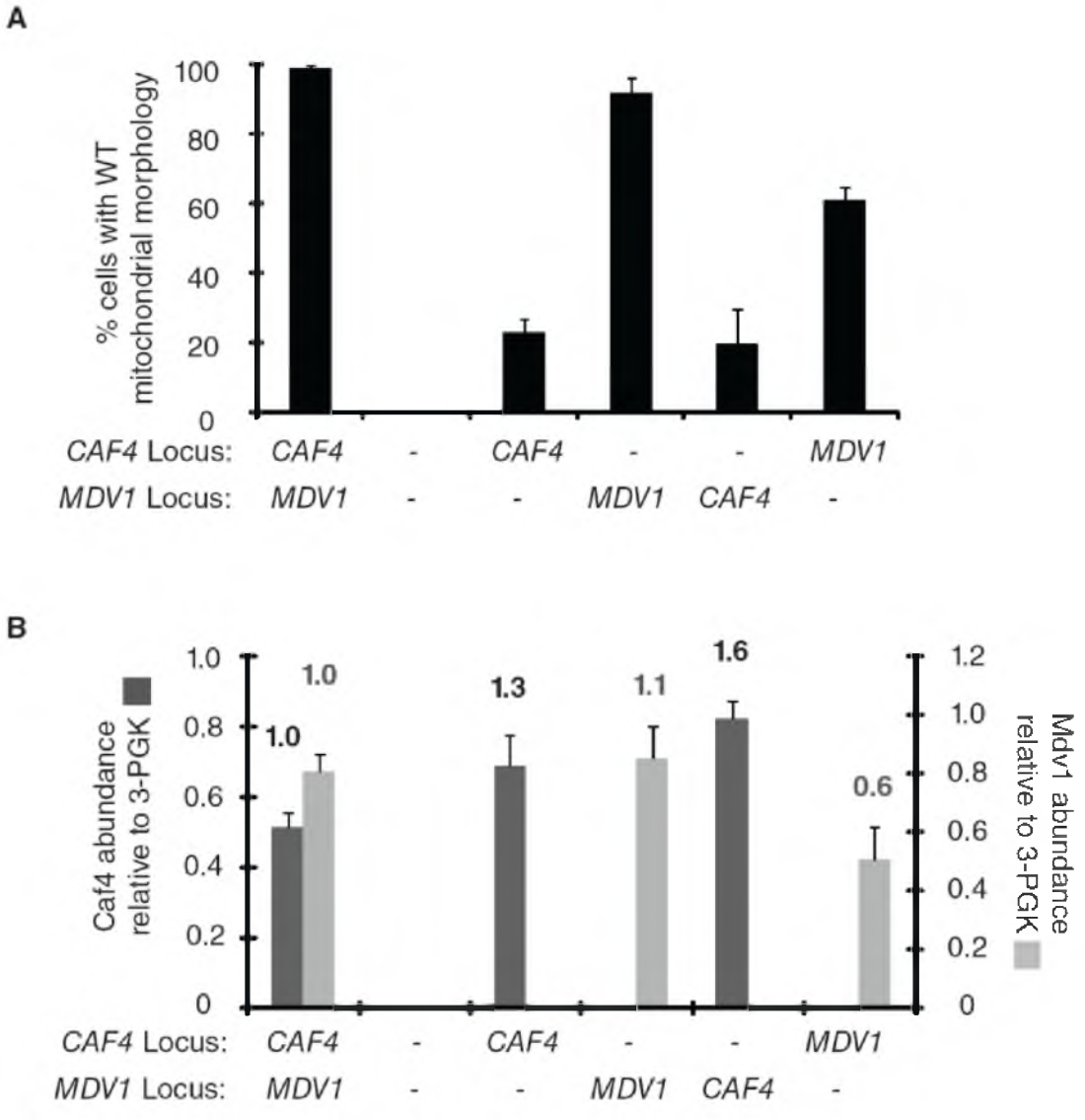
A
% cells with WT mitochondrial morphology
100
80
60
40
20
0
CAF4 Locus: CAF4 - CAF4 - - MDV1
MDV1 Locus: MDV1 - - MDV1 CAF4 -
B
Caf4 abundance relative to 3-PGK
Mdv1 abundance relative to 3-PGK
1.0
0.8
0.6
0.4
0.2
0
1.2
1.0
0.8
0.6
0.4
0.2
0
1.0
1.0
1.3
1.1
1.6
0.6
CAF4 Locus: CAF4 - CAF4 - - MDV1
MDV1 Locus: MDV1 - - MDV1 CAF4 -

function together during mitochondrial fission. To address this question, we examined the extent and function of Caf4 and Mdv1 colocalization *in vivo*.

We began by quantifying the colocalization of GFP-Caf4 with RFP-Caf4 and GFP-Mdv1 with RFP-Mdv1 in cells lacking WT versions of the two proteins. Since fluorescent puncta in these experiments contain a single fission adaptor coassembled with Dnm1, these numbers represent the maximum colocalization we would expect to observe. Representative images of the categories scored are shown in Figure A.4A (colocalized, a-c; not colocalized, d-f). Using this approach, 85% of Caf4 and 82% of Mdv1 signals colocalized in these studies, with the majority of puncta displaying the colocalization pattern shown in Figure A.4A, a and b (72% and 81% respectively).

Next we quantified the colocalization of GFP-Caf4 and RFP-Mdv1 in mitochondrial puncta. We observed that 56% of RFP-Caf4 puncta colocalized with GFP-Mdv1 puncta (Figure A.4B). Of these 56%, (t = 0s, white signal in overlay) were able to mediate fission of an mCherry-labeled mitochondrial tubule. In the example shown, fission was complete after 80 seconds, at which point Caf4 and Mdv1 disassembled and dispersed along the surface of the majority (77%) displayed the colocalization pattern shown in Figure A.4A, a and b. Similar results were obtained with GFP-Caf4 and RFP-Mdv1 (data not shown), indicating that placement of the fluorescent protein tags did not affect the experimental results.

Further analysis established that mitochondrial fission occurred at sites where Caf4 and Mdv1 colocalized. As shown in Figure A.4C, time-lapse imaging studies of cells expressing Cerulean-Caf4 and EYFP-Mdv1 showed that puncta containing both adaptors (t = 0s, white signal in overlay) were able to mediate fission of an mCherry-

Figure A.4. Mitochondrial Puncta Containing both Caf4 and Mdv1 Are Fission Competent.

Large panel at the left shows a representative image of *caf4Δ mdv1Δ* cells expressing GFP-Caf4 and RFP-Mdv1. Scale bar: 5 μm. a-f marks puncta enlarged from the image in (A) at the left. Examples of partially or completely co-localized (**a-c**) versus isolated (**d-f**) puncta are shown. Scale bar: 0.2 μm. (**B**) Quantification of Caf4 and Mdv1 colocalization. GFP- or RFP-tagged Caf4 and Mdv1 were expressed in *caf4Δ mdv1Δ* cells in the pair-wise combinations indicated. The number of GFP puncta colocalized with RFP puncta was quantified and normalized to the total number of RFP puncta in each cell (n=10 cells). Bars and error bars are the mean and SD of three independent experiments. (**C**) Time lapse imaging of a mitochondrial fission event at a site where Caf4 and Mdv1 co-localize. Cerulean-tagged Caf4 (shown in cyan pseudo-color) and EYFP-Mdv1 were integrated at the *HO* and *MDV1* loci, respectively. Mitochondria were visualized using plasmid-borne mt-mCherry. The overlay contains true color images of all three channels. White areas indicate regions where signals from all three fluorescent proteins overlap. Scale Bar: 0.6 μm

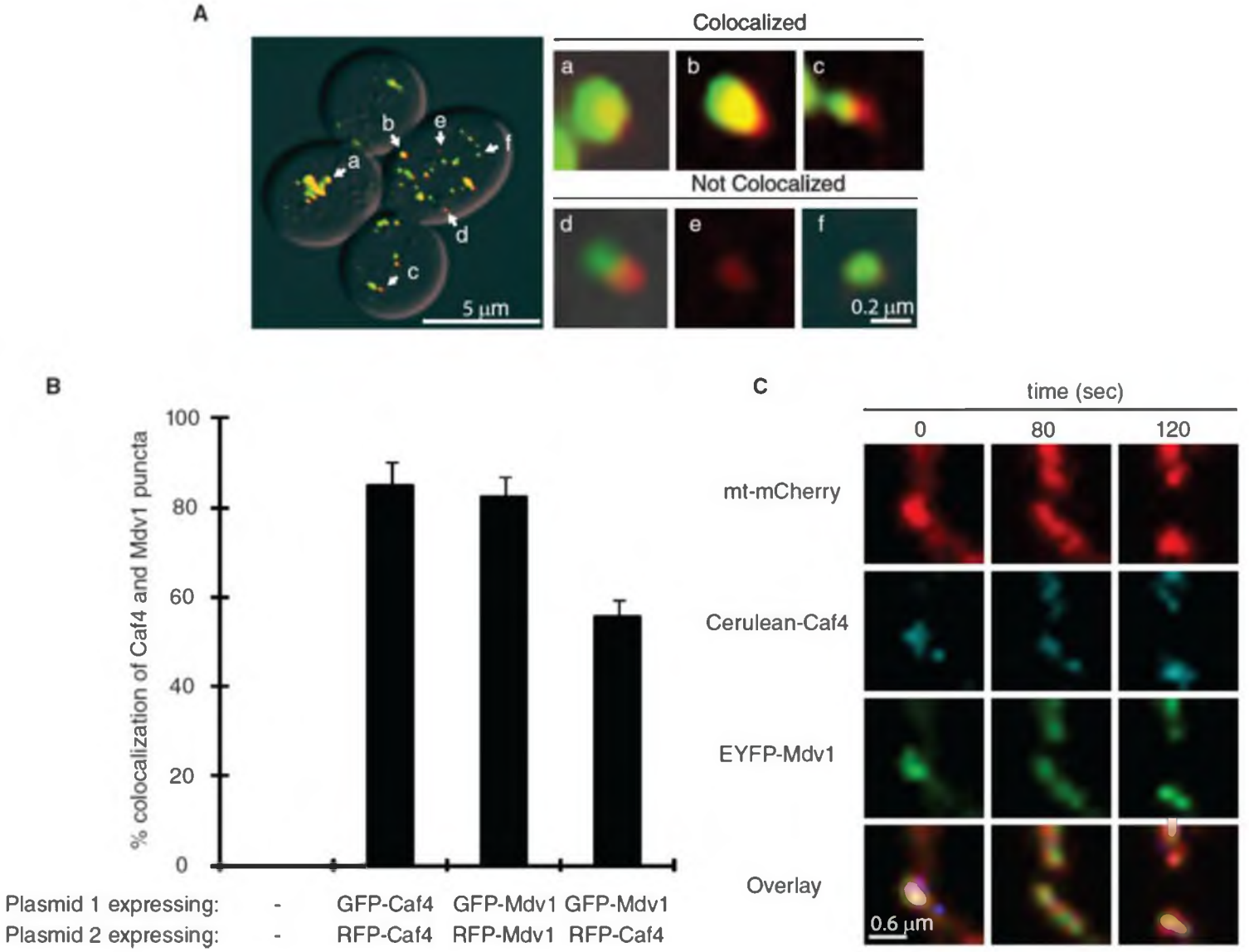
A
Colocalized
Not Colocalized
a
b
c
d
e
f
5 µm
0.2 µm
B
% colocalization of Caf4 and Mdv1 puncta
100
80
60
40
20
0
Plasmid 1 expressing: - GFP-Caf4 GFP-Mdv1 GFP-Mdv1
Plasmid 2 expressing: - RFP-Caf4 RFP-Mdv1 RFP-Caf4
C
time (sec)
0
80
120
mt-mCherry
Cerulean-Caf4
EYFP-Mdv1
Overlay
0.6 µm

labeled mitochondrial tubule. In the example shown, fission was complete after 80 seconds, at which point Caf4 and Mdv1 disassembled and dispersed along the surface of the separated tubules. These data provide a direct demonstration that Caf4 and Mdv1 can work together at the same mitochondrial fission site in vivo.

Eolution of the Fungal Fission Adaptors

A major event in the evolutionary history of *Saccharomyces cerevisiae* was an ancestral whole genome duplication, which was followed by elimination of many redundant gene copies during the divergence of species in the genus *Saccharomyces* (Kellis et al., 2004; Wolfe and Shields, 1997). Our phylogenetic analysis indicates that *CAF4* and *MDV1* are among those redundant gene copies that have been retained during evolution. As shown in Figure A.5, *Pichia pastoris*, *Lachancea thermotolerans* and *Aspergillus fumigatus* contain only a single gene that is homologous to *CAF4/MDV1*. Duplication of this ancestral gene gave rise to *CAF4* and *MDV1* in most *Saccharomyces* species, consistent with an origin resulting from whole genome duplication. The increased branch lengths in the Caf4 clade compared to the Mdv1 clade indicate that the Caf4 protein has undergone more amino substitutions than Mdv1 since the original duplication event. This observation suggests that Mdv1 is under tighter constraints to perform its essential function in mitochondrial fission, consistent with our functional analysis. One possible outcome of this accelerated rate of Caf4 protein evolution is that the *CAF4* gene will ultimately be lost from the *Saccharomyces* genome. However, it appears that *MDV1*, but not *CAF4*, was lost from *Saccharomyces kudriavzevii*. Thus, Caf4 can either substitute for Mdv1 function or a completely different protein has assumed the essential role in membrane fission in this species. An alternative outcome in

Figure A.5. Phylogenetic Relationship of Caf4 and Mdv1 in Representative Fungi. The amino acid sequences of paralogs from fully sequenced fungal genomes were aligned using ClustalW2 and a phylogenetic tree was constructed using the maximum-likelihood method. Bootstrap values above 50 are shown at the nodes of the branches. Branch lengths are proportional to the number of amino acid substitutions per site. The Caf4 and Mdv1 clades are marked by vertical lines. Scale bar: 0.1 substitution per site in the protein.

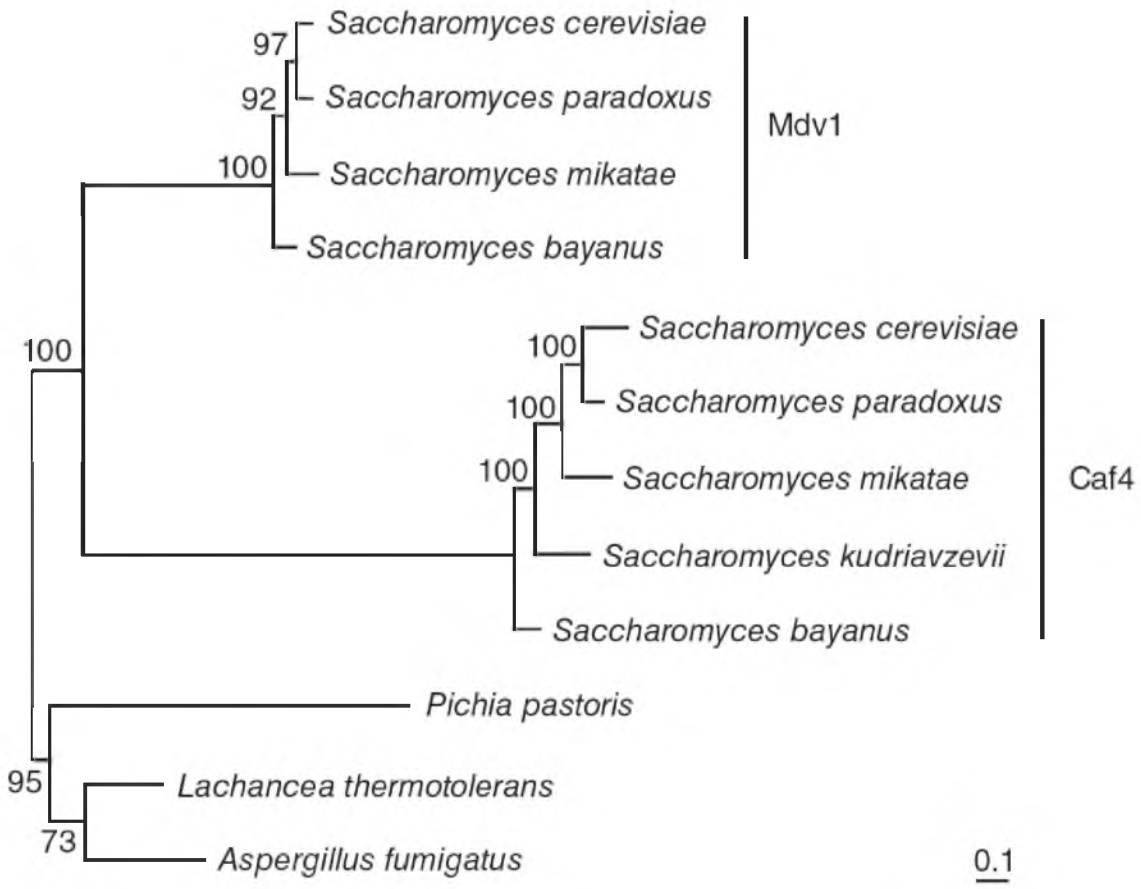
Saccharomyces cerevisiae
97
Saccharomyces paradoxus
92
Mdv1
100
Saccharomyces mikatae
Saccharomyces bayanus
100
Saccharomyces cerevisiae
100
Saccharomyces paradoxus
100
Saccharomyces mikatae
Caf4
Saccharomyces kudriavzevii
Saccharomyces bayanus
Pichia pastoris
95
Lachancea thermotolerans
73
Aspergillus fumigatus
0.1

species with both proteins is that Caf4 will acquire additional or novel function(s) (see discussion).

Discussion

Prior to this study, the Caf4 adaptor was known to function early in fission to recruit Dnm1 to the outer mitochondrial membrane. However, whether Caf4 participated in mitochondrial membrane fission after Dnm1 recruitment was unclear. Our results provide a direct demonstration that, in the absence or presence of Mdv1, Caf4 localizes in complexes on mitochondria that carry out membrane division.

It has been suggested that Caf4 serves as regulator of mitochondrial fission. We think it is unlikely that Caf4 acts as a positive regulator, since its presence or absence has little effect on Mdv1-mediated fission in WT cells. Several observations also suggest that Caf4 does not act as a negative regulator. When Caf4 is expressed in the absence of Mdv1, fission occurs and the time course of fission is similar to WT. In addition, when Caf4 and Mdv1 are both present in mitochondrial puncta, fission appears to occur normally. However, Caf4 and Mdv1 are not functionally equivalent. When expressed at maximum levels from the *MET25* promoter, Caf4 (but not Mdv1) causes dominant-negative fission defects. Moreover, expression of the *CAF4* gene from the *MDV1* promoter in the genome is not sufficient to restore mitochondrial fission to levels observed in an *MDV1 caf4*Δ strain.

In many instances, one member of a duplicated gene pair is retained during evolution because it develops a specialized function (subfunctionalization) within a cellular process or because it acquires an entirely new function (neofunctionalization) (Kafri et al., 2009). There is evidence that Caf4 has acquired a specialized function in

mitochondrial biology. Jakob and colleagues showed previously that Caf4 (but not Mdv1) plays a role in orienting a subset of mitochondrial Dnm1 puncta toward the yeast cell cortex (Schauss et al., 2006). This Dnm1 orientation is proposed to anchor mitochondria near the plasma membrane and distribute them at the cell periphery. Caf4 has also been shown to participate with Dnm1, Mdv1 and Fis1 in peroxisome division (Hofmann et al., 2009; Motley et al., 2008). Although it is possible that Caf4 has acquired specialized functions in peroxisome division, we do not observe changes in peroxisome morphology in *caf4*Δ cells relative to WT (data not shown). Moreover, cells lacking Caf4 grow as well as WT on carbon sources that require peroxisome function (i.e. oleate, data not shown). If Caf4 had acquired a new function in a critical cellular process, loss of Caf4 would be expected to affect yeast fitness. However, our extensive analyses of *caf4*Δ cells has not uncovered conditions that confer a fitness advantage or disadvantage relative to WT with respect to cell growth, sporulation, mtDNA maintenance, mitochondrial respiratory function, or drug sensitivity (data not shown). Future studies competing a *caf4*Δ mutant against wildtype strains under additional conditions may uncover a more subtle fitness cost.

Our phylogenetic analysis revealed a slightly accelerated rate of amino acid substitution for Caf4 relative to Mdv1. However, both adaptors have retained roles in mitochondrial fission, arguing against the idea that the *CAF4* gene is likely to be lost, like many other paralogs originating from whole gene duplication. Instead, Caf4 and Mdv1 appear to work synergistically, with Mdv1 carrying out the majority of fission in proportion to its higher level of expression. Consistent with this model, we find that Caf4 and Mdv1 are cross-regulated, with Caf4 expression increasing when Mdv1 is absent.

The fact that Caf4 has acquired the ability to orient Dnm1 at the cell cortex (Schauss et al., 2006) also supports the idea that the *CAF4* gene has been retained because it confers some type of selective advantage. It remains to be determined whether/how the Dnm1-orienting ability of Caf4 measurably contributes to overall fitness in yeast, and how species like *S. kudriavzevii* have compensated for the loss of Mdv1.

Acknowledgements

We thank Jane Macfarlane for expertise in mutagenesis and plasmid construction, members of the Shaw laboratory for critical discussions, Nels Elde for guidance with phylogenetic tree construction and Markus Babst for use of his DeltaVision microscope. We also thank Beverly Wendland for use of her lab space while performing experiments in the Johns Hopkins Integrated Imaging Center. Sequencing and oligonucleotide synthesis services were provided by University of Utah Core Facilities.

References

Bleazard, W., McCaffery, J.M., King, E.J., Bale, S., Mozdy, A., Tieu, Q., Nunnari, J., and Shaw, J.M. (1999). The dynamin-related GTPase Dnm1 regulates mitochondrial fission in yeast. Nature Cell Biology *1*, 298-304.

Cerveny, K.L., and Jensen, R.E. (2003). The WD-repeats of Net2p interact with Dnm1p and Fis1p to regulate division of mitochondria. Mol Biol Cell *14*, 4126-4139.

Cerveny, K.L., McCaffery, J.M., and Jensen, R.E. (2001). Division of mitochondria requires a novel DMN1-interacting protein, Net2p. Mol Biol Cell *12*, 309-321.

Ghaemmaghami, S., Huh, W.K., Bower, K., Howson, R.W., Belle, A., Dephoure, N., O'Shea, E.K., and Weissman, J.S. (2003). Global analysis of protein expression in yeast. Nature *425*, 737-741.

Goffeau, A., Barrell, B.G., Bussey, H., Davis, R.W., Dujon, B., Feldmann, H., Galibert, F., Hoheisel, J.D., Jacq, C., Johnston, M., et al. (1996). Life with 6000 genes. Science *274*, 546, 563-547.

Gorsich, S.W., and Shaw, J.M. (2004). Importance of mitochondrial dynamics during meiosis and sporulation. Mol Biol Cell *15*, 4369-4381.

Griffin, E.E., Graumann, J., and Chan, D.C. (2005). The WD40 protein Caf4p is a component of the mitochondrial fission machinery and recruits Dnm1p to mitochondria. J Cell Biol *170*, 237-248.

Guthrie, C., and Fink, G.R. (1991). Guide to yeast genetics and molecular biology. Methods Enzymol *194*, 1-863.

Hofmann, L., Saunier, R., Cossard, R., Esposito, M., Rinaldi, T., and Delahodde, A. (2009). A nonproteolytic proteasome activity controls organelle fission in yeast. J Cell Sci *122*, 3673-3683.

Ingerman, E., Perkins, E.M., Marino, M., Mears, J.A., McCaffery, J.M., Hinshaw, J.E., and Nunnari, J. (2005). Dnm1 forms spirals that are structurally tailored to fit mitochondria. J Cell Biol *170*, 1021-1027.

Kafri, R., Springer, M., and Pilpel, Y. (2009). Genetic redundancy: new tricks for old genes. Cell *136*, 389-392.

Karren, M.A., Coonrod, E.M., Anderson, T.K., and Shaw, J.M. (2005). The role of Fis1p-Mdv1p interactions in mitochondrial fission complex assembly. J Cell Biol *171*, 291-301.

Kellis, M., Birren, B.W., and Lander, E.S. (2004). Proof and evolutionary analysis of ancient genome duplication in the yeast Saccharomyces cerevisiae. Nature *428*, 617-624.

Koirala, S., Bui, H.T., Schubert, H.L., Eckert, D.M., Hill, C.P., Kay, M.S., and Shaw, J.M. (2010). Molecular architecture of a dynamin adaptor: implications for assembly of mitochondrial fission complexes. J Cell Biol *191*, 1127-1139.

Kushnirov, V.V. (2000). Rapid and reliable protein extraction from yeast. Yeast *16*, 857-860.

Legesse-Miller, A., Massol, R.H., and Kirchhausen, T. (2003). Constriction and Dnm1p recruitment are distinct processes in mitochondrial fission. Mol Biol Cell *14*, 1953-1963.

Maniatis, T., Fritsch, E.F., and Sambrook, J. (1982). Molecular Cloning: A Laboratory Manual (Cold Spring Harbor, NY: Cold Spring Harbor Laboratory Press).

Motley, A.M., Ward, G.P., and Hettema, E.H. (2008). Dnm1p-dependent peroxisome fission requires Caf4p, Mdv1p and Fis1p. J Cell Sci *121*, 1633-1640.

Mozdy, A.D., McCaffery, J.M., and Shaw, J.M. (2000). Dnm1p GTPase-mediated mitochondrial fission is a multi-step process requiring the novel integral membrane component Fis1p. J Cell Biol *151*, 367-380.

Musso, G., Zhang, Z., and Emili, A. (2007). Retention of protein complex membership by ancient duplicated gene products in budding yeast. Trends Genet *23*, 266-269.

Nunnari, J., Marshall, W.F., Straight, A., Murray, A., Sedat, J.W., and Walter, P. (1997). Mitochondrial transmission during mating in Saccharomyces cerevisiae is determined by mitochondrial fusion and fission and the intramitochondrial segregation of mitochondrial DNA. Mol Biol Cell *8*, 1233-1242.

Okamoto, K., and Shaw, J.M. (2005). Mitochondrial morphology and dynamics in yeast and multicellular eukaryotes. Annu Rev Genet *39*, 503-536.

Otsuga, D., Keegan, B.R., Brisch, E., Thatcher, J.W., Hermann, G.J., Bleazard, W., and Shaw, J.M. (1998). The dynamin-related GTPase, Dnm1p, controls mitochondrial morphology in yeast. J Cell Biol *143*, 333-349.

Schauss, A.C., Bewersdorf, J., and Jakobs, S. (2006). Fis1p and Caf4p, but not Mdv1p, determine the polar localization of Dnm1p clusters on the mitochondrial surface. J Cell Sci *119*, 3098-3106.

Sesaki, H., and Jensen, R.E. (1999). Division versus fusion: Dnm1p and Fzo1p antagonistically regulate mitochondrial shape. J Cell Biol *147*, 699-706.

Tieu, Q., and Nunnari, J. (2000). Mdv1p is a WD repeat protein that interacts with the dynamin-related GTPase, Dnm1p, to trigger mitochondrial division. J Cell Biol *151*, 353-366.

Tieu, Q., Okreglak, V., Naylor, K., and Nunnari, J. (2002). The WD repeat protein, Mdv1p, functions as a molecular adaptor by interacting with Dnm1p and Fis1p during mitochondrial fission. J Cell Biol *158*, 445-452.

Wolfe, K.H., and Shields, D.C. (1997). Molecular evidence for an ancient duplication of the entire yeast genome. Nature *387*, 708-713.

Zhang, Y., and Chan, D.C. (2007). Structural basis for recruitment of mitochondrial fission complexes by Fis1. Proc Natl Acad Sci U S A *104*, 18526-18530.

Zhang, Y., Chan, N.C., Ngo, H.B., Gristick, H., and Chan, D.C. (2012). Crystal structure of mitochondrial fission complex reveals scaffolding function for mitochondrial division 1 (Mdv1) coiled coil. J Biol Chem *287*, 9855-9861.